Håkon Johan Kirkesæther Brun
Erlend Hansen
Edvard ove Zimmer

Development of a parametric workflow, form finding and structural analysis for timber gridshells

Master's thesis

NTNU
Norwegian University of Science and Technology
Faculty of Engineering
Department of Structural Engineering

NTNU
Norwegian University of
Science and Technology

Håkon Johan Kirkesæther Brun
Erlend Hansen
Edvard ove Zimmer

Development of a parametric workflow, form finding and structural analysis for
timber gridshells

NTNU

Norwegian University of
Science and Technology

Department of Structural Engineering
Faculty of Engineering
NTNU – Norwegian University of Science and Technology

MASTER THESIS 2020

SUBJECT AREA:	DATE:	NO. OF PAGES:
Conceptual Structural Design	2020-06-09	157

TITLE:

Development of a parametric workflow, form finding and structural analysis for timber gridshells

Utvikling av en parametrisk arbeidsflyt, formfinning og kontruksjonsanalyse av gitterskall av tre

BY:

Håkon Johan Kirkesæther Brun
Erlend Hansen
Edvard Hove Zimmer

SUMMARY:
In this thesis, the potential of the parametric workflow environments for real time conceptual design and analysis of discrete, segmented timber gridshells, is investigated. The opportunities of generating repeating node networks in the design, without compromising the structural performance to a large extent, is also examined. Timber has become a popular material to use in Norway, due to its sustainability, light weight and availability. This combined with the possibility to mass produce some of the otherwise unique configurations of building materials needed, could make gridshells a more viable structure, also in Norway. This is investigated through the development of a parametric workflow environment where grid pattern design and real time feedback of structural behaviour is combined with custom developed components for both global and local geometrical form finding and evaluation. The culmination of the thesis is a case project in which the Great Court Roof of the British Museum served as the basis for redesigns and optimization.

The parametric design environment developed proved not only useful, but crucial for any of the design comparisons of the case project to be made. For the Great Court Roof, the weight of the nodes was found to be negligible compared to the other loads acting on it. The structural performance greatly depends on the global shape, and it was found that the Great Court Roof is not optimized for structural efficiency in terms of curvature. It was shown how the structural efficiency of gridshells are completely dependent upon its curvature, and how increasing the height of the Great Court Roof make a stronger structure that deflects less. The grid pattern topology turned also out to greatly affect the structural performance. It was found that generating new grid patterns can be done quickly with parametric design, but irregular boundaries can make it more difficult to find a design that facilitates repeating node networks. It was found that facilitating either an effective structure or one easier to manufacture, will to at least some degree involve compromising the other.

RESPONSIBLE TEACHER: Nils Erik Anders Rønnquist

SUPERVISORS: Nils Erik Anders Rønnquist and Steinar Hillersøy Dyvik

CARRIED OUT AT: Department of Structural Engineering, NTNU, Trondheim

Abstract

Gridshells are geometrical complex structures where the borders between architectural design and engineered optimizations become blurred. The global shape of the gridshells largely determine the structural performance. In recent years, parametric modelling through digital software have gotten more prevalent. These parametric environments lend themselves perfectly for the design and analysis of gridshell structures, as the different design choices taken will all be intertwined and dependant upon each other. Although gridshells can be aesthetically beautiful, it is not common to build in Norway. This is partly due to the environmental factors imposed by heavy snow loads, but mostly because of the complexity in both fabrication and construction that make them very expensive.

In this thesis, the potential of the parametric workflow environments for real time conceptual design and analysis of discrete, segmented timber gridshells, is investigated. The opportunities of generating repeating node networks in the design, without compromising the structural performance to a large extent, is also examined. Timber has become a popular material to use in Norway, due to its sustainability, light weight and availability. This combined with the possibility to mass produce some of the otherwise unique configurations of building materials needed, could make gridshells a more viable structure, also in Norway. This is investigated through the development of a parametric workflow environment where grid pattern design and real time feedback of structural behaviour is combined with custom developed components for both global and local geometrical form finding and evaluation. The culmination of the thesis is a case project in which the Great Court Roof of the British Museum served as the basis for redesigns and optimization.

The parametric design environment developed proved not only useful, but crucial for any of the design comparisons of the case project to be made. For the Great Court Roof, the weight of the nodes was found to be negligible compared to the other loads acting on it. The structural performance greatly depends on the global shape, and it was found that the Great Court Roof is not optimized for structural efficiency in terms of curvature. It was shown how the structural efficiency of gridshells are completely dependent upon its curvature, and how increasing the height of the Great Court Roof make a stronger structure that deflects less. The grid pattern topology turned also out to greatly affect the structural performance. It was found that generating new grid patterns can be done quickly with parametric design, but irregular boundaries can make it more difficult to find a design that facilitates repeating node networks. It was found that facilitating either an effective structure or one easier to manufacture, will to at least some degree involve compromising the other.

Oppsummering

Gitterskall er geometrisk komplekse strukturer, der grensene mellom arkitektur og konstruksjonoptimalisering blir visket ut. Konstruksjonsutnyttelsen bestemmes i stor grad av gitterskallets globale form. De siste årene har parametrisk modellering gjennom digitale verktøy blitt mer utbredt. Disse parametriske miljøene egner seg ideelt til design og analyse av gitterskall, ettersom de forskjellige parametere vil påvirke hverandre. Selv om gitterskall kan være estetisk vakre konstruksjoner, så er det ikke vanlig å bygge i Norge. Det skyldes delvis miljøfaktorene, som blant annet at konstruksjoner i norske forhold må . Likevel er det nok hovedsakelig på grunn av kompleksiteten i både fabrikasjon og konstruksjon som gjør dem veldig dyre.

I denne avhandlingen blir potensialet til de parametriske arbeidsflytmiljøene for sanntids konseptuell design og analyse av diskrete, segmenterte gitterskall i tre undersøkt. Mulighetene for å generere repeterende nodenettverk, uten at det går ut over konstruksjonsytelsen i stor grad, blir også undersøkt. Tre har blitt et populært materiale i Norge på grunn av dets bærekraft, lette vekt og tilgjengelighet. Det kombinert med muligheten for å masseprodusere noen av de ellers unike konfigurasjonene av byggematerialer som trengs, kan gjøre gitterskall til mer gjennomførbare konstruksjoner, også i Norge. Dette undersøkes gjennom utviklingen av et parametrisk arbeidsflytmiljø der gittermønsterdesign og tilbakemeldinger i sanntid er kombineres med egenutviklede komponenter for både global og lokal geometrisk formfinning. Oppgaven ledes frem til et case prosjekt der the Great Court Roof, taket til British Museum, blir lagt som grunnlag for redesign og optimalisering av gitterskall.

Det parametriske arbeidsflytmiljøet viste seg ikke bare å være nyttig, men avgjørende for gjennomføre case prosjektet. For the Great Court Roof ble nodevekten funnet å være ubetydelig sammenlignet med andre laster. Konstruksjonsytelsen avhenger i stor grad av den globale formen, og det ble funnet at the Great Court Roof ikke er optimalisert for konstruksjonseffektivitet. Det blir vist hvordan gitterskalls konstruksjonseffektivitet påvirkes av kurvatur, og at å øke høyden på the Great Court Roof kan gjøre konstruksjonen mer effektiv og gi mindre nedbøyninger. Topologien viste seg også å påvirke konstruksjonsytelsen i stor grad. Det ble funnet at nye gittermønstre enkelt kan gjøres i et parametrisk arbeidsflytmiljø, men de asymmetriske grensebetingelsene som kommer med the Great Court Roof gjør det vanskeligere å finne et design som gir økt repetisjon av nodenettverk. Det ble funnet at tilrettelegging av enten en effektiv konstruksjon eller en konstruksjons som er enklere å produsere, vil til en viss grad gå ut over den andre.

Preface

This master thesis was written on behalf of the Department of Structural Engineering, as the concluding part of our Master of Science Degree at the Norwegian University of Science and Technology (NTNU), in collaboration with the Conceptual Structural Design Group (CSDG). The research and writing of this thesis has been conducted through 20 weeks in the period between January and June 2020.

During our studies at the Civil and Environmental Engineering study program, there has been limited topics related to the field of conceptual structural design and using methods as parametric designing in the work of a structural engineer. The desire to explore the topics of parametric design and conceptual structural design more in detail, made us choose this path for our thesis. The study has been related to the work of PhD candidate Steinar Hillersøy Dyvik at the Department of Architecture and Technology, focusing on global shape of free form timber gridshells using parametric modelling.

We want to thank our supervisors Professor Nils Erik Anders Rønnquist and PhD candidate Steinar Hillersøy Dyvik for guidance and assistance throughout the semester. We are very grateful that you have spent so much time and energy helping us finishing our thesis. We appreciate the fact that we have been able to explore the topic of conceptual structural design after our own premises. We also want to thank Marcin Luczkowski and Bunji Izumi for valuable contributions to the study. Finally, we want to thank our fellow students Ragnhild Myrnes, Kristin Kilvik Skeide, June-Marie Jacobsen Esjehold, Daniel May Instanes and Sverre Magnus Haakonsen for help and sharing of knowledge throughout the semester.

Trondheim, 2020-06-09

Håkon Johan K. Brun	Erlend Hansen	Edvard Hove Zimmer

Contents

List of Figures

List of Tables

1 Introduction

In the planning phase of a building project, architects and structural engineers tend to focus on different areas of design. While architects works with form and aesthetics of a building, the structural engineer is concerned with load bearing capacities, structural systems and project costs. This distinction between contributions from architects and engineers is not necessarily inadequate, but a closer collaboration in the conceptual design phase could benefit many projects. Conceptual structural design is a field exploring the platform in between these two professions. The intention is to develop structures which not only create space and carries loads, but also appear meaningful and aesthetically pleasing. It is about uniting structural functionality and visual form.

Development of new technology has provided opportunities in design of structures with complex geometry at lower costs. Utilizing digital parametric environments provide architects and engineers the opportunity to work more tightly together from the earliest stages of the design process, and all the way to finished drawings. This concept is especially relevant for the design of shell structures, which are recognized for their complex geometrical configurations. Often designed with doubly curvature, these structures can either be continuous or reticulated, where the latter is referred to as a gridshell. The curvature enables a highly efficient transportation of gravity loads, which allow them to span large areas unsupported. However, this characteristic means that the shape of a shell is paramount for its structural efficiency. This thesis will mainly focus on a specific type of shell, namely timber gridshells with discrete segmentation.

In this thesis, tools for design, optimization and evaluation of discrete timber gridshells are investigated and developed for a parametric environment. Starting with a background chapter, the expressions parametric design and conceptual design are established. Moreover, some inspiring gridshells are investigated and discussed. The next chapter includes relevant theory about gridshells, node connections, geometric optimization, and software tools utilized for this thesis. There will also be a chapter involving design according to the Eurocode for the norwegian climate, where both snow loads and timber is discussed. There will be a chapter revolving around the development of custom design and evaluation components, and how they are implemented in the parametric environment. Proceeding, a parametric workflow is established to showcase the process of establishing and evaluating a gridshell model using form finding tools and structural analysis. Furthermore, the parametric workflow is used to implement a study of the Great Court Roof of the British Museum. In the case project, the Great Court Roof will be transformed from the steel gridshell of London, to one of timber set in Norway. Different optimization criteria will be investigated based on structural performance and repetitive building parts, which can contribute to make manufacturing both cheaper and less time consuming. Finally, some conclusive thoughts on the methods and results are presented, in addition to suggestions

for further work.

This thesis, along with two others, are a part of the PhD project of Steinar Hillersøy Dyvik. The others are; Ragnhild Myrnes and Kristin Kilvik Skeide, who did a parametric structural analysis of two aluminium node designs, and June-Marie Jacobsen Esjeholm, Daniel May Instanes and Sverre Magnus Haakonsen, who has implemented trust network analysis (TNA) in Grasshopper, and tested the method's performance on discrete gridshells.

2 Background

Shell structures are characterized by their slender, curved geometry and light weight. Shells refer to both continuous shells, where the surface is unbroken, and reticulated shells, so-called gridshells. The curvature makes them very efficient at transferring gravity loads, and allows for a span-thickness ratio not seen with any other structure. Due to this ability to span long distances and at the same time stand out aesthetically from other types of buildings, make them interesting for both architects and engineers alike. Even though shells have been built for their aesthetic and structural properties since ancient times, the complexity they present in design and construction make them challenging to engineer and construct cost-effectively, even today.

One of the earliest constructed shells is the roof of the former temple *Pantheon* in Rome, which is displayed in figure 2.1. Completed around 126 A.D, the structure consist of a portico, which is a porch entrance, with large granite columns in front of a cylindrical building with a concrete dome roof with a top opening to the sky. The height and diameter of the roof is the same length of 43 meters, and is still the world's largest unreinforced concrete dome. Nearly 2000 years after its completion, the Pantheon is still an impressive work of architecture and engineering.

Shell structures as a doubly curved roof with arbitrary geometry can be masterly pieces of architecture. However, they are difficult to design and construct for a reasonable price. Historically, designers had to rely on physical models for structural verification, as hand calculations were either extremely difficult or downright impossible to implement. This made the design of these structures both expensive and difficult. Today, the use of computers and parametric design environments have provided new opportunities for the viability of the shell structures.

(a) Pantheon, Rome   (b) Pantheon, inside the dome

Figure 2.1: The Pantheon in Rome[1].

2.1 Parametric and conceptual design

Figure 2.2: The Trondheim HolzBau Pier (2014). Architects: John Haddal Mork and Anders Gunleiksrud. Photo: Sophie Labonnote-Weber [2]

Conceptual structural design is a platform in between the fields of structural engineers and architects [7]. The aim for the designing is to create structures which is both aesthetically pleasant and carry loads in a efficient or interesting way. The Holzbau Pier (figure 2.2), located in Trondheim, is an example of conceptual structural design. The architectural intention with the timber pier was to visualize forces within the structure and minimize the expression of the object in its landscape by optimizing the structural pattern.

The topic of conceptual structural design includes the use of software tools and parametric design is highly related. Parametric design is a design process in the planning phase of a building project. It uses algorithms to model a structural geometry based on specified parameters, which can be altered anytime in the designing process. This design approach is different from the more conventional design process by building a model step by step. Parametric design is a method to develop several design options for a given form, boundary conditions and parameters. Several techniques has been developed over the past 50 years, whereas before the software tools provided from computers, pioneers as Antoni Gaudi developed analoge physical models as the hanging-chain model [14].

Parametric design fits well in between the professions of architects and structural engineers,

where both form and structural integrity is evaluated simultaneously. Antoni Gaudi's work with designing the church of Colònia Güell in 1898, which was never completed, is one of the first structures to use what is defined a parametric design [14]. The uniqueness of his work was the physical upside-down model he made of the church, shown in figure 2.3. Using cables only supported at the ends, he attached weights to make arches and vaults. The principal was that the upside-down model with tension cables would become compression forces for a mirrored structure. This design method was first developed by Robert Hooke in 1676, which described it as; *"As hangs the flexible line, so but inverted will stand the rigid arch"* [15]. This was a new approach to design, where the designer could visualize the construction as a whole and how changing of parameters as length of the cables and weights could influence the rest of the structure.

Figure 2.3: Hanging chain model of Colònia Güell [3].

Since the invention of the computer, digital modelling tools and analysis software has changed the way of designing radically, and today computer programming tools are exclusively used. Architecture has moved from Computer Aided Design (CAD) to a more complex environment as Building Information Modeling (BIM), where various consultants works with design and optimizations in the same digital environment. Over the last years, parametric design has become more popular among consultant engineers and architects as development of visual programming tools has accelerated. It is advantageous during the early stages of the design process to use parametric software tools to explore innovative and irregular forms. Using these software tools, the geometry can be optimized based on

parameters of the designers choosing. The traditional way of project planning, with the architects carrying out the building design and the engineers analysing the structure, is more joined in a parametric environment. The software tools used in this thesis will be described more in detail in chapter 3.5.

Digital parametric design as known today, was first introduced in the book *The fold* from Gilles Deluze in 1988 [16]. In mathematics, (x, y) represent variables and (a, b, c) represent parameters. Use of parameters instead of fixed numbers, will describe a generic family of curves from the use of a script with specific functions. For example, the function $y = ax^2 + bx + c$ would describe all parabolas, while the function $y = 4x^2 + 2x + 4$ would describe one specific parabola. Deluze was fascinated by the parametric notation and all the possibilities for a geometry to be described by the use of parameters. He found that in order to utilize this, it was necessary to combine the generic way of describing forms with the use of digital programs. Patrik Schumacher introduced the term *parameterism* through his texts, and since the early 1990s, digital parameterism has changed both engineering and architecture: *"... Parametricism is the most potent movement and avant-garde style in architecture today."* [17].

The use of parametric design in software tools allows the designer to create various geometries and evaluate them rapidly. Therefore, it is crucial that both architects and engineers knows how to use the software tools, and knows their possibilities and limitations. The application of these software tools has enabled complex and expensive structures, such as shell structures, to be built in a much greater extent.

2.2 Reference buildings

In the following subsections, three gridshell structures, Mannheim Multihalle, the Great Court Roof of the British Museum and the Pods Sport Academy, is presented. These gridshell structures presented are both beautiful and complex structures, and they have been inspirational and helpful when learning about different gridshell structures. Moreover, the geometry of the Great Court Roof of the British Museum is used in the case project in chapter 7.

2.2.1 Mannheim Multihalle

When Mannheim was going to host the horticultural exhibition *Bundesgartenschau*, which is held every other year in Germany, the architects Carlfried Mutschler and Joachim Langner won the compitetition for the design of a temporary structure to accommodate the exhibition. They received help from the well known architect Frei Otto to create the structure where he introduced the timber gridshell design which he had worked with for some years [4]. Frei Otto (1925-2015) was a German architect and is seen among many as one of the pioneers in the use of parametric design. Patrick Schumacher mentioned him as the most original, profound and brilliant architectural innovator ever, and said Otto was the ”*...only true precursor of parametricism*” [18]. He explored geometry using physical models, inspired by shapes in the nature.
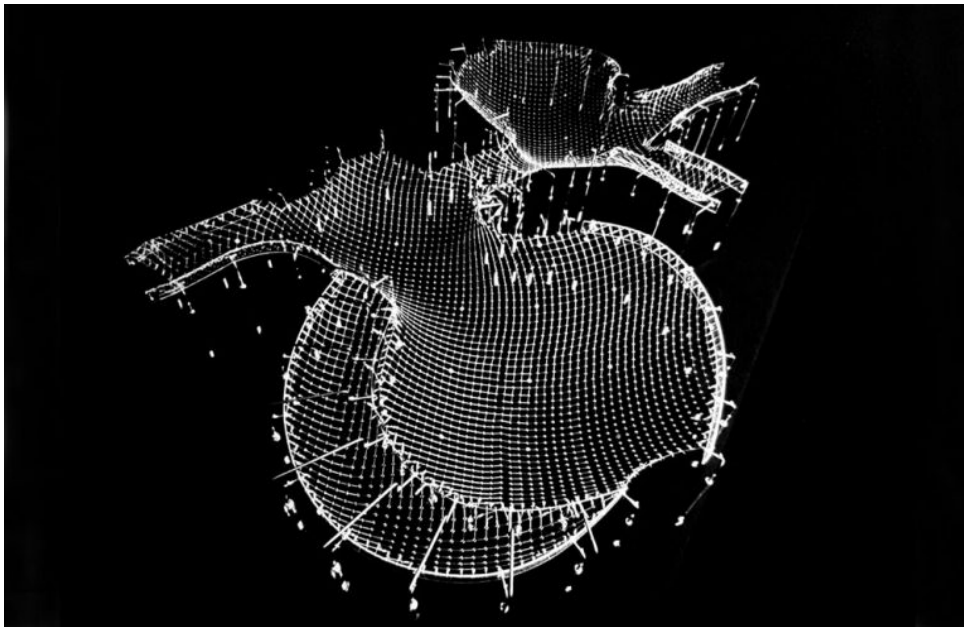
Figure 2.4: Model of Mannheim Mulithalle. Photo: Daniel Lukac [4]

Frei Otto was the main architect behind the gridshell structure Mannheim Multihalle, and collaborated with Ove Arup & Partners as the structural engineers. It was built in 1975 and was ment as a temporary structure but it is still the largest timber gridshell roof per 2020. This unique state-of-the-art structure is often referred to when talking about

gridshells. In the design process, Otto made an up-side-down model of the structure using finely woven fly screen and multi-coloured pins to fix it flexibly to a wood plate, as shown in figure 2.4. Frei Otto used a lot of physical models in his design work of structures and especially the hanging-chain method as Antoni Gaudí did.

(a) Mannheim Multihalle from above.   (b) Inside Mannheim Multihalle.

Figure 2.5: The Multihalle in Mannheim. Photos: Daniel Lukac
[4]

The structure was built as a kinematic gridshell, and can be seen in figure 2.5. The grid was assembled flat on the ground with straight timber laths and pinned connections in a square grid pattern. Then it was erected using multiple scaffolding as supports before tightening the connections when the final shape is secured. Tightening of the connections gave fixed actions in the joints to secure a rigid quadrilateral diagrid network, along with bracing from diagonal steel cables to increase the in-plane stiffness [19]. The timber laths needed to be slender to make them flexible enough during the erection process but at the same time stiff enough to avoid buckling and deflections when constructed. The laths have a cross-section of 50x50 mm, laid in a double layer with pieces of shear blocks between. The grid could have been built as a single-layer shell with bigger cross-sections but this would have lead to increased bending stresses and different architectural expression.

2.2.2 British Museum and the Great Court Roof

The British Museum building was designed by Sir Robert Smirke and built in the 19th century [20]. The building consist of four wings of galleries arranged around a central quadrangle, measuring the courtyard as 96 x 72m. Later on, the Reading Room was constructed which is a circular building in the middle of the courtyard. The popularity of the museum and the need for more space, resulted in the project of creating the roof over the Great Court. The roof is designed by Foster and Partners with Buro Happold as the structural engineer [21]. The lightweight roof is design to let in light and give cover for rain, which creates a indoor plaza for the public to move freely. The geometry of the Great Court Roof is used as a part of the case project in chapter 7.

Figure 2.6: Great Court at the British Museum [5].

The doubly curved shape of the roof is defined by a surface where the steel grid nodes lie. The height of the surface is obtained by analytical and numerical expressions presented in a paper by Chris J.K. Williams [22], which defined the geometry of the roof. The roof itself is a steel triangular lattice construction with glass panels, which can be seen in figure 2.6 and in figure 2.7. The geometry of the doubly curved roof is chosen to give the museum a significantly architectural characteristic, and to transfer loads more efficient than a flat roof would have achieved. The final geometry was a result of several constraints regarding roof height, boundary conditions, minimization of loads on to existing buildings and manufacturing [23]. The size of all triangles in the steel mesh is determined by maximum glass size available. In the grid, all nodes intersect six members each. The connections are welded to achieve fixed nodes, in order to transfer forces and bending moments. In total, the grid structure consists of 5178 steel members, 1806 nodes and 3312 glass panes. Since the Reading Room is slightly off centered, it spans about 5 m longer towards north than south [21]. Thus, the mesh facade has only one line of symmetry. The span in the northern direction is 28.8 m, with an arch height of 5.48 m. The span in the eastern and western direction is 14.4 m, with arch height of 5.1 m. And the span in the southern direction is of 23.8 m, with arch height of 6.4 m. By not having two lines of symmetry makes the geometry more complicated and cause all of the node connections unique.
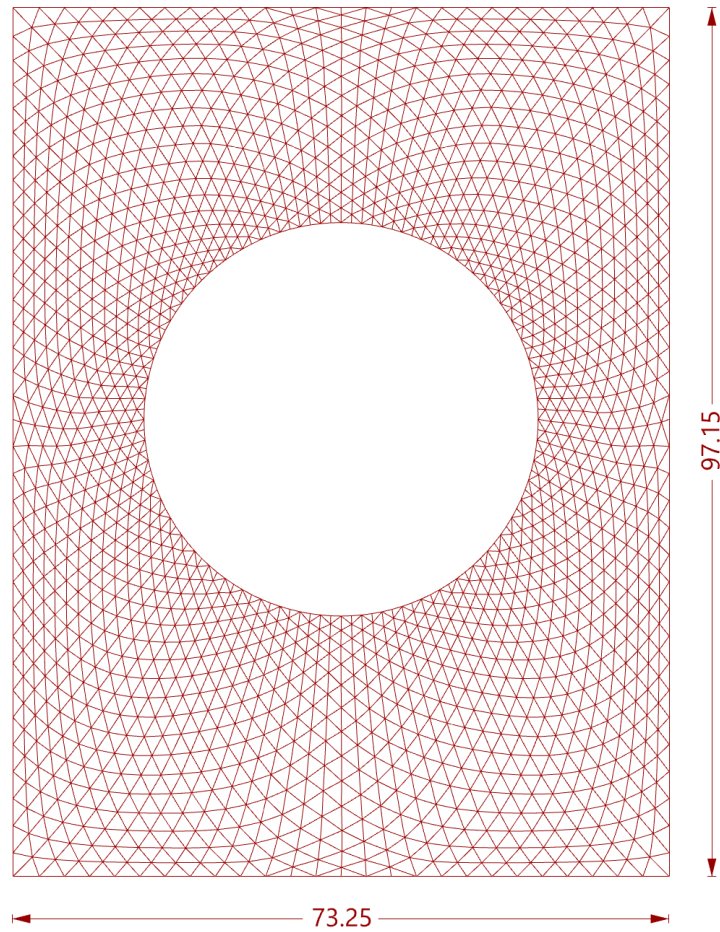
Figure 2.7: Overview mesh of the Great Court Roof. Mesh obtained by model in Rhino.

The roof spans from supports around the quadrangle on to the inner circle, as displayed in figure 2.7. The boundary conditions for the roof is described in details in an article by Johan Sisckha [23]. The existing buildings of British Museum cannot carry additional loads and extra supports was needed to carry the loads from the Great Court roof. To carry the roof, additional columns around the circular Reading Room and the outer perimeter was constructed to transfer vertical loads down to the foundations. As no horizontal forces could be transferred to the existing buildings, a continuous horizontal steel beam with vertical posts provided stiffness to the roof. Slightly below this steel beam, a big new horizontal concrete ring is positioned which is rigidly fixed horizontally to the columns. All posts sit on sliding bearings to avoid horizontal loads.

The roof members at the perimeter and inner circle is connected to a horizontal steel beam which is supported by gliding bearings. The supports do not transfer loads horizontally normal to the perimeter. They only provide vertical support and horizontal support longitudinal to the perimeter beam. The support conditions have a major influence on the structural behaviour of the roof. The usual arch effect of the double curved roof could not be achieved due to sliding bearings at the outer perimeter, allowing the roof to

deflect outwards. This induces bending moments and shear forces in addition to normal forces. The stresses are transferred trough the members which requires stiff elements and sufficiently fixed connections. As the forces increases towards the outer rectangular boundary, the cross-sectional properties is optimized with varying size. The height of the members varies from 80 mm to 200 mm, with the same width of 80 mm [21], based on the moment working in the beams. The steel beams are hollow to obtain a light weight structure. An alternative solution was to use solid sections to achieve a slender structure, but it did not fulfill the structural requirements.

The Great Court Roof is a structure of interest in this thesis. In chapter 7, the steel gridshell is transformed to a timber gridshell and used in an analysis of timber gridshells in Norwegian conditions.

2.2.3 The Pods Sport Academy

The Pods Sport Academy is a timber gridshell structure located in Scunthorpe, England, and was opened in 2011. The design were developed in interactive collaboration between the architects of Andrew Wright Associates and engineers from Buro Happold, which resulted in a structure comprised of five interconnected domes [6], with a maximum span of 65 metres. In contrast to the Mannheim Multihalle, The Pods' domes were designed and constructed as *discrete segmeneted* gridshells, where every individual building part is straight and the curved shape is instead a result of the connections between them.

(a) Global overview   (b) Gridshell detail

Figure 2.8: The Pods from both outside and inside the building [6].

As for any timber gridshell, the outstanding strength to weight ratio means that snow and wind loads can be significant [6]. As shown in figure 2.8b the structural system is comprised of a triangulated timber beam grid connected at steel nodes, with additional stiffeners in between in a perpendicular pattern. At the interfaces steel beams were used

to give the structure additional strength, as the structure has to carry the external loads from panel installations and especially greenery.

The optimizations in the design phase was based on minimizing the angle variations between the beams at each node, which was done by equalizing each beam length as much as possible. The structure is highly asymmetric, however, and therefore building elements are not repetitive. To make the construction cost-effective, it relied on state-of-the-art fabrication methods as well as partial construction of the connections with bolts on site. This assembly method also enabled small tolerances to be incorporated due to the rearrangement effect from the nodes, but the larger tolerances had to be accounted for by filling in any gaps [6]. In addition to this, the design also emphasized the use of a minimal number of nodes in the finished structure, which lead to the faceted finish seen in figure 2.8a.

3 Theory

3.1 Shell and gridshell structures

Shell structures has fascinated the human eye since the rise of Pantheon in ancient Rome. They create both spatial housing and transfer loads efficiently, while being aesthetically appealing. Some may define shell structures as simply a curved surface. In this section both shell structures and gridshells will be described in more detail.

Shell structures in building design is a system of three-dimensional curved surfaces where the thickness of the shell is relatively small compared to the other dimensions [24]. Hence, shells resist external loads as dead weight and pressure loads predominantly through in-plane membrane stresses, which will be explained in chapter 3.2.1, and should mainly be subjected to compression forces. They are form-passive, meaning they do not significantly change shape due to varying loads unlike form-active systems as cables or membrane structures. Shells can be constructed with a continuous surface, such as the Pantheon, described in chapter 2, or with a non-continuous mesh surface, as the gridshells Mannheim Multihalle, the Great Court Roof and the Pods Sport Academy, described in chapter 2.2.

According to *Shell structures for architecture* [24], geometry of a shell can be described in three different ways:

- Analytical functions. Mathematical expressions can describe the curvature of a shell perfectly with polynomials, such as elipsoids, hyperboloids and hyperbolic or elleptical paraboloids, trigonometric or hyperbolic functions.

- Freeform shells. Generated by drawing on *free hand* without taking structural performance into consideration.

- Form found shells. Shell geometry found form physical models or from digital software using form-finding-methods to find an optimal shape based on structural performance.

Designing shell geometry based on form finding methods is a sophisticated but effective way of finding an optimal shape. There are several form finding methods with different approaches. In this thesis, the method *dynamic relaxation* (DR), which is described in chapter 3.4.1, is described further in chapter 3.4.1.

3.1.1 Gridshells

A subcategory of shell structures are as mentioned the non-continuous *gridshells*. While continuous shells typically are made of concrete, gridshells is typically built of members of steel or timber. This allows for an even lighter structure compared to continuous shells, and opens up the surface. The pattern can be everything from quadratic, triangular or

hexangular, depending on aesthetics, structural needs and manufacturing constraints. The members can be curved or straight in the surface plane, depending on construction method and constraints in the cladding material. Curved members are usually implemented as a *kinematic gridshell*. Kinematic gridshells are built flat on the ground with loose-fitting connections, and then lifted up to its predefined shape before the connections are tightened [24]. The members are then strained, utilizing the elastic deformation to the members to give it curvature. Figure 3.1 displays a kinematic gridshell, erected in 2015 as part of the master thesis of Steinar Hillersøy Dyvik and John Haddal Mork. The members in the grid are continuous through the nodes. The timber members are spliced together instead of connected only in the nodes, which are typical for a kinematic gridshell. The stiffness of a gridshell is largely determined by the rigidity of the connections, grid pattern and material choice. Mannheim Multihalle, which was described in chapter 2.2.1, is another example of a kinematic gridshell construction.

Figure 3.1: Trondheim Gridshell (2015). Architects: John Haddal Mork and Steinar Hillersøy Dyvik. Photo: Sophie Labonnote-Weber [7]

This thesis will be focusing on *discrete gridshells*, rather than kinematic gridshells. In discrete gridshells, the members are not strained into a curvature but instead straight between each joint, allowing for planar cladding materials as glass panes [24]. This means that the shells curvature is obtained only through the geometry of the connections. With steel members these connections can be welded together, but timber members demand more complex connection designs. Both the Pods Sport Academy and the Great Court Roof of the British Museum, which are described in respectively chapter 2.2.3 and chapter 2.2.2, is examples of discrete gridshells. The Pods Sport Academy is a timber gridshell with steel nodes [6], while the Great Court Roof is a steel structure with the beam elements welded together [21].

3.2 Structural behaviour

The curvature is what makes the shell structures so efficient, and enables their uniquely long-spanned and slender geometry. This is due to the fact that the shape allows structural action from transverse loading to be directed as in-plane *membrane stresses* to its supports.

3.2.1 Membrane action

Membrane action refers to a type of structural action that only allows for uniform in-plane stress-fields, in the shape of normal and in-plane shear forces. The curved shell will primarily transfer loads through these actions, whereas a flat plate will have to rely on out-of-plane bending and shear to transfer loads to supports. This is displayed in figure 3.2. Most materials are naturally resilient to these forces compared to out-of-plane bending or shear. It is for example much easier to deform a plate by bending it, than to deform a plate by stretching or compressing it [25, p. 499].

(a) Straight beam.   **(b)** Arched beam.
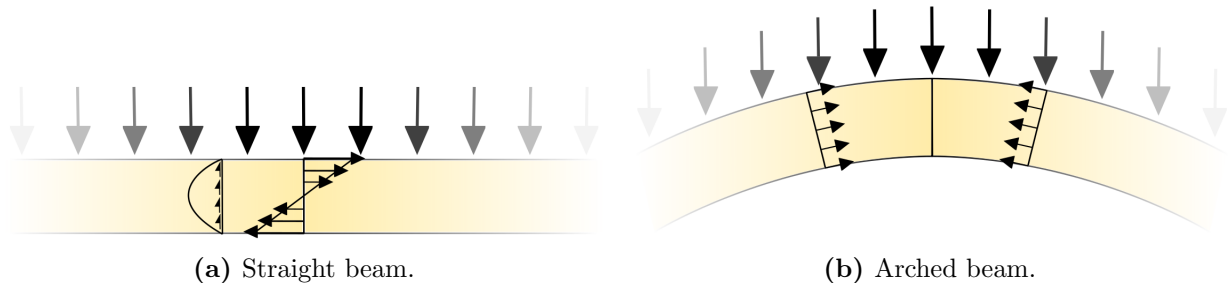
Figure 3.2: Comparison of stress distribution for curved and straight beam.

This concept relates to the membrane theory of shells, which will not be explored in depth in this thesis, as it involves complex mathematics with limited practical use. For this reason *true* membrane behaviour is rare in architecture, and experimental physical modelling has traditionally been needed to analyse shells before the introduction of the finite element method (FEM) and computers. The theory has in some cases, however, been implemented as a solution to design problems where out-of-plane bending and shear forces have been small enough to be considered negligible and the solutions obtainable [26]. Figure 3.3 displays how for example the supports must be designed for the membrane theory to be applicable.
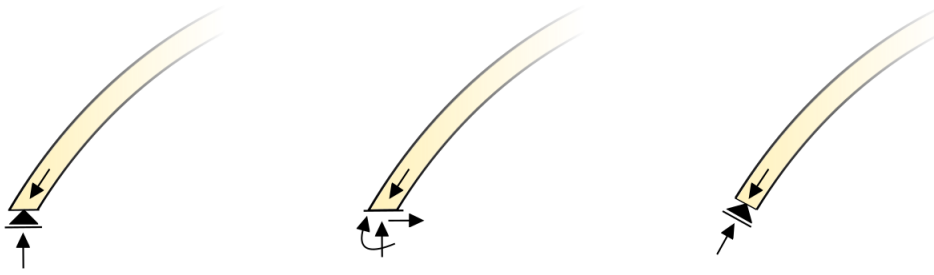
Figure 3.3: Different support conditions. Only the rightmost is compatible with membrane theory.

Shells are considered optimized for efficiency when the shape, boundary and thickness is so that it produces the smallest possible out-of-plane bending and shear. This shape can be determined via form finding and numerical analysis, which will be explained further in chapter 3.4.1. Numerical analysis is usually done using FEM with shell elements for continuous shells and beam elements for gridshells, however, structural behaviour can still be complicated enough to warrant physical testing even today [24, p.26].

3.2.2 Buckling

If a gridshell can endure inextensional derformation, bending stiffness and strength will probably be dimensional when designing the structure. Gridshells are slender structures, and when they deflect, they become less resistant to compression forces. This may lead to collapse by buckling, without the material yielding. Gridshells that cannot endure inextensional deformation, however, are efficient and stiff, but also very sensitive to imperfections, and small deformations can lead to sudden collapse. Structures which can endure inextensional deformations are less efficient, but also less sensitive to imperfections [24, p. 242-243].

For gridshells, buckling can occur in one or more individual beam element, and it can occur globally. Being slender structures makes them prone to the latter. It is therefore important to include global buckling in the structural analysis, and the buckling load factor needs to be taken into consideration. The buckling load factor is used to determine the loads required for the structure to buckle. It could be useful to visualize buckling modes and the modal shapes to understand which part of the structure is collapsing due to buckling. In this thesis, global buckling will be included in the analysis in the case project in chapter 7, which is done with the software tools described in chapter 3.5.

In summary, the structural behaviour of shells and gridshells can be described with both membrane and bending action. Membrane action characterize an efficient structure, but bending action must be relied upon to tackle buckling and inextensional deformations. The complexity of the structures makes it practical, and often a necessity, to carry out structural analysis with FEM and computer models.

3.3 Node structure

Discrete timber gridshells, described in chapter 3.1, are constructed with each member being connected in nodes. These node connections are extremely important for the structural integrity of gridshells, and parameters that need to be considered include material, capacity and stiffness. As is explained in chapter 3.4.2, fabrication of, and construction with these nodes are also economically costly. Complete node design is a complicated issue, and in this thesis they will not be evaluated or calculated in detail. However, the effect of the node weight on gridshells will be investigated in later chapters.

There are many different ways for nodes to be designed in discrete timber gridshells. A specific design will present their own benefits, drawbacks and aesthetic for both construction and realized structure. In this thesis the node design will be integrated as two plates, as the one displayed in figure 3.4. The figure shows how the two plates is structured. The two plates consists of one hexagonal plate in the middle, connecting the six plates protruding on each side.
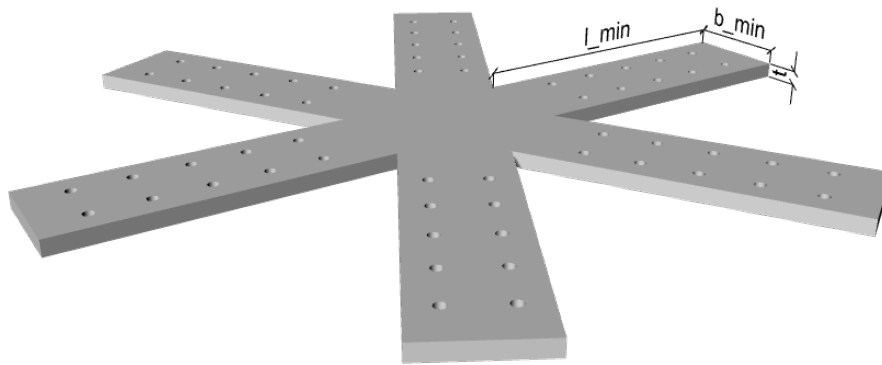
Figure 3.4: Node design used in this thesis. The measurements in (b) is used to calculate the weight for the nodes in chapter 7. The calculations can be found in appendix D.

The most common material used for nodes in discrete timber gridshells, is steel. Comparing aluminium to steel, aluminium has better corrosion resistance, is lighter and has the possibility for manufacturing by for example extrusion [27]. However, aluminium is a more expensive material than steel. Aluminium is used extensively for projects that need to retain light weight, for instance in ships and the car industry. In structural elements, however, aluminium is rarely used. When aluminium is recycled, it usually is reused as cast aluminium, for example as car engine parts. Because of the need for new applications of cast aluminium, aluminium will be investigated as a material for nodes. Specifically, how the global structural performance of timber gridshells are affected by the weight difference of aluminium and steel nodes.

The joint stiffness of the node is also dependent on the material used. In this thesis, the nodes are assumed to be fixed and completely rigid. In reality, nodes in a gridshell will

be semi-rigid, which is somewhere in between fixed and pinned. With the right design, however, they can be expected to behave close to rigid. This topic will be investigated further in the master thesis written by Myrnes and Skeide, which is a part of the same PhD project as this thesis. They provided the node data used in this thesis, which can be found in appendix D.

3.4 Geometric optimization

Geometric optimization is generally segmented into two categories for gridshell structures: *structural geometry* and *panel geometry* [28]. Structural geometry refers to the global shape of a shell, which can be determined by some kind of form finding method, as mentioned in chapter 2.1. Panel optimization refers to the local geometry of nodes, and is linked to both the economic cost of fabrication and complexity of construction for gridshells. The latter is more open-ended in terms of approach, which is elaborated on in chapter 3.4.2. In this project, *dynamic relaxation* is used to optimize the structural geometry of gridshells. This is incorporated in the parametric framework described in chapter 6, as a Grasshopper component developed in C#.

3.4.1 Dynamic Relaxation

Dynamic relaxation is a popular numerical form finding method, developed in the sixties by Alistair Day [24]. The method can be implemented for solving various non-linear physical systems, and is essentially the computational equivalent of the physical *hanging-chain* method used by Gaudí, as seen in figure 2.3. As software applicable to all kinds of different geometries and boundary conditions, means that dynamic relaxation is much less time consuming than any physical model could ever be.

The summary of the dynamic relaxation in this section is based on the explanation given in the book *Shell structures for architecture - Form finding and optimization* [24, p.93-95]. The essence of the method is to use a numerical integration scheme for Newton's second law of motion on lumped masses or point loads, acting on nodes. These nodes are interconnected by discrete finite elements, representing lines in a mesh or grid. To find the form of a shell, these forces should be applied 'upwards'. Nodes that represents supports must be left out of the computation, so that they remain fixed in space during the process. By 'following' the position of the nodes as the geometry is deformed, and updating the velocity based on the residual forces in the system, a step-by-step movement towards a state of equilibrium can be achieved for each iteration of the algorithm. As the residual forces weaken, the motion of the structure will start to oscillate around a static solution, moving back and forth over the equilibrium position defined by the initial and boundary conditions.

This method will not converge, however, as the residual forces will only get smaller and smaller, but never actually zero. Therefore, a form of velocity damping must be introduced to speed up the calculation and avoid the movement of the structure becoming unstable. There are two types of velocity damping commonly implemented for the dynamic relaxation method, viscous and kinetic damping [24, p.95]. Viscous damping is applied as a nodal velocity factor acting opposite to the direction of the system, decelerating the motion. Kinetic damping utilizes the fact that the kinetic energy peaks at the equilibrium position

as the system oscillates. When a peak has occurred, the nodal velocities are set to zero and the method restarts with the position updated. This will lead to increasingly smaller energy peaks. These methods are often implemented together with a threshold on acceptable kinetic energy in the system, since at some point it will be small enough to be negligible for any practical purpose.

Approach

Because the method updates each individual element in turn for each iteration, it can be implemented without the need for calculating stiffness- or branch-node matrices. Only the internal forces and position of the elements need to be stored and updated [29]. The lumped masses do not need to be related to the actual mass of the structure either, as it is only the ratio between stiffness and loads that affect the final shape. Using fictitious mass values can help accelerate the speed of which the process converges.

The framework that will be used for the component developed, and described in chapter 5.2, is to simplify the geometry in to a particle-spring-system. This method represent the geometry of the grid as a discrete collection of lumped masses in the nodes (referred to as 'particles'), connected by linear elastic springs [30]. As springs are stretched or compressed from the initial length, they generate a force that act opposite the direction of the displacement caused by the fictitious load-case. This force can be defined by Hooke's law:

$$F = K * \delta \tag{3.1}$$

Where K is the stiffness, and δ is the strain in the disturbed spring. The dynamic relaxation method then acts as the numerical *solver* for this discretized system. Viscous damping will be used in this thesis, as it is easier to implement in the code. The process is visualised in figure 3.5.

Figure 3.5: A hanging chain modelled with Dynamic Relaxation.

Numerical integration scheme

The equations needed for the numerical integration of the dynamic relaxation method was obtained from the journal *Finding the form of an irregular meshed steel and glass shell based on construction constraints* [31]. Starting from Newton's 2nd and Hooke's law, the equation of motion for discrete systems can be written as:

$$m_i a_{ij}(t) + C v_{ij}(t) + K_{ij}\delta_{ij}(t) = P_{ij} \tag{3.2}$$

Where

m: mass

a: acceleration in direction j at time t

C: damping factor (constant)

v: velocity in direction j at time t

K: spring stiffness

δ: displacement in direction j at time t

P: external applied force

i refers to the ith node and j the specified direction (x,y,z), respectively.

Defining the residual forces, F, as the difference between the internal and external force, equation 3.2 can be rewritten as:

$$F_{ij} = m_i a_{ij}(t) + C v_{ij}(t) \tag{3.3}$$

To calculate the velocities and positions of the nodes, a numerical integration scheme of the motion equation must be implemented. By double numerical integration of the acceleration in equation 3.3, and expressing the terms in central difference form, the equation becomes:

$$F_{ij}(t) = m_i \left(\frac{v_{ij}(t + \Delta t/2) - v_{ij}(t - \Delta t/2)}{\Delta t}\right) + C\left(\frac{v_{ij}(t + \Delta t/2) - v_{ij}(t - \Delta t/2)}{2}\right) \tag{3.4}$$

Introducing viscous damping in the form $A = \frac{1 - C/2}{1 + C/2}$ and $B = \frac{1+A}{2}$ the recurrence equation for the velocities can be obtained from equation 3.4 as:

$$v_{ij}(t + \Delta t/2) = A v_{ij}(t - \Delta t/2) + B\frac{\Delta t}{m_i} F_{ij}(t) \tag{3.5}$$

The geometry can thus be updated to time $t + \Delta t/2$:

$$j_i(t + \Delta t/2) = j_i(t) + \Delta t v_{ij}(t + \Delta t/2) \tag{3.6}$$

Once the positions are updated, the residual force for each node can be calculated by:

$$F_{ij}(t + \Delta t) = P_{ij} - \sum_n K_{ijk}\delta_{ijk}(t + \Delta t) \tag{3.7}$$

Where k is the number of elements connected to node i. The implementation of the computational algorithm is elaborated upon further in chapter 5, and the complete code can be found in the attachments, see appendix A.

3.4.2 Local geometric optimization

The efficient load bearing capacity of the doubly curvature obtained through form finding methods, also greatly increase the complexity in fabrication and construction processes of the structure. Nodes have been identified as a large contribution to costs in discrete segmented gridshells in particular. Ways to increase the number of identical node configurations, generate support for planar panels, and minimizing node torsion are all important both from a structural, constructional and aesthetic point of view [32]. A torsion-free node means that the elements axis of symmetry intersects along a shared axis at that particular node. Identical node configurations in this case is connected to the concept of repetitive structure elements and is always a factor of consideration in complex free-form construction projects. The ultimate economic cost is often the deciding factor in whether a project is feasible or not. Coupled with the fact that the basic cost of labor in Norway is high, makes this issue highly relevant to address in a parametric workflow framework for gridshells.

Repetitive building parts

Applying the concept of repetitive building parts in the case of gridshells, repetitive node networks is desirable to make real world construction both simpler and cheaper. The concept of using identical parts in construction have been implemented in engineering for as long as there have been buildings to engineer [19]. Moreover, this can also provide more options for architects, who can stand to gain more control in a design process, instead of solely relying on the most advanced production and fabrication tools available for complex designs. In the worst case, the design could be altered due to engineering or economic limitations in production, which neither the architects or the contractors wants, but nonetheless happens. To control shape, segmentation and structural elements in a non-problematic way, makes it easier to find the best rationalizations, topology options and fabrication methods, and streamlines the process all the way from conceptual design through a finished structure.

The focus of this thesis is on gridshells with discrete segmentation, meaning each member in itself has zero curvature. If one were to generate a discrete grid mesh from a free form doubly curved surface, the grid would only intersect the surface at the nodes. This characteristic simplifies the geometry of panels and members in gridshells, but at the same time concentrates the geometric complexity in the nodes [19]. This complexity is further affected by boundary conditions and type of topology chosen. A triangular mesh, which is displayed in figure 3.6a, is often used as it provides stiffness to the structure, but a drawback is that it requires six elements to meet at the connections of each node. A quadrilateral mesh, as displayed in figure 3.6b, is also a popular alternative. This configuration has a smaller topological edge/area-ratio which means less material is needed. In addition each node becomes less complex with fewer elements attached. If planar panels

can be achieved, it also supports more efficient fabrication for panels compared to the triangular alternative. The drawback is that a quadrilateral topology will not have as stiff connections, and will often require additional stiffeners to the mesh configuration. Obtaining planar panels can also be challenging for complex forms, compared to the triangulated mesh where panels are automatically planar by default.
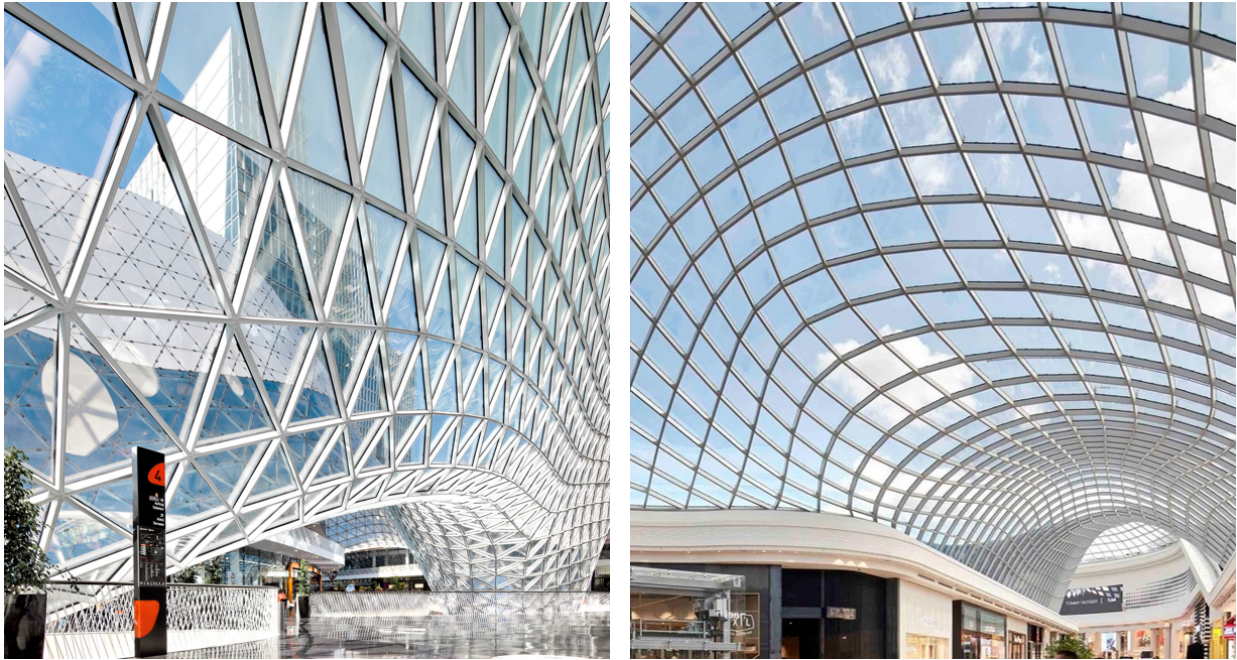
(a) MyZeil Shopping Mall, Frankfurt [33]. **(b)** Chadstone Shopping Centre, Melbourne [34].

Figure 3.6: Different grid patterns utilized for similarly implemented steel gridshells.

As mentioned in the start of this chapter, there are different aspects that should be considered when approaching the local geometry of nodes in discrete gridshell design. The concept of *repetitive building parts* is the aspect focused most upon in further chapters.

Generalized approach

From an optimization point of view, the aim should be to include repetitive node networks in a bottom-up design strategy, which means it is facilitated for from the very start of the design process. This was strategy implemented for The Pods Sport Academy, as described in chapter 2.2.3. On the other hand, construction restraints, asymmetrical boundaries or general irregularity can make this difficult to implement. As seen with the British Museum in chapter 2.2.2, the issue of repetitive building parts were not prioritized in the design phase partly due to this. Since both the design and optimization for shell structures are so closely intertwined, some facilitating of construction and fabrication should not be neglected in a parametric workflow framework, either.

The orientation and amount of members joined at a node, in combination with a normal axis, make up the local geometry of a specific node. This normal axis can be defined in

various ways, as it only reflects the orientation of the connection that will be used in the node. This means that in principal, all node normal axis could be uniquely defined to achieve certain properties. The standard ways however, include summation of the unit vectors defined by the elements at a node, or by drawing lines from some reference surface or point in the interior of the gridshell to each node [35]. The angles needed to define the unique geometry of a node in relation to the normal axis are based on [19], and displayed in figure 3.7. These are;

- The geodesic angle (U) that measures to mesh angle projected on to the tangent plane of the normal axis, and relates to the geodesic curvature of the structure.

- The normal angle (V) is the angle between the mesh edges and the the normal vector, and relates to the normal curvature.

- The torsion angle (W) is the twisting of the normal axis from one node to another.

Alternatively, the U angle can be substituted by the mesh angle of the gridshell. All U, V, W angles for one node need to be identical to the equivalent angles of another node for them to be geometrically identical. Without relying on a specific connection design, all three angles are necessary for general fabrication of a connection.
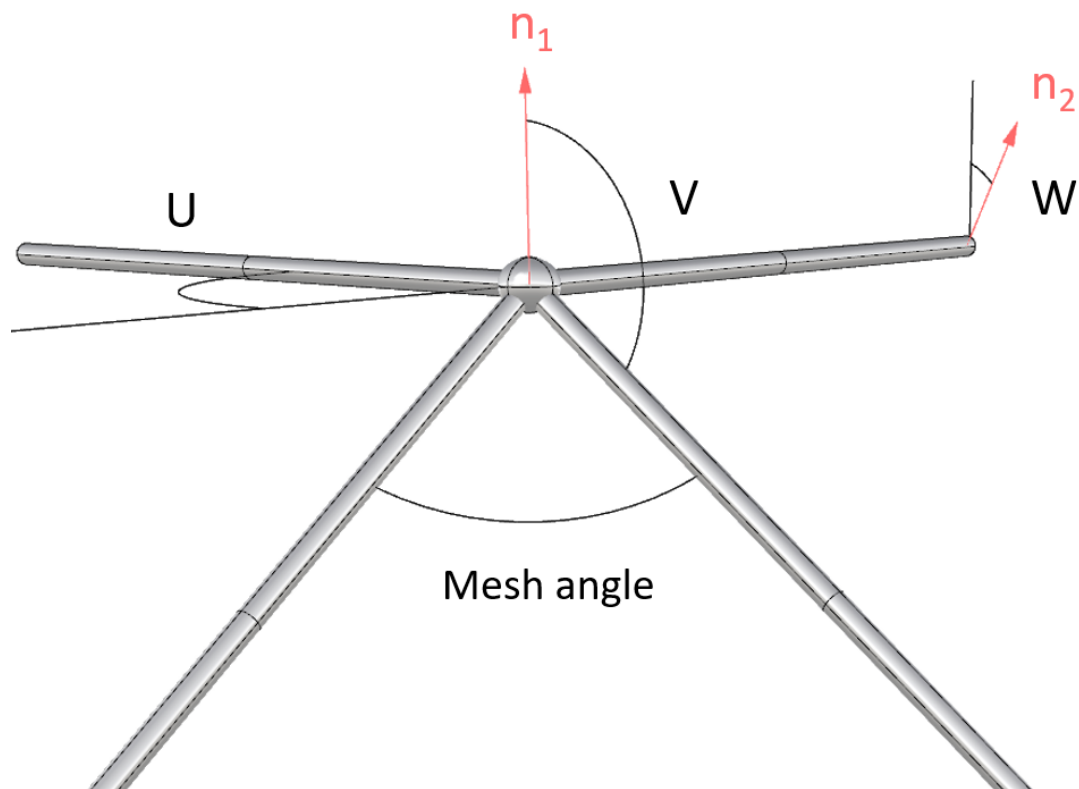
Figure 3.7: How the angles U, V and W are defined both by geometry and normal vector orientation.

Some tolerance should also be allowed, as built complex structures often have relied on

tolerances or deformation to adjust for identical building parts in the fabrication process [19]. This concept is included in the parametric workflow in chapter 6 in the form of a custom Grasshopper component developed in C#. This component is elaborated upon in chapter 5, and the complete code can be found in the attachments, see Appendix A.

3.5   Software tools

The software tools used in this thesis will be described in this section.

3.5.1   Rhinoceros 5.0

Rhinoceros 3d, commonly called Rhino or Rhino 3d, is a three-dimensional computer graphics and computer-aided design (CAD) application software developed by Robert McNeel & Associate [36]. The viewport in Rhino provides an interface illustrating three-dimensional geometry. The geometry in Rhino is based on non-uniform rational basis spline (NURBS), which is a mathematical model commonly uses in computer graphics for developing curves and surfaces. Geometry can be modelled directly in Rhino or it can be imported from another software, such as for example AutoCAD. Because Grasshopper runs within Rhino, Rhino is the basis for all of the coding done in Grasshopper with the various plugins, which is described later in this chapter.
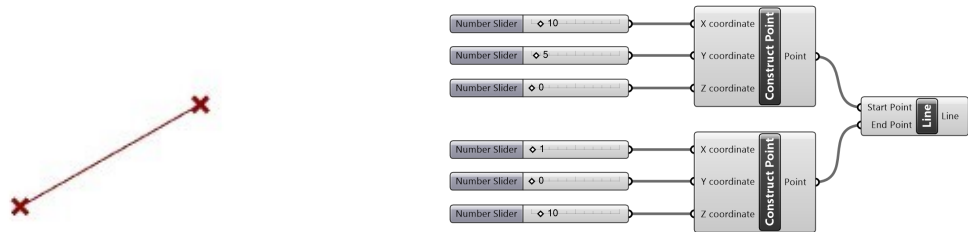
Figure 3.8: Illustrating how components in Grasshopper (right window) works and how the geometry is visualized in the Rhino viewport (left window).

3.5.2   Grasshopper

Grasshopper is a visual programming language (VPL) also developed by Robert McNeel & Associates, and it runs within Rhino. Grasshopper is a fully integrated parametric environment where so-called components is used in the VPL. Each component usually has one or more input parameters and one or more outputs. Figure 3.8 demonstrates the component called *Construct Point*, where the inputs are a value for the X, Y and Z coordinate and the output is a point in those exact coordinates. The output is also displayed in Rhinos viewport. In figure 3.8, this is done for two different points, and further the points are taken in as inputs in a new component called *Line*. The line component takes two different points as input and makes straight line between them. The geometry made in Grasshopper can easily be adjusted by using *Number Sliders*. In figure 3.8, the *Number Sliders* are connected to *Construct Point* component. If the numbers are adjusted, the geometry will change accordingly. The geometry in Grasshopper can be made parametrically as described, or it can be retrieved from Rhino.

There are a standard set of components implemented in Grasshopper. If a desired function does not exist, it is possible to create its own components. This is usually done with programming languages such as Python or C#. The homemade components can be implemented in Grasshopper as plugins. There is an online community that makes such plugins and uploads them to an Internet site called food4rhino.com. At food4rhino.com there are many popular plugins, in which some of them are used in this thesis. Some of the desired functions for this thesis did not exist already and was therefore scripted in C# in the development environment Microsoft Visual Studio (3.5.3). A list of all plugins used in the Grasshopper scripts in connection to this thesis is proved in appendix C.4. In addition to this, the most important plugins is discussed in the following sections.

Kangaroo Physics

Kangaroo Physics is a live physics engine for simulation, form finding and optimization [37]. The Kangaroo plugin is a library which consist of a set of Grasshopper components and some different solvers. *Kangaroo 2* is the newest version of Kangaroo Physics, and it is the version used in this thesis. The solver in Kangaroo is a form finding tool [37], which it takes in different *GoalObjects* as inputs. The *GoalObjects* can for example be loads and anchor points. The solver moves points of a geometry to a state where they are in or close to equilibrium. In this thesis, the Kangaroo solver are used for form finding. The geometry of a mesh, the anchor points and a load is taken in as *GoalObjects* to the Kangaroo solver, and the solver finds a global shape for the geometry where as much of the geometry is in equilibrium.
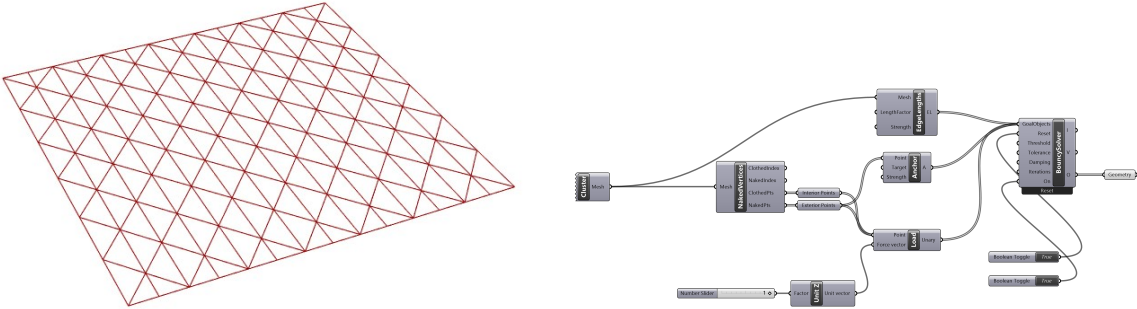
Figure 3.9: *Reset* input set as true. The *BouncySolver* will not do anything.
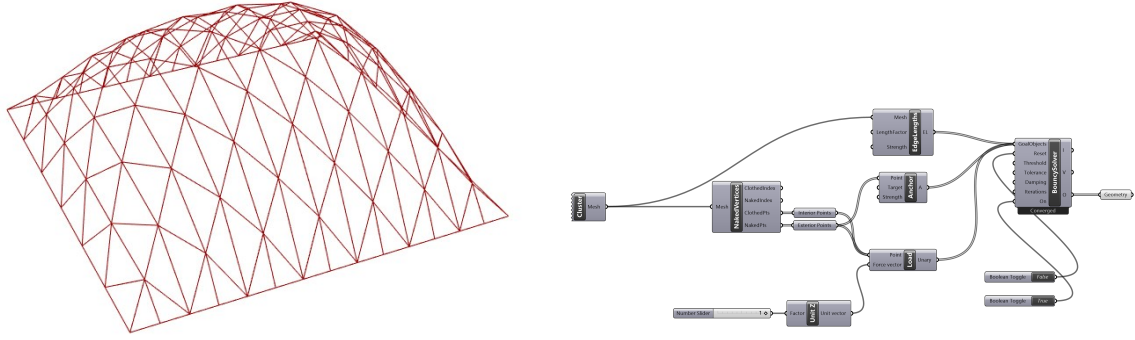
Figure 3.10: *Reset* input set as false. The *BouncySolver* will change the geometry and it will converge when in equilibrium.

Figure 3.9 and 3.10 illustrates the *BouncySolver* component from Kangaroo 2. The geometry from a mesh is stripped down to lines and points. The exterior points are used as anchor points and an arbitrary load in z-direction is set at all points. Load, anchor points and the lines from the mesh are put in as *GoalObjects*. As long as the *Reset* input is true, which is shown in figure 3.9, the *BouncySolver* will not do anything. When the *Reset* input is set as false, the *BouncySolver* will change the global shape of the mesh. It will converge when in equilibrium, which is displayed in figure 3.10.

The Kangaroo solver will merely change the global shape of a mesh based on the coordinates of the points. Combined with an analysis software, this however, will be useful. When a Kangaroo script is combined with an analysis script from Karamba3D, the shape can be manipulated as desired based on various parameters.

Karamba 3D

Karamba3D [38] is a parametric finite element analysis (FEA) software application developed by Clemens Preisinger in collaboration with Bollinger und Grohmann ZT GMbH in Vienna [39]. Karamba3D is a plugin for Grasshopper. Hence, it is possible to connect the parametric model made in Grasshopper directly to the FEA software. This makes the it easy to combine parameterized models, optimization scripts like Kangaroo can provide, and FEA [10].

When using Karamba, the component called *Assemble Model* is the key. The inputs in this component is the boundary conditions for the model, including the geometry, loads, support points, cross section type and material. *Assemble Model* will then give a model as an output, which can be used to get the analysed model. The configuration of Karamba is discussed in detail in chapter 6.4.

LunchBox

LunchBox is a plugin for Grasshopper for exploring and manipulating mathematical shapes, paneling and structures. LunchBox also provides components for machine learning components [40]. In this thesis it is used as a way to explore different grid patterns. Thus, LunchBox is used as an optimizing tool.

Geometry Gym

Geometry Gym is a plugin for Grasshopper that enable BIM generation and exchange [41]. For this thesis it is used to export Grasshopper and Karamba3D models to the structural analysis program, Robot, described in chapter 3.5.4.

3.5.3   Microsoft Visual Studio

Visual Studio is an integrated developer platform for Microsofts .NET platform. It supports a number of programming languages, most notably the C-languages, which are built into the program. Since Grasshopper is a .NET (RhinoCommon) plugin developed with C#, it is the most advantageous language for targeting the framework when developing Grasshopper Component Libraries. Microsoft Visual Studio has a built in template for Grasshopper written in C#, which makes the creation of an add-on simple to implement in to the program. Being a class-based, object-oriented programming language, it is easy to create new classes, which helps the developers workflow, and makes it easier to run tests and avoid 'nesting'. The Rhino.Geometry namespace is also available through Visual Studio, which gives access to geometric definitions like 3d-points, curves and vectors, as well as methods which are useful for both simulations and geometric calculations.

3.5.4   Robot Structural Analysis

Robot Structural Analysis is a BIM (Building Information Modeling) software provided by Autodesk [42]. Robot provides structural engineers tools to evaluate a model by structural analysis as the finite element method (FEM). Models can be built in Robot or imported through other CAD software for analysis. In this thesis, it is convenient to use Robot as a FEM tool for analyses of structures made in Grasshopper. It can be used to compare results obtained from the Karamba3D plugin in Grasshopper, and perform design checks according to the Eurocode for materials as steel, timber and aluminium.

4 Design according to the Eurocode

4.1 Design values of actions

According to NS-EN 1990, Eurocode: Basis of structural design, actions are classified based on their duration [8]. There are three action classes:

- *Permanent actions (G)*, e.g. self weight of the structure;

- *Variable actions (Q)*, e.g. snow and wind loads;

- *Accidental actions (A)*, e.g. car crash or explosions. Accidental actions is not considered in this thesis.

The ultimate limit state (ULS) is safety design for a structure and its users by reducing the capacity of the materials. The ULS verified in this thesis will be STR, which is failure or excessive deformation in the structure or the structural parts [8]. ULS is used to calculate the capacity of a structure, such as utilization factors and buckling load factors. When displacements are calculated, servicability limit state (SLS) is used. The intend with SLS is to prove that the structure satisfy the specified criteria under characteristic action values.

Persistent and transient design situations	Permanent actions		Leading variable action (*)	Accompanying variable actions (*)
	Unfavour-able	Favour-able		
(Eq. 6.10a)	$\gamma_{Gj,sup}G_{kj,sup}$	$\gamma_{Gj,inf}G_{kj,inf}$	$\gamma_{Q,1}\psi_{0,1}Q_{k,1}$	$\gamma_{Q,i}\psi_{0,i}Q_{k,i}$
(Eq. 6.10b)	$\xi\gamma_{Gj,sup}G_{kj,sup}$	$\gamma_{Gj,inf}G_{kj,inf}$	$\gamma_{Q,1}Q_{k,1}$	$\gamma_{Q,i}\psi_{0,i}Q_{k,i}$

Figure 4.1: NA.A2.4B from NS-EN 1990 [8].

The design values of loads will be calculated using either 6.10a or 6.10b from figure 4.1, depending on which of the equations that will give the least favourable load case. The following set of γ, ξ and ψ are used when using the formulas 6.10a and 6.10b [8]:

$\gamma_{Gj,sup} = 1.35$;

$\gamma_{Gj,inf} = 1.00$;

$\gamma_{Q, 1} = 1.50$ where unfavourable (0 where favourable);

$\gamma_{Q, i} = 1.50$ where unfavourable (0 where favourable);

$\xi = 0.89$;

$\psi_0 = 0.7$ for snow loads;

$\psi_0 = 0.6$ for wind loads.

4.2 Determination of snow loads

For the analysis in this thesis to be adequate, snow loads has to be considered. Snow load calculations is done in accordance with Eurocode 1 (EC1), NS-EN 1991-1-3 [9].

The magnitude of the snow loads depend on where the location of the structure is set to be. The focus of this thesis is on design for Trondheim, Norway. The geography of the set location is to be used later in this section. Some of the districts of Trondheim city is displayed with their respective height above sea level (H) in table 4.1.

Table 4.1: Height above sea level for some districts of Trondheim [11].

District name	Midtbyen	Lade	NTNU Gløshaugen	NTNU Dragvoll	Byåsen
Meters above sea level (H)	8.0 m	31.0 m	46.6 m	164.8 m	135.8 m

The characteristic snow load, s_k, is dependent on the height above sea level for the structure in question. If $H > H_g$ (EC1 NA.4.1, [9]):

$$s_k = s_k 0 + n \Delta s_k \tag{4.1}$$

Where
$s_{k0} = 3.5$ kN/m^2 for Trondheim (EC1 Table NA.4.1(901)).
$\Delta s_k = 1.0$ kN/m^2 for Trondheim (EC1 Table NA.4.1(901)).
$n = (H - H_g)/100$, and n is rounded upwards to the closest integer.
$H_g = 150$ m for Trondheim (EC1 Table NA.4.1(901)).

Even though most districts of Trondheim is below 150 m above sea level, the height for NTNU Dragvoll is used. This is because the structures discussed in this thesis do not have a specified location. Thus, NTNU Dragvoll is the conservative choice of location.

$$n = (H - H_g)/100 \tag{4.2}$$

$$n = (164.8 - 150)/100$$

$$n = 0.148 => n = 1$$

This gives:

$$s_k = 3.5 + 1 \cdot 1 = 4.5 kN/m^2$$

According to the National Annex of NS-EN 1991-1-3 (EC1 NA.2), snow loads in Norway should not be considered as exceptional or accident loads. Hence, EC1 5.2(3) gives the following expression for the snow loads, s [9]:

$$s = \mu_i C_e C_t s_k \tag{4.3}$$

Where:
μ_i is the snow load form factor (see table 4.2).
C_e is the exposure coefficient.
C_t is the thermal coefficient.

The exposure coefficient is determined in EC1 Table 5.1, and it is dependent on how exposed the structure is to wind. Topography exposed to wind ($C_e = 0.8$) is defined as flat areas without obstacles, where the structure is exposed to wind from all sides. Shielded topography ($C_e = 1.2$) is defined as topography where the structure is significantly lower than its surroundings. As most buildings in Trondheim is not within any of the two definitions, normal topography ($C_e = 1.0$) is used for the calculations. C_t is defined as 1.0 in EC1 5.2(8) [9].

EC1 5.3 describes the snow load form factor, μ, and in which situations they should be applied, and they are displayed in 4.2. According to the Eurocode, μ_1 is to be used for shed roofs, μ_2 should be used on gable roofs and μ_3 should be applied for shed roofs next to each other. For curved roofs, however, μ_4 should be applied. According to EC1 5.3.5 μ_4 should not be greater than 2.0 [9]. Which snow load form factor μ_i to use, depends on the global shape of the structure. Most gridshells, at least the ones investigated in this thesis, has a curved shape, as can be seen in figure 4.2. Hence, μ_4 is the snow load form factor used in this thesis.

EC1 also explains that snow loads should not be taken into consideration if the angle of the strcuture, α, is larger than 60° relatively to the xy-plane. The magnitude of the snow load form factor also depends on the angle, α. This can be seen in table 4.2.

Table 4.2: Snow load form factors (from Table 5.2 in NS-EN 1991-1-3 [9]).

Angle α	0°<α<30°	30°<α<60°	$\alpha \geq$60°
$\mu_1(\alpha)$	0.8	$0.8 \cdot \frac{60°-\alpha}{30°}$	0
$\mu_2(\alpha)$	0.8	$0.8 \cdot \frac{60°-\alpha}{30°}$	0
$\mu_3(\alpha)$	$0.8 + 0.8 \cdot \alpha/30$	1.6	—
$\mu_4(\alpha)$	$0.2 + 10 \cdot h/w$	$0.2 + 10 \cdot h/b$	0
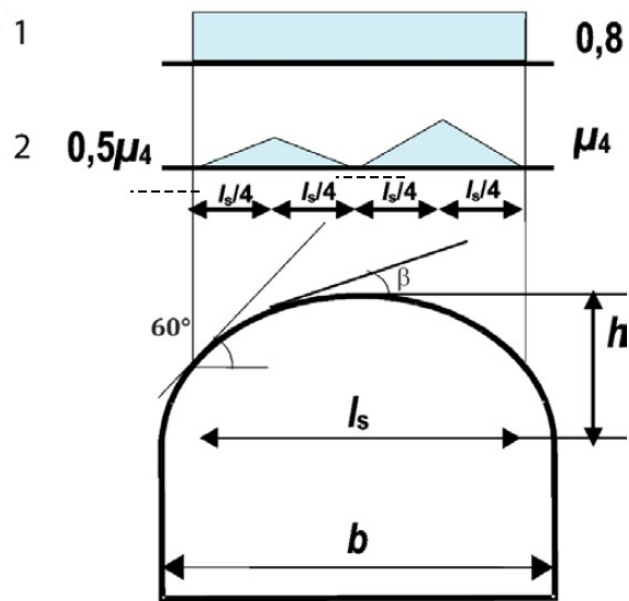
Figure 4.2: The parameters, h, b and l_s, needed to calculate μ_4 (from Figure 5.5 in NS-EN 1991-1-3 [9]). Case 1 and 2 is for respectively undrifted and drifted conditions.

The numbers 1 and 2 in figure 4.2 indicates respectively undrifted and drifted snow loads. If the conditions are undrifted it indicates that the structure is not particularly affected wind loads. l_s from figure 4.2 is defined in EC1 5.3.6 as 2h. Figure 4.2 also displays the parameters h and b from table 4.2. The h/b-ratio from table 4.2 is needed to calculate μ_4, which is needed to calculate the dimensional snow load, s.

Whether to assume drifted or undrifted conditions, depends on what kind of situation that will be investigated. If the snow load is to be seen as one continuous distributed load, undrifted conditions will have to be assumed, and $\mu_4 = 0.8$. If it is desired to look at different scenarios where the snow load only works on certain areas of the structure, drifted conditions has to be assumed.

4.3 Design of timber structures

Timber structures should be designed according to Eurocode 5 (EC5), NS-EN 1995-1-1 [13]. For a structure not to collapse, the utilization of the structure must be considered. Numerous design rules can be found in EC5 for different loading scenarios.

For practical design, the timber element is given two material directions; longitudinal direction, parallel to grain, and normal direction, transverse to grain. For these two directions exist different values for the material properties as modulus of elasticity (E), shear modulus (G), tensile strength (f_t), compression strength (f_c) and shear strength (f_v). Tension and compression parallel to grain gives the highest strength and stiffness, while compression and tension perpendicular to grain is much lower. Timber can also contain imperfections as notches which reduces the cross-sectional strength in the area. Knowledge about the characteristics and constraints regarding timber is essential when designing structures using this material. EC5 gives general common rules and requirements when designing in timber [13]. Designing and calculating value for capacity of timber elements in ULS requires a k_{mod} factor taking into account moisture content and duration of loads. Hence, the design strength will be:

$$X_d = k_{mod} \cdot R_k / \gamma_M$$

Displacements and deflections of timber elements should be calculated for the serviceability limit state (SLS). In EC5, the deflection of a beam due to bending and shear deformation is calculated as a result of instant deflection (w_{inst}) and deflection due to creep (w_{creep}). Global displacements and beam deflections in timber beams can change over time due to long term effects as creep.

Robot Structural Analysis, described in chapter 3.5.4, can perform cross section validations based on EC5. This is elaborated on in chapter 6.5, and implemented in the case project in chapter 7.

5 Developing and integrating custom components in Grasshopper

If the visual scripting available through Grasshopper is inadequate to specific design or analysis issues, there are two implementation options available. Finding and installing existing custom plugin packages, as described in chapter 3.5.2, is one option. This requires some effort into research of existing software, as well as understanding how it operates. There is, in any case, no guarantee that the specific features needed already exist somewhere at all. Option number two is to program custom components from scratch. Both options come with their own benefits and disadvantages. Developing a component from scratch *can* be a time consuming endeavor, depending on the scope of the task and coding experience. On the other hand, it allows for completely tailor-made components for whatever need is to be filled. In order to be productive, the different options available should therefore always be considered carefully.

The components presented in this chapter was developed as tools for geometrical design and evaluation of gridshells, and is incorporated in the case project presented in chapter 7. However, this chapter can also be thought of as a more general feasibility study for the potential of parametric design and Grasshopper. For some specific operations, developing simple components from scratch can be much quicker than constructing potentially long and winding visual scripts in Grasshopper. Looking up preexisting plugins that may or may not exist can also be time consuming, and potentially fruitless. However, the needs of an operation should be thoroughly established before the actual coding begins. Chapter 3.4 provides some background for the components described further in this chapter. Both components were developed specifically for the case project in chapter 7 .

5.1 Programming utility components in C#

Writing code is essentially breaking down a problem in to the most basic step-by-step instructions to which the programming language can interpret. This means that in addition to programming the actual computation one wants to run in the Grasshopper framework, the physical representation of any geometry needed must also be defined in the code. Specifically for a gridshell model, the geometry of nodes and lines should be represented in a way that is practical for the operation one want to accomplish. Class-based programming, as mentioned in chapter 3.5.3, allows the programmer to create objects with specific, relevant properties. A node object, shown in figure 5.1, can for instance have the properties *index* and *position*, and a list of *element-objects* representing the lines connected to it. Furthermore, an element-object can have the properties of a *node-object* at the start and end of its length. These properties can then be initialized and defined by input provided by geometric data in Grasshopper.
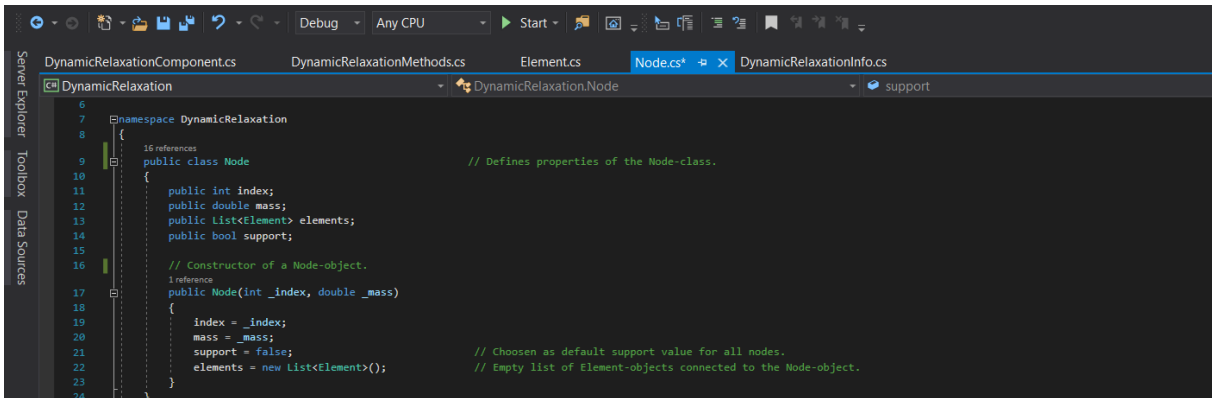
Figure 5.1: A *Node-class* written with C# in Visual Studio. The class can be used to create *Node-objects* with specific properties.

For output there are three different options available in the Grasshopper framework, which are *item*, *list* and *Data Tree*. The first two are fairly straight forward - an item refers to a single data unit, whilst a list consists of several data units in an arrangement. The *Grasshopper Data Trees* is more complex, however, and deals with hierarchical data structures for nested lists. Simplified for its use in this paper, it can be described as a list of sub-lists, or more precisely as a list of *Paths* that each contains another list.

To supplement the parametric workflow framework for gridshells established in chapter 6, two custom utility components were developed. The first being the *Dynamic Relaxation* form finding component presented in chapter 5.2 for global shape design of gridshells. This is explained more in-depth in chapter 3.4.1. The second being the *Angler* component presented in chapter 5.3, used for analysis and identification of local node geometry as described in chapter 3.4.2.

5.2 Dynamic Relaxation component

The Dynamic Relaxation component was developed as a form finding tool for gridshell structures, operating as a simple physics engine for specific geometry. Displayed in figure 5.2, the component uses Rhino Geometry lines and points as input. The input-data is used to construct a node-element system by generating element-objects representing the geometry of the lines, and node-objects at the start and end of each element. A grid or mesh of lines can be created with Rhino Geometry in a multitude of different ways, which is discussed in chapter 6.2. Additionally, there are four number inputs. The mass/stiffness-ratio and damping factor discussed in chapter 3.4.1. This is needed for the numerical integration. The Threshold input is referencing the kinetic energy in the system, and will stop the computation as specified. The finished component can be seen in 5.2, and information about the C#-script for the Dynamic Relaxation component can be found in appendix A.
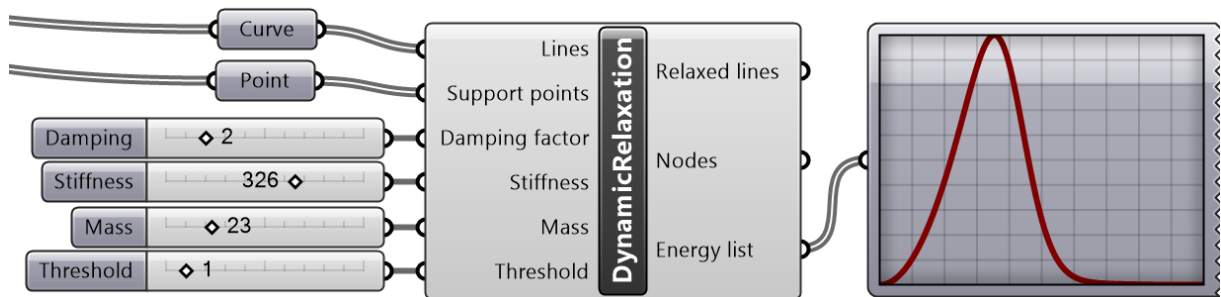
Figure 5.2: The *Dynamic Relaxation* component and required input parameters. The *Energy list* output can be plotted to evaluate computational convergence.

The component uses fictional mass and stiffness values, as explained in chapter 3.4.1. Therefore, the resulting shapes will not necessarily be structurally efficient for explicit load cases or materials. To find an optimal shape, the form finding must be done in conjunction with structural analysis for the specific case. A parametric environment can simplify this process, as one can obtain structural data in real time for different shapes. The ultimate shape will be determined by the mesh pattern, support points and the fictional stiffness/mass-ratio. Figure 5.3 shows how different support points affect the relaxed shape of a simple, quadrilateral mesh.

(a) Mesh + boundary points **(b)** All support points **(c)** Two edges only **(d)** Corners only
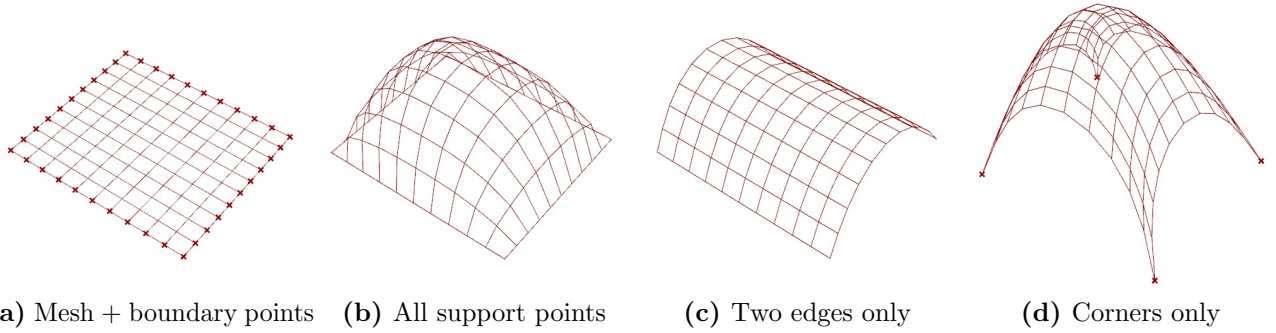
Figure 5.3: Shapes obtained through the Dynamic relaxation component for different support points.

The algorithm defining the code of the Dynamic Relaxation component can be described very simply like this:

1) A *node-element* system is generated from input data. This keeps track of how nodes and elements are related to one another in the code. Current positions of the nodes and initial length of the elements are stored. Current velocity is zero.

2) Gravitational acceleration is applied to the lumped 'masses' in the nodes. As the nodes are accelerated from their initial position, the elements are stretched from their initial lengths.

3) The internal force generated in each element is calculated using Hooke's Law, and the residual forces in the system are updated.

4) The current node velocities and positions are calculated using the numerical integration of Newton's 2nd law of motion, based on the previous velocities and positions. The complete formula for the numerical integration scheme can be found in chapter 3.4.1.

5) If convergence is reached within the given tolerance, the algorithm is terminated and the process completed. If not, steps 3 through 5 are repeated. If the process takes to long, the computation breaks.

Both the time-step used for the numerical integration in the code, and the damping factor used as input require some trial and error to achieve a stable solution. A break-function was included in the code, to terminate a computation if it went on for too long. A simplified descriptive flowchart of the algorithm coded for the component can be seen in figure 5.4. The methods referred to as *generating node-element system* and *dynamic relaxation numerical integration* could warrant having their own flowcharts in and of itself, due to the intricacy of the methods. The complete C# code with comments can be found in the attachments, and information about the attachments can be found in appendix A.

Dynamic Relaxation component flowchart
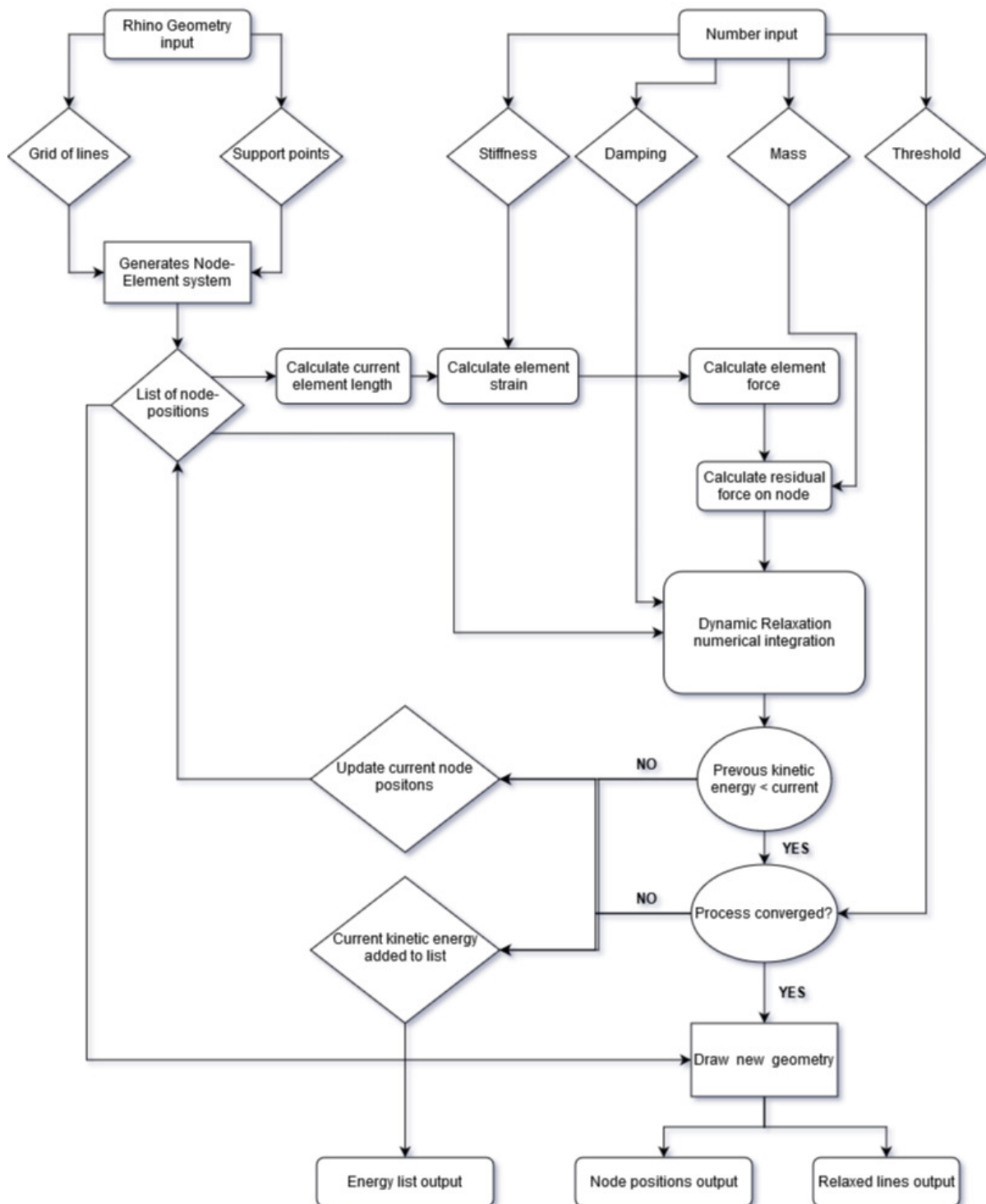
Figure 5.4: Dynamic Relaxation component flowchart.

Form finding methods are by now a well explored subject, but it is still important as an engineer to understand the mechanisms behind the tools in use. Even though the mathematics of it might be similar to other tools, developing ones own open up possibilities for tailoring a component for a specific parametric workflow environment in terms of inputs and outputs. The custom Dynamic Relaxation component was replaced by the Kangaroo form finding component in the parametric workflow described in chapter 6.3. This was done because Kangaroo was found to be a lot more efficient with computing power, which became limiting for the case project detailed in chapter 7. Comparing results obtained from the Dynamic Relaxation component with what was found with Kangaroo in 6.3 on the same mesh, it is apparent that they output similar geometries, as seen in figure 5.5, although the exact inner workings probably differ with regards to the inputs.

(a) Kangaroo   (b) Dynamic Relaxation component
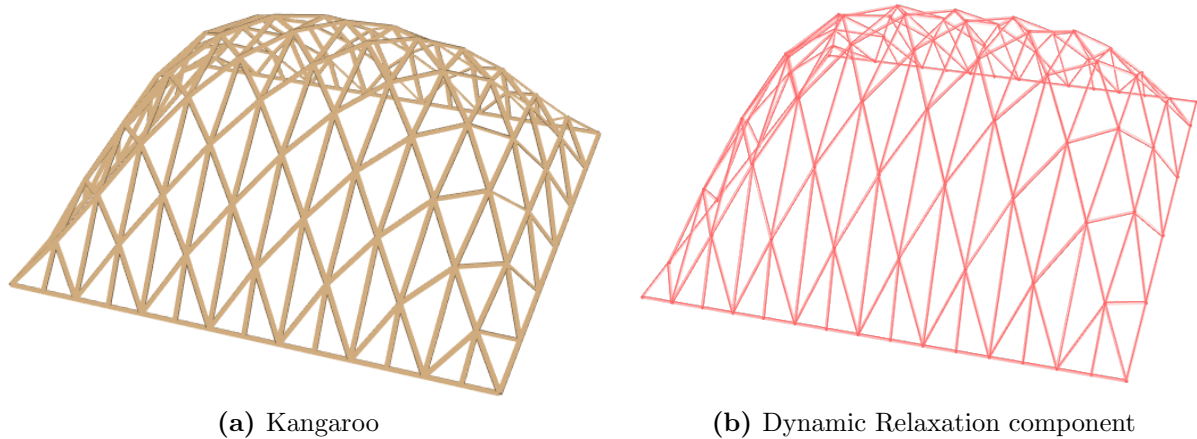
Figure 5.5: Form comparison of the different components.

Having developed a custom form finding component, this highlights a possible pitfall one can encounter as an engineer - where the inner logic of a program is not open for inspection by the user, a so-called 'black-box', which can only be viewed in terms of inputs and outputs. Coding the algorithm from scratch ensures that the process and possible limitations are understood by the user, and allow for tailoring to ones specific need. It does, however, demand a lot of time and effort. In this case the form finding provided by Kangaroo where found to be adequate for the task of the case project in chapter 7. However, it would not be possible to control check the reliability of Kangaroo without the Dynamic Relaxation component, and therefore it is found to be an important part of making the case project in chapter 7 a reliable study.

5.3 Angler Component

In chapter 3.4 it is explained that optimizing for structural efficiency is not the only factor influencing the economic and construction feasibility of a gridshell. The local geometry of the nodes is a substantial source of complexity when it comes to both construction and fabrication. This is in part because large numbers of unique node configurations are not eligible for mass production. Investigating shapes or grid pattern topology that supports repetitive or identical building parts, should therefore be an aspect considered in the conceptual design phase. The definitions obtained in figure 3.7 was used as a basis for the *Angler* component, which can calculate local node geometry for a gridshell and identify identical nodes. As with the Dynamic Relaxation component, Angler was also specifically developed to be used in the evaluations of the British Museum case project in chapter 7. As mentioned in chapter 2.2.2, the British Museum gridshell did not emphasize repetitive node configurations in the design. Because of the unique boundaries imposed by the existing structures on the Great Court roof, it is interesting to see if other grid pattern designs will perform better in this respect. The *Angler* component, seen in figure 5.6, can act as a specialized geometrical analysis tool for gridshells. Information about the C# script can be found in appendix A.
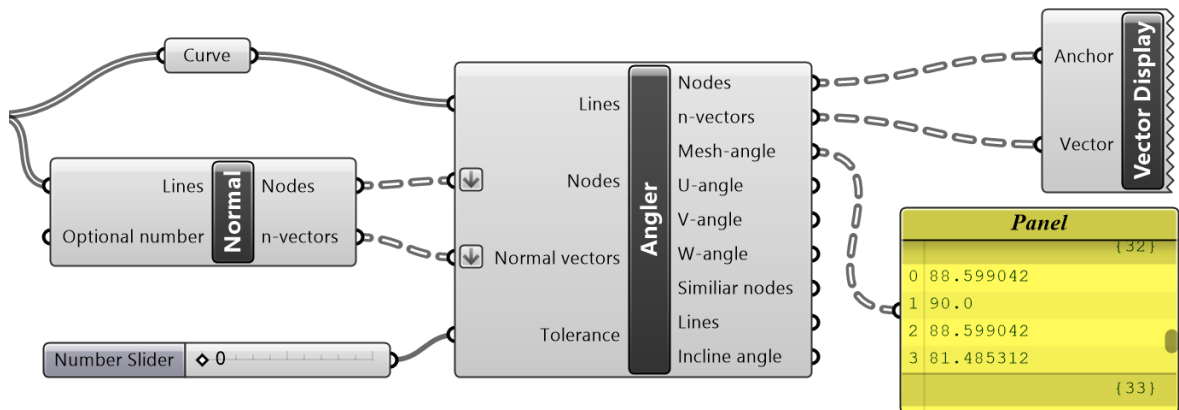
Figure 5.6: The *Angler* component and *Normal* utility component on a quadrilateral grid. The output shows mesh angles sorted counter-clockwise around nodes.

As explained in chapter 3.4.2, three different angles are needed to define the unique configuration of a specific node geometry in 3d-space. These are further defined in relation to a node *normal-vector*. The *Normal* utility component, also seen in figure 5.6, generates normal vectors used to identify the unique geometry of a node, as seen in figure 3.7. The component itself is derived from a method originally implemented in the Angler component. Because it can be beneficial to adjust the normal vector of a node manually or by genetic algorithms, for instance torsion optimization, it was split into its own component to serve as input instead. The two components work as a pair, but any normal-vector generation method can be used as desired. The only restriction is that the list of input nodes must correspond to the list of input vectors. Because of this, the Normal component itself will

not be explained further, except for that it can generate normal vectors by two different methods. The default method uses unit vector summation, which means that the vector orientation, and thus node orientation, follows the global curvature implied by a discrete gridshell. In other words, it is perpendicular on the global 'curvature'. The other vector generation option included in the component, is by unit vector conversion of a straight line drawn from the centroid of the model and up to each node. This is done when feeding a number to the *Num* input, which slides this point downwards and enable this method. This is displayed in figure 5.7, which also visualise these vectors.

(a) Vector summation method.　　　　(b) Vectors by internal point.
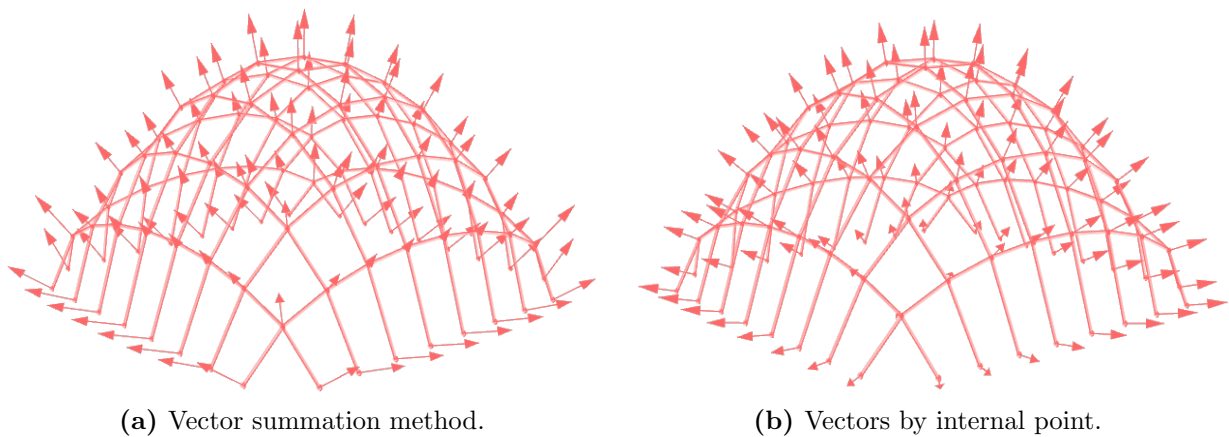
Figure 5.7: The vector generation methods of the Normal component, visualized with the Grasshopper Vector Display. The vectors represent the physical orientation of each node in space.

The Angler component is the main algorithm, and has a multitude of different outputs. The *Mesh-angle*, *U-angle*, *V-angle* and *W-angle* outputs are Grasshopper data trees, with each sub-list path corresponding to the *Nodes* output indexes, which means that any specific node can be examined manually. All angles are calculated counter-clockwise around a node, starting from the line with the smallest coordinate x-value. The *n-vectors* outputs the normal vectors used for the calculations, which can be checked to verify that they correspond to the ones input from the *Normal* component. The main output, however, is *Similar nodes*. This is a data tree where each sub-list contains all node positions with equal U, V and W angles within the given tolerance input.

A simplified descriptive flowchart of the algorithm coded for the component can be seen in figure 5.8. As with the Dynamic Relaxation component, some methods in the flowchart would require their own unique flowcharts in order to be fleshed out sufficiently. The complete C# code with comments can be found in the attachments, see Appendix A.

Angler component flowchart
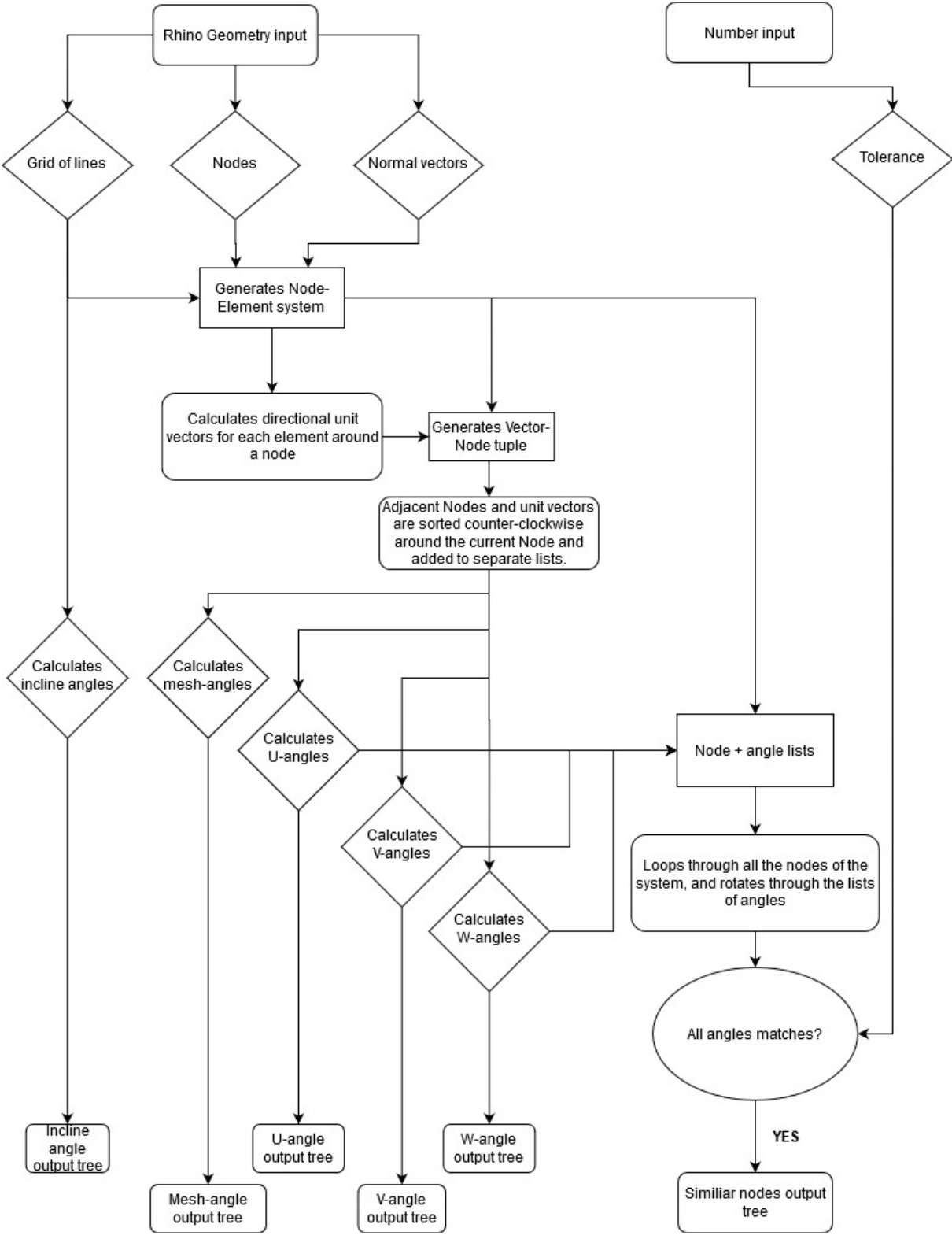
Figure 5.8: Angler component flowchart.

In order to get the best use out of the Angler component, it should be incorporated with other Grasshopper components. Combining the *Similiar Nodes* output with a color grading component, displayed in figure 5.9, allows the user to receive real-time feedback in the viewport on the current status of repetitive nodes - specifically the amount and size of the different identical node groups.

(a) Grasshopper algorithm with Colour Wheel.

(b) Identical node groups by color coding.
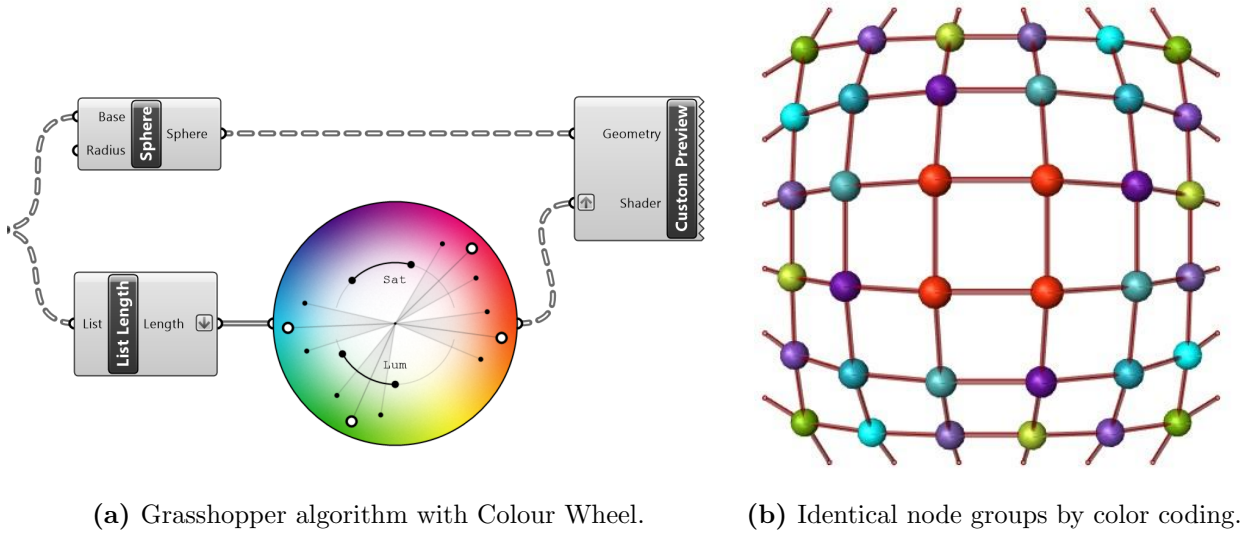
Figure 5.9: Colour coding algorithm on the *Similiar nodes* output. The result results are exemplified on a symmetrical quadrilateral gridshell. Seen from above.

This is less accurate the more different groups there are, as they become harder to discern by sight. But once again, it can be desirable for quick visual evaluations. The colour coding has been further demonstrated on a few simple vault gridshell, which is displayed in figure 5.10. The figure is meant to provide a better idea of how identical nodes are distributed in very simple structures, as the concept is taken further for more complex forms in chapter 7.

(a) Quadrilateral.

(b) Quadrilateral w/ bracings.

(c) Triangulated.
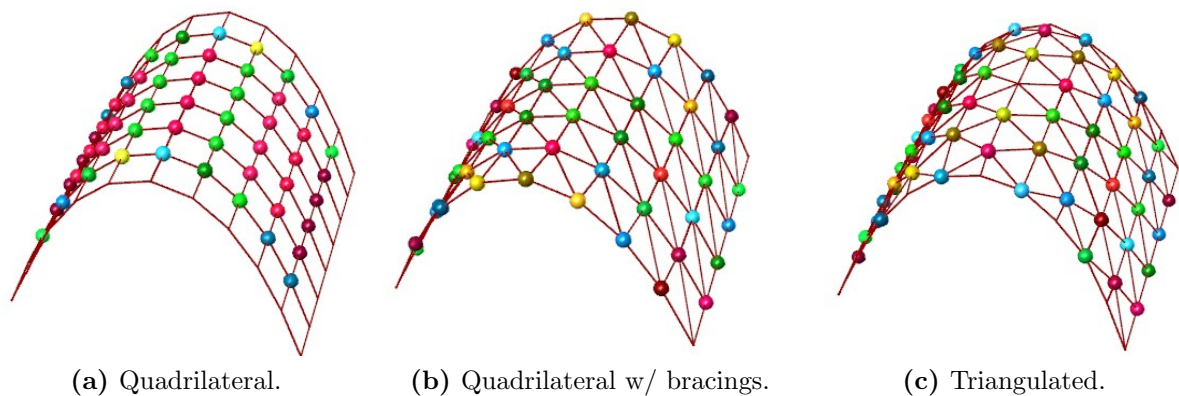
Figure 5.10: Identical nodes distribution for simple vault gridshells of varying grid patterns.

Although optimizing for repetitive building parts is a complex issue that should be investigated in depth, including real time feedback in the parametric workflow framework for gridshells, gives the user an extra aspect for consideration in addition to aesthetics and structural efficiency when evaluating a design. Comparing different free form designs, for instance, the real time feedback can give an indication of to what degree the current configuration can support repetitive node networks. A Grasshopper algorithm is simple to implemented for evaluating the size of the identical node groups as well, which can be used to comparatively evaluate different designs. This can be seen in figure 5.11.
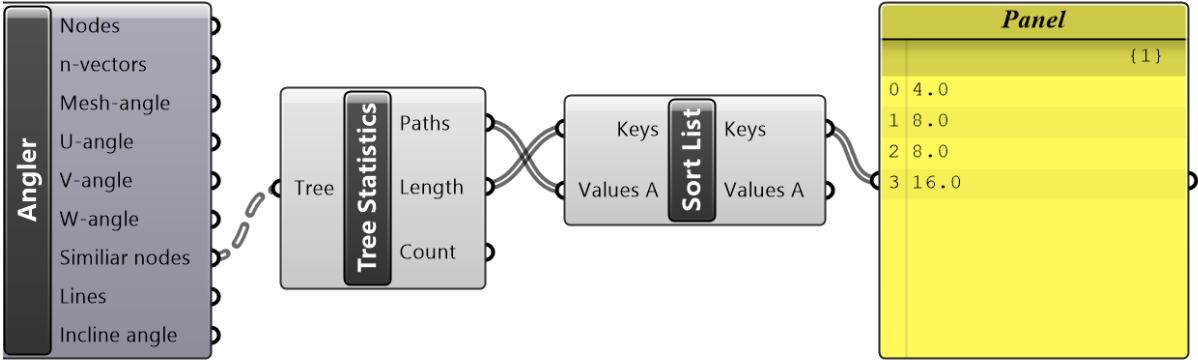
Figure 5.11: Grasshopper sorting algorithm for branch lengths. The first group contain 16 identical nodes. The next 8, and so on.

The final feature of the Angler component is the *Incline angle* output. In chapter 4.2, it is explained that snow loads will not be considered for parts of gridshell structures where the shell is more than 60° relative the horizontal plane. The Incline angle output provides a list of all element orientation relative the horizontal plane. This way, snow loads can be applied exclusively to areas of a gridshell with angles flatter than 60°. This is demonstrated in the parametric workflow in chapter 6.4. The Angler component have been implemented in both chapter 6 and in the case project in chapter 7.

6 Gridshell design in a parametric workflow

6.1 Introduction of the parametric workflow

In this chapter the procedure of parametric modelling and analysis of gridshells, using the software tools explained in chapter 3.5, will be thoroughly explained. The idea is to create a parametric workflow where it is possible to change all kinds of parameters in a simple fashion, when designing a discrete gridshell, which are described in chapter 3.1. Both how the parametric workflow is created, which software tools are used, and how to get results from the analysis, is explained throughout this chapter. The procedure is displayed in the flow chart in figure 6.1. The advantage of the parametric design, which is introduced in chapter 3.1, is that every parameter can be changed no matter where the designer is in the designing process. Hence, if the first, the second or the fiftieth design proposal is not good enough for some reason, every parameter can easily be changed as desired. The parametric design also makes it easier for the designer to correct errors throughout the designing process.
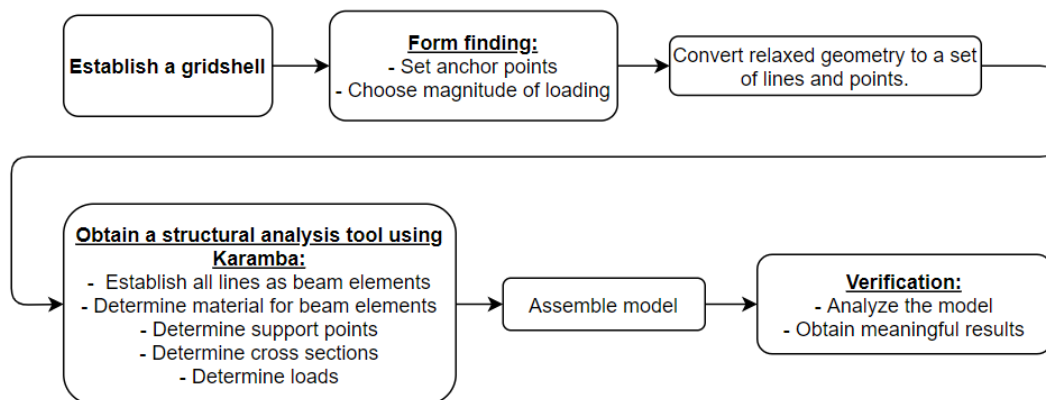
Figure 6.1: A flow chart describing the process which is the parametric workflow described in this chapter.

Further, to emphasize how the parametric modelling is working, a structural analysis is done on gridshells for three different heights, which are displayed in figure 6.2. In addition to the different heights, a global analysis for two different node types will be done, as discussed in chapter 3.3. The nodes in a gridshell structure is of great importance to the structure. Even though the node capacities will not be analyzed in this thesis, the node configurations will be considered during the form finding. Therefore, nodes of steel and aluminium will both be considered during the form finding and analysis of the gridshells.

As a verification of the procedures created in this chapter, structural analysis of simple gridshells will be carried out. The results in this chapter are not important in itself, as the geometry and material of the gridshell studied is randomly chosen. Hence, the intention of this chapter is not to actually design the gridshells in the most efficient way, but to illustrate the development of a parametric workflow for gridshell structures. This is done through Rhino, Grasshopper, various plugins and creating a framework for real time structural analysis through Karamba. The simplicity of changing parameters should be emphasized, and it should be easy for the reader to understand how to design gridshells with these parametric modelling software tools. Furthermore, the parametric workflow obtained in this chapter will be used in the case project in chapter 7.

(a) Gridshell with h = 3.0 m   **(b)** Gridshell with h = 4.5 m   **(c)** Gridshell with h = 8.0 m
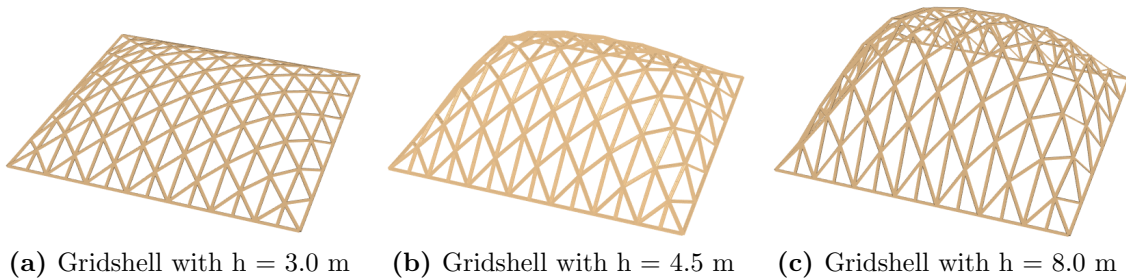
Figure 6.2: The gridshells and corresponding heights that will be evaluated.

6.2 Establishing a gridshell in Grasshopper

In chapter 3.5 it is described that Rhino and the Rhino plugin Grasshopper are the main software tools used in this thesis. In the parametric workflow, Grasshopper is used for modelling, form finding and finite element analysis. To make the model as parametric as possible, Rhino will be used merely as a viewport, and the geometry will be modelled directly in Grasshopper. As both the form finding and the analysis can be done within the Grasshopper interface, it will be easy to make changes and compare different shapes, materials and load cases.
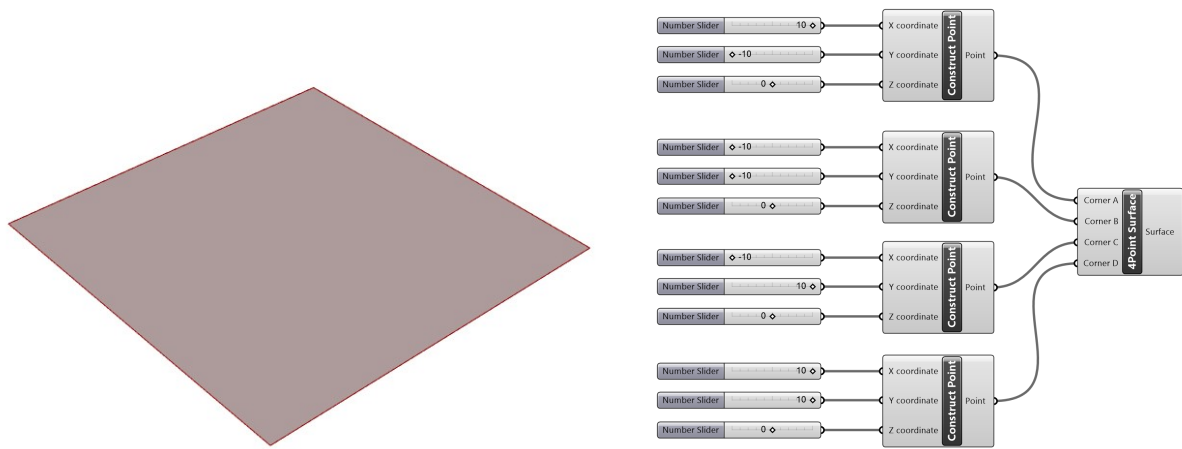
Figure 6.3: A quadratic surface made of four points.

There are many different ways one could go about creating a gridshell model in Grasshopper. The plugin called LunchBox, which is described in chapter 3.5.2, is mostly used throughout this thesis to generate different grid patterns. These can then be formed in to a shell shape with a form finding component. LunchBox includes a number of different pattern variations, and therefore the grid can be altered easily using this plugin. This method is also used for the topology optimization in the case project in chapter 7.5.2. A grid pattern can also be drawn by hand, for instance, but would quickly become time consuming for testing many different designs.

To generate a grid pattern using LunchBox, a surface must be created first. A surface can be created in many ways in Grasshopper, and it depends on the initial shape desired. Figure 6.3 displays one way to do it. Four different points is constructed using different *Number Slider* components to decide the coordinate of the points. The *4Point Surface* component takes in four corner points and makes a surface between them. In figure 6.4 the LunchBox component *Triangle Panels B* takes in a surface as input and sends a certain amount of panels as output. The density of the grid is determined by the inputs *U Divisions* and *V Divisions*. The divisions are decided by *Number Sliders*. Each panel

from the *Triangle Panel B* component is classified as a boundary representation (Brep) in Grasshopper. To convert the Breps from the *Triangle Panel B* component into one mesh the *Simple Mesh* component is used. This component converts all the Breps into meshes. There are plural useful components from the Kangaroo plugin as mentioned in chapter 3.5.2. Three of them are used in the script shown in figure 6.4. The *Combine&Clean* component converts multiple meshes into one. Both *Mesh Edges* and *NakedVertices* takes in a mesh as input. While *Mesh Edges* separates between exterior and interior lines in the mesh, *NakedVertices* separates the exterior and interior points in the mesh. These components will be used both for form finding with Kangaroo and the analysis with Karamba.
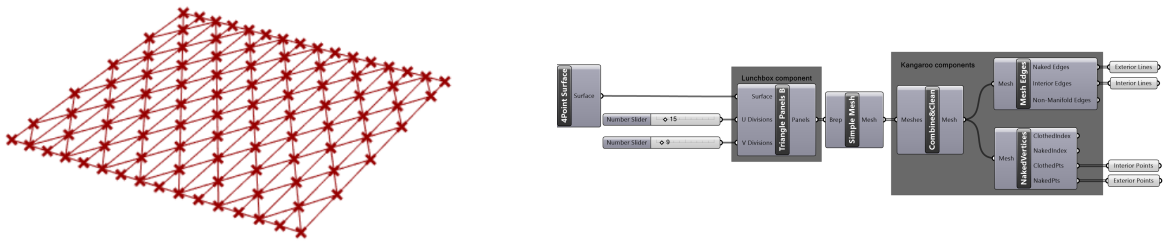
Figure 6.4: Convert one surface into a specific mesh. *Triangle Panel B* is from the LunchBox plugin. *Combine&Clean, Mesh Edges* and *NakedVertices* is from the Kangaroo plugin.

After the mesh is made in Grasshopper, as in figure 6.4, the form finding and eventually the analysis can be done. Both form finding and analysis can be done within the Grasshopper interface. The following sections describes the form finding using Kangaroo Physics, and the finite element analysis done with Karamba3D, respectively.

6.3 Form finding in the parametric workflow

As explained in chapter 3.1, a gridshell with a curved form will be more resilient to lateral forces, than a flat gridshell. The boundary conditions can make it hard to see clearly how the global shape of the grid shell should be, and it will be easier to change the global shape of the structure based on the analysis, if the form finding in the model is parametric. The Dynamic Relaxation component presented in chapter 5.2, was specifically developed to do the form finding in this thesis. It was, however, found to be too computationally ineffective for the case project in chapter 7. Since the Dynamic Relaxation component has already been described, an alternative method will be showcased here instead.

Form finding using Kangaroo

As explained in chapter 3.5.2, the *BouncySolver* takes in parameters such as geometry, loads and supports as inputs. In this case the mentioned geometry is the mesh from figure 6.4. The *BouncySolver* is not compatible with meshes as an input. However, Kangaroo have made a component to convert meshes to lines, *EdgeLengths*. In figure 6.5 all the exterior points are chosen as support points. The support points could be changed to for example the corner points by taking the points shown in figure 6.3 as inputs in the *Anchor* component instead of the exterior points.
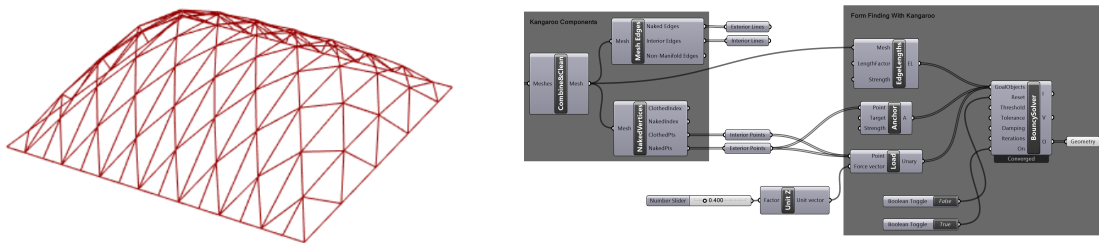
Figure 6.5: The *BouncySolver* component uses dynamic relaxation to change the global shape of the structure.

The global shape will be influenced by the *Load* component. The global height of the structure is proportional to the input value of the *Load* component. The number taken in as an input in the *Load* component is not an intuitive number, but that number is not important in it self. The structure height, however, can be found after the *BouncySolver* has converged. Both the height of the structure and the h/b-ratio, which is the height divided by the smallest width, is of importance in this thesis. In this chapter, the gridshell will be investigated especially for three heights, displayed in figure 6.2. This is to emphasize the fact that it is easy to change the global shape of the gridshell and get results for the different shapes.

6.4 Obtain a structural analysis tool using Karamba

After the form finding, a structural analysis tool can be made using components from Karamba, which was introduced in chapter 3.5.2. To create an analysis tool with Karamba, a model must be assembled. The model is assembled with the Karamba component *Assemble Model*, which was explained in chapter 3.5.2. For the component to work, it must take in a number of parameters such as beam elements, cross sections, material, support points and loads. The following sections suggest a procedure for making a geometry, in this case the relaxed geometry from Kangaroo's *BouncySolver*, into a Karamba model.

Conversion to mesh

The output of the Kangaroo component, *BouncySolver*, is a geometry. Karamba however, works easier if the geometry is sorted in exterior and interior lines and points. One way to get the points and lines is to convert the geometry to a mesh and then do the same as in figure 6.4. To convert geometry to a mesh, a Grasshopper plugin component called *Weaverbird's Mesh From Lines* is used, from the plugin *Weaverbird*. Figure 6.6 shows how the plugin component takes in a geometry and convert it to a mesh.
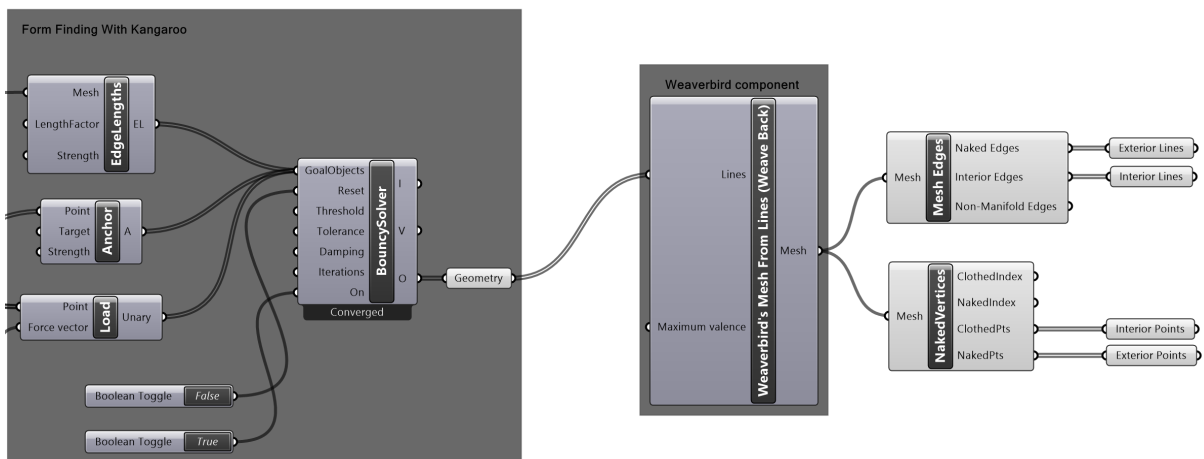
Figure 6.6: *Weaverbird's Mesh From Lines* takes in the relaxed geometry from the *BouncySolver*, and convert it to a mesh.

Beam elements

Further, the Karamba software will be used. For Karamba to work, however, the interior and exterior lines needs to be characterized as *beam elements*. This is done with Karamba's *Line To Beam* component, as shown in figure 6.7. The component takes in all the lines and convert them to beam elements. It is recommended to use one *Line To Beam* component for each of the beam element group. In this parametric workflow, interior beams, exterior beams and beams with an angle under 60° are the three beam element groups in use. The beam elements with an angle under 60° are used to determine which beam elements

should carry snow loads, which is discussed in chapter 4.2. If it is desired to have different materials or cross sections for different parts of the structure, multiple *Line To Beam* components can be used. However, the exterior and interior beam elements will have the same properties in this parametric workflow.
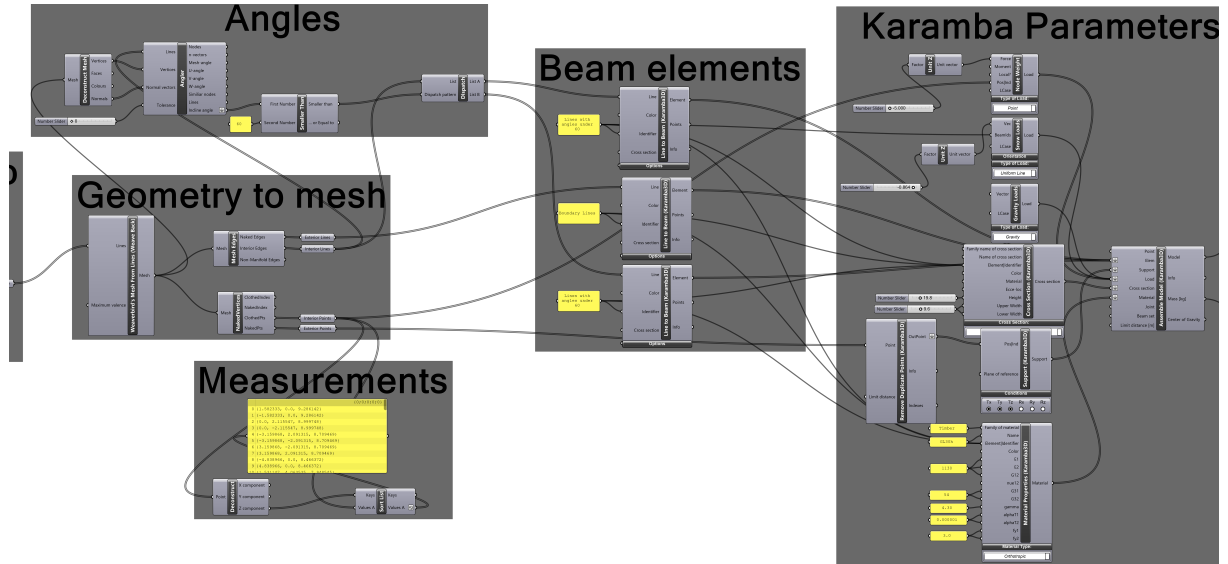
Figure 6.7: The *Line To Beam* components converts the geometry to beam elements. Further, material properties, cross sections, support points and loads are inputs in *Assemble Model*. The output is a model ready to be analyzed.

Determination of cross section and material

As mentioned, the cross sections are set as the same for both the exterior and the interior elements. For both the *Cross Section* and the *Material* component to recognise which elements they should affect, identifiers are made in the *Beam Elements*-group. Both the cross section and material can be chosen as desired, and in this parametric workflow, they are chosen at random. A timber cross section with cross-sectional dimensions, bxh = 96x198 mm, is selected for this parametric workflow.

Karamba provides a set of material types to choose from. If, however, the desired material is not among the standard materials from Karamba, the material can be self made. With *Material Properties* from Karamba, the material properties can be set as desired. In this parametric workflow, the material in use will be GL30h.

Table 6.1: Material properties for GL30h [12].

Material	E [MPa]	G [MPa]	f_y [MPa]	ρ[kN/m^3]	α_T [1/C°]
GL30h	11300	540	30	4.3	$5.0 \cdot 10^{-6}$

Table 6.1 displays the parameters the *Material Properties* component from Karamba takes as inputs. The parameters could easily be changed if desired. In this part of the thesis,

the exact material is not as important as the fact that the material properties are correct and equal for all the variations of the gridshell that are evaluated. The material properties is found in NS-EN 14080 from Norsk Standard [12].

Determination of support points

The support points were defined during the form finding, in this case all the exterior points are used. After the support points are set, the support conditions needs to be decided. The *Support* component in Karamba is specified with six degrees of freedom, three translational and three rotational, where the six degrees of freedom can be set as desired. The support conditions depend on the boundary conditions for the specific project. In this case, pinned supports are chosen (no translational moment, but free to rotate), as can be seen in figure 6.7.

Determination of loads

The last parameter in this chapter is the loads. If preferred, plural loads can be included in the model. Some variations of the *Loads* component is displayed in figure 6.8. If gravity is chosen, the component does not need any inputs as the *assemble* component contributes with the necessary information about the materials and cross sections. In many cases, it would be useful to combine the gravity load with other loads, like point loads, line loads or uniform loads of various sorts. In this chapter, snow actions is added. The prevalent load type for the snow actions depends on the structure. In this parametric workflow, no cladding are included. Thus, *Uniform Line* is the most prevalent to use. If a kind of cladding, such as glass panels, had been included, the load type should have been chosen as *MeshLoad Constant*, which is a distributed load, in the *Loads* component. When *Uniform Line* is used, the direction and intensity of the load must be set as an input. Typically, snow load and wind load can be applied. The purpose of this parametric workflow however, is not to examine how structures behave in given, different load combinations. Therefore, only gravity forces and snow loads are chosen. ULS, which is introduced in chapter 4.1, could have been used to get the design loads acting on the gridshell. This is not done in this chapter, however. In the case project in chapter 7, ULS and SLS calculations is taken into account.
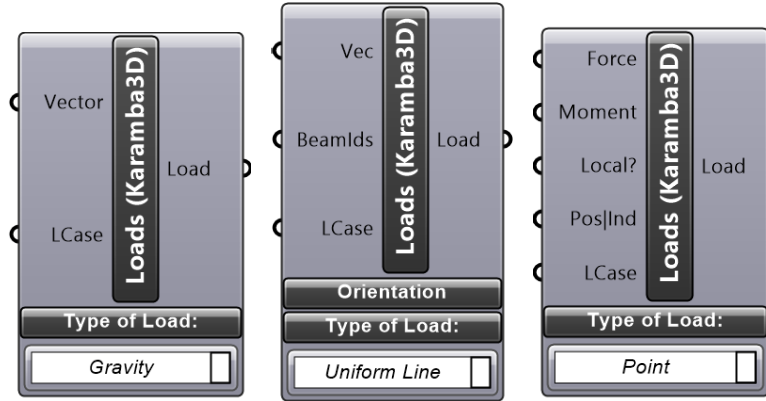
Figure 6.8: Different variations of the *Load* component from Karamba.

Determination of snow loads

As explained in chapter 4.2, the snow load, s, depends on conditional factors. This can be seen in equation 6.1. The snow load form factor, μ_4 depends on the h/b-ratio. In chapter 4.2 it was explained that both C_e and C_t equals to 1.0, and $s_k = 4.5$ kN/m². This makes μ_4 the only changing parameter for the three different gridshells that will be analyzed in this chapter.

$$s = \mu_4 C_e C_t s_k \tag{6.1}$$

The three gridshells to be analyzed have a height of 3.0 m, 4.5 m and 8.0 m. The floor area are 20x20 meters, and thus the width of the gridshells is 20 m in both X- and Y-direction. Hence, the h/b-ratio for the three gridshells is respectively 0.150, 0.225 and 0.400.

$$\mu_4 = 0.2 + 10 \cdot h/b, \tag{6.2}$$

$$\mu_4 \leq 2.0$$

Table 6.2: According to EC1 5.3.5, $\mu_4 \leq 2.0$ [9].

Gridshell height	h = 3.0 m	h = 4.5 m	h = 8.0 m
$\mu_{4,\text{ undrifted}}$	0.8	0.8	0.8
$\mu_{4,\text{ drifted}}$	min{1.70; 2.00}	min{2.45; 2.00}	min{4.20; 2.00}
$\mu_{4,\text{ drifted}}$	1.7	2.0	2.0

If the conditions are assumed undrifted, $\mu_4 = 0.8$, according to chapter 4.2. If undrifted conditions on the other hand, is to be analyzed, μ_4 has to be calculated for that specific structure. The results of μ_4 can be found in table 6.2.

Table 6.3: The dimensional snow load, s, for drifted and undrifted conditions.

Gridshell height	h = 3.0 m	h = 4.5 m	h = 8.0 m
$s_{undrifted}$	3.6 kN/m^2	3.6 kN/m^2	3.6 kN/m^2
$s_{drifted}$	7.7 kN/m^2	9.0 kN/m^2	9.0 kN/m^2

Both drifted and undrifted conditions can be analyzed for a roof structure. The undrifted conditions is where the snow works as a continuously distributed load over the structure. In this chapter it will be assumed undrifted conditions for the gridshell structures. Hence, the snow loads will be as displayed in table 6.4.

Table 6.4: The dimensional snow load, s, given parameters h, α and w.

Gridshell height	h = 3.0 m	h = 4.5 m	h = 8.0 m
s(α≤60°)	3.60 kN/m^2	3.60 kN/m^2	3.60 kN/m^2
s(α≤60°; w=96mm)	0.346 kN/m	0.346 kN/m	0.346 kN/m
s(α>60°)	0	0	0

Parametric modelling of snow loads

The magnitude of the snow loads is investigated according to EC1 in chapter 4.2. In this thsis, undrifted conditions are considered. Thus, the dimensional snow load, s, can be found in table 6.4. As explained in chapter 4.2, snow loads will not affect beam elements with an angle, α, larger than 60° relative to the xy-plane. To get a list with only the beam elements with an angle smaller than 60°, a component, *Angeler* is programmed with C#, using Microsoft Visual Studio. The Angler component is described in chapter 5.3, and can be used, inter alia, to get a list of all areas in a geometry with an angle below 60°. Figure 6.6 displays that the Angler component takes in all the lines from *Mesh Edges*. In addition to the lines, the Angler component takes in the normal vectors and the vertices from the mesh obtained by the Weaverbird component. The tolerance of degrees is set to 0 in this case, because it should not be a tolerance of degrees to the 60° limit. The output used in this part of the parametric modelling is the *Global Incline angle*. Global Incline angle sends a list with all the beam element angles, α. With a *Smaller than* component, which is a standard math component from Grasshopper, a new list can be made with only the angles smaller than 60°.

Figure 6.9 displays how the new list of lines with angles smaller than 60° is made using the Angler component. The new list of lines can be sent to a *Line To Beam* component as described in chapter 6.4, and displayed in figure 6.7. The Loads component for snow loads is connected to the new Line To Beam component and the vector input is set as table 6.4 displays.
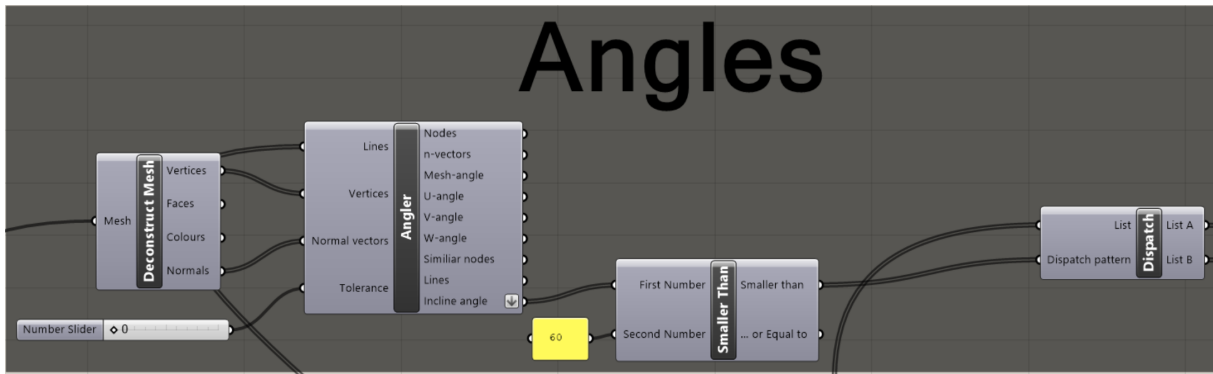
Figure 6.9: The *Angler* component takes in all the lines in the geometry, and together with *Smaller Than* and *Dispatch* it sends a list with all the lines with angles smaller than 60° as an output.

Nodes

In this thesis, all connection nodes in the gridshell is assumed fixed. The nodes used in this thesis is discussed in chapter 3.3 and the node weight calculation can be found in appendix D. The design of the nodes used in this thesis, independent of material, is shown in figure 6.10.
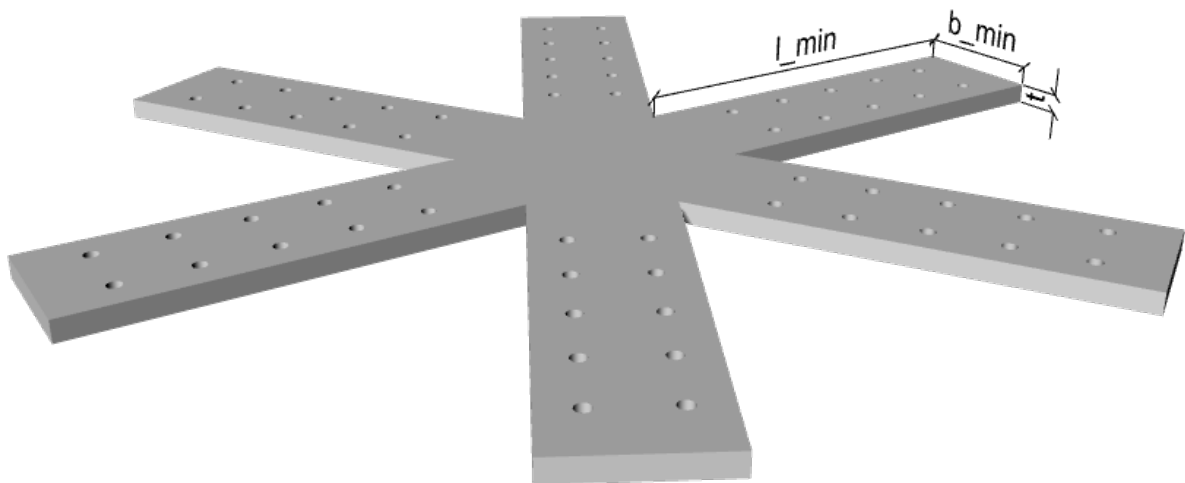
Figure 6.10: The nodes used in this thesis consists of two plates like the one in this figure.

To include the node weight in the parametric workspace in Grasshopper, a new *Loads* component has to be made. The most suitable would be to consider the node weight as a point load, P, in every node. It can be seen in figure 6.8, that point loads can be chosen in the Karamba component.

$$P = m \cdot g \cdot 0.001 [kN] \tag{6.3}$$

In appendix D calculation of the node masses can be found. The steel nodes has a m = 86.2 kg and the aluminium nodes has m = 47.4 kg. From equation 6.3, the loads from the steel nodes is P = 0.846 kN, and the loads from the aluminium nodes is P = 0.465 kN. In the analysis, the point load, P, will be working on all the nodes in the gridshell structure. Further, the gridshells with node weight will be analyzed and compared with a gridshell where the node weight is neglected.

The design of the foundations will depend on the global weight of the structure. To find the global weight including the node weights, the number of nodes has to be considered. This is because of the fact that the nodes is considered as point loads in the model, and not actual metal structures with its own weight in the model. The number of nodes can be found in the Grasshopper model. The model featured in this chapter has 72 interior nodes and 40 exterior nodes. For simplicity, it is assumed that the exterior nodes weigh the same as the interior nodes. Thus, the global weight of the structure should be the combined weight of the nodes, which is 9654 kg for the steel nodes and 5309 kg for the aluminium nodes, plus the weight of the timber beam elements. The foundations are not calculated and therefore they will not be discussed thoroughly. However, the weight of the nodes will be considered later in this chapter, both with regards to the foundations, and to a general consideration.

Assembled model

After the model is assembled, it can be sent to *Beam View*, which is a component that shows the structure with proportional beam size. Figure 6.11 displays how the analysis in Karamba can be set up, and how it will look in the Rhino port view.
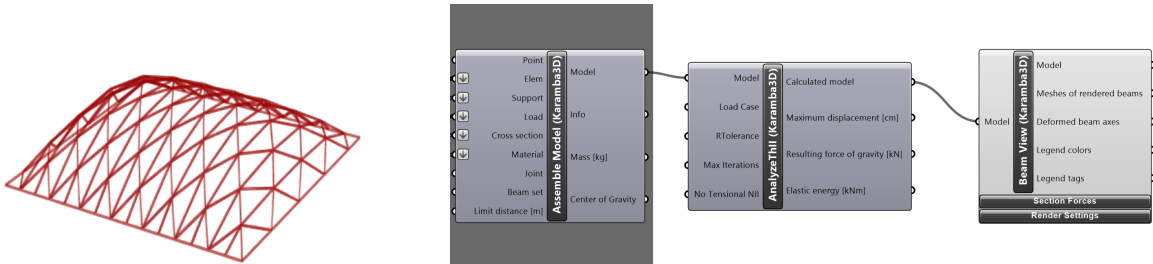
Figure 6.11: The Rhino port view (left) displays what the *Beam View* component in the Grasshopper window (right) does.

Beam View is merely used for the visualization. To get a calculated analysis, an analysis component has to be added. Karamba includes three alternative analysis components, *Analyze*, *AnalyzeThII* and *Large Deformation Analysis*. Small deformations refer to situations where the displacements virtually do not affect the global shape of the structure. Therefore, *Large Deformation Analysis* should not be used in this thesis. The difference between *Analyze* and *AnalyzeThII* is the use respectively first order theory for small

deformations and second order theory for small deformations. *AnalyzeThII* is used because it will be slightly more accurate [38] [10].

The calculated model from *AnalyzeThII* is ready to be analysed and it can be sent to *Beam View* through *Model View*. *Model View* lets the user inspect the state of the model and is used in cooperation with *Beam View*. The order of the components is shown in figure 6.12. From the figure, it can be seen that the Rhino port view is showing displacements between 0.00 and 0.20 cm, and that for the particular model in figure 6.12, the largest displacement is 0.1946 cm. The Rhino port view displays the magnitude of the displacements in the model. It can also be seen that both normal forces, shear forces, bending moments, maximum displacements, structure weight and buckling length factors is a part of the analysis.
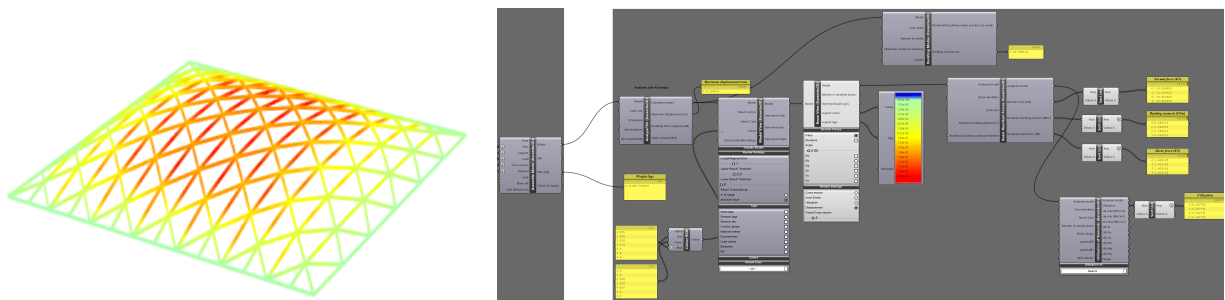
Figure 6.12: The calculated model. The Rhino port view displays where the displacements will be. The Grasshopper window displays how Karamba components can be used to get displacements, forces and buckling length factors from a model.

Karamba gives the opportunity to to examine normal forces, shear forces and bending moments in the model. In order to make an evaluation on the geometry from an engineer's point of view, the forces must be taken into account. As described in chapter 3.2.2, shell structures are exposed to buckling as they are relatively slender geometries. Slender structures may fail to buckling even though the stresses in the structure are below those needed to cause failure in the material. Karamba has a component for buckling analysis, *Buckling Modes*. The component takes in the calculated model and gives *Buckling-load-factors* (BLF) as an output, as illustrated in figure 6.13.
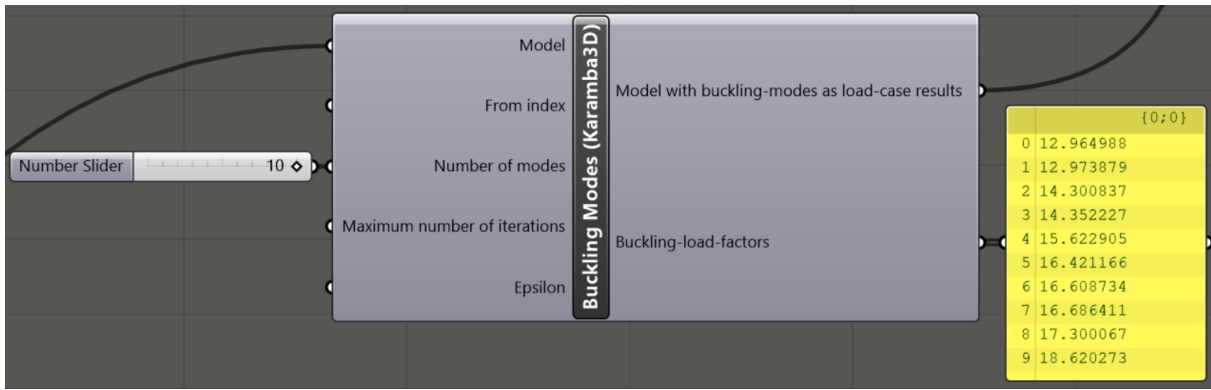
Figure 6.13: The component calculates the BLF for a given model.

$$BLF < 1.0 \Leftrightarrow \text{Buckling occurs} \qquad (6.4)$$

As can be seen from equation 6.4, the BLF needs to be larger than 1.0 if buckling is not to occur. The *Buckling Modes* component takes in the analyzed model and the BLF is affected by both the normal forces and moments. The buckling load factors is given as the lowest number for the particular buckling mode. If multiplied with the current normal force, it would lead to collapse due to global buckling [10].

The *Buckling-load-factors* component calculates the BLF for a given number of buckling modes. In figure 6.13 10 buckling modes is given. It is most important to keep the buckling load factors above 1.0, to avoid global buckling. If the BLF is below or close to 1.0, a visualization of the buckling modes can be useful. The visualization of the buckling modes displays where the buckling is going to occur for that particular mode. In this way, the designer will know where to strengthen the structure if necessary. Figure 6.14 displays the first three buckling modes of the gridshell with h = 8.0 m as an example.
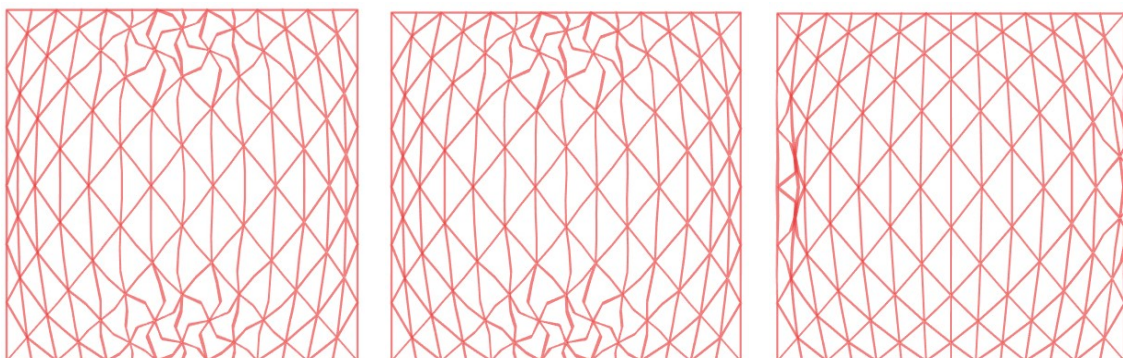
(a) The first buckling mode. (b) The second buckling mode. (c) The third buckling mode.

Figure 6.14: The three first buckling modes for a gridshell with h = 8.0 m, as an example of how the buckling modes can be useful when designing a gridshell.

6.5 Timber design checks in Robot Structural Analysis

Designing timber structures needs to be verified according to design checks in EC5 [13]. Design checks in EC5 of timber design was introduced in chapter 4.3. The computer software Robot, which were introduced in chapter 3.5.4, can both compute FEM analyzes and design checks according to EC5, and is used to check the utilization of members in the structure. This is because Karamba does not provide the possibility to check the utilization for timber structures. Robot is a well used finite element software in the industry and is considered as a trustworthy source of validation. Therefore, Robot will be used both to find the utilization of selected gridshells, and as a validation check for the results obtained from the Karamba analysis.

Import model from Grasshopper

Robot provides the opportunities to model a structure from scratch or import a model from CAD files. In this thesis, it is desirable to export a model from Grasshopper. This is done by using the Grasshopper plugin *Geometry Gym*, mentioned in chapter 3.5.2. The model from the *Assemble model* component in Karamba is used as input. When the model is imported into Robot, the structure can be viewed and analyzed by the loads obtained in Karamba. Figure 6.15 displays the setup in Grasshopper with the use of Gemetry Gym.
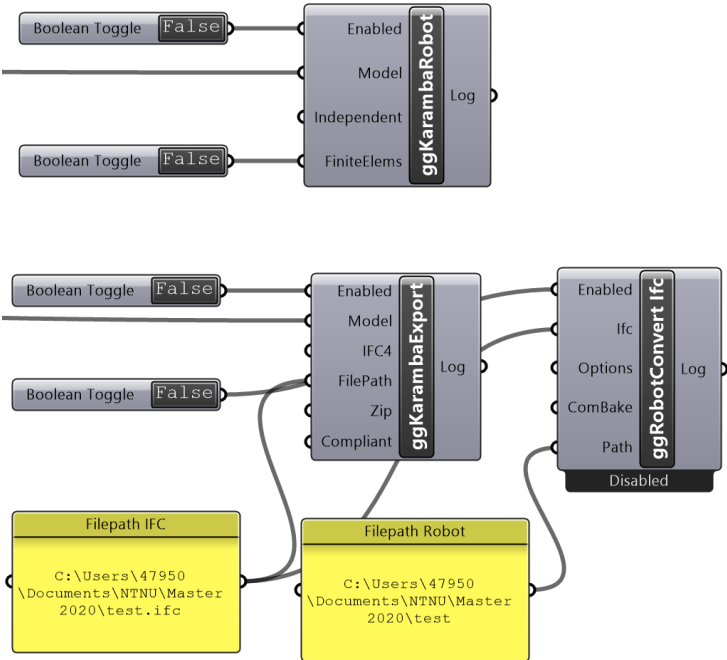
Figure 6.15: Geometry Gym plugin which exports the model assembled by Karamba in Grasshopper to Robot Structural Analysis.

Assigning loads and analyzes

In Robot there is possible to assign varies of loads, load combinations and structural analyzes to the model. The default settings in Robot calculates the model using linear static analysis but can be changed to run nonlinear analysis. Nonlinear behaviour of a structure can be due to nonlinear relation between forces and deformations in the structure, generating moments resulting from second order effects [43]. For long spans structures as gridshells, it would be convenient to use nonlinear analysis taking in second order effects in the calculations. The loads obtained by Karamba is combined in Robot as ULS and SLS combinations and calculated. Design values for the combinations is presented in chapter 4.1.

Timber design checks

Robot gives an utilization value for each member where the user can view all calculations and ensure which design verification were most critical. Figure 6.16 displays the interface from a timber verification with the results from one member. The factors and parameters has to be controlled according to the EC5. Buckling length factor, β, must comply with the support constraints for the members. In the case for fixed joint between members, the buckling length is set to $L_k = 0.5L$.
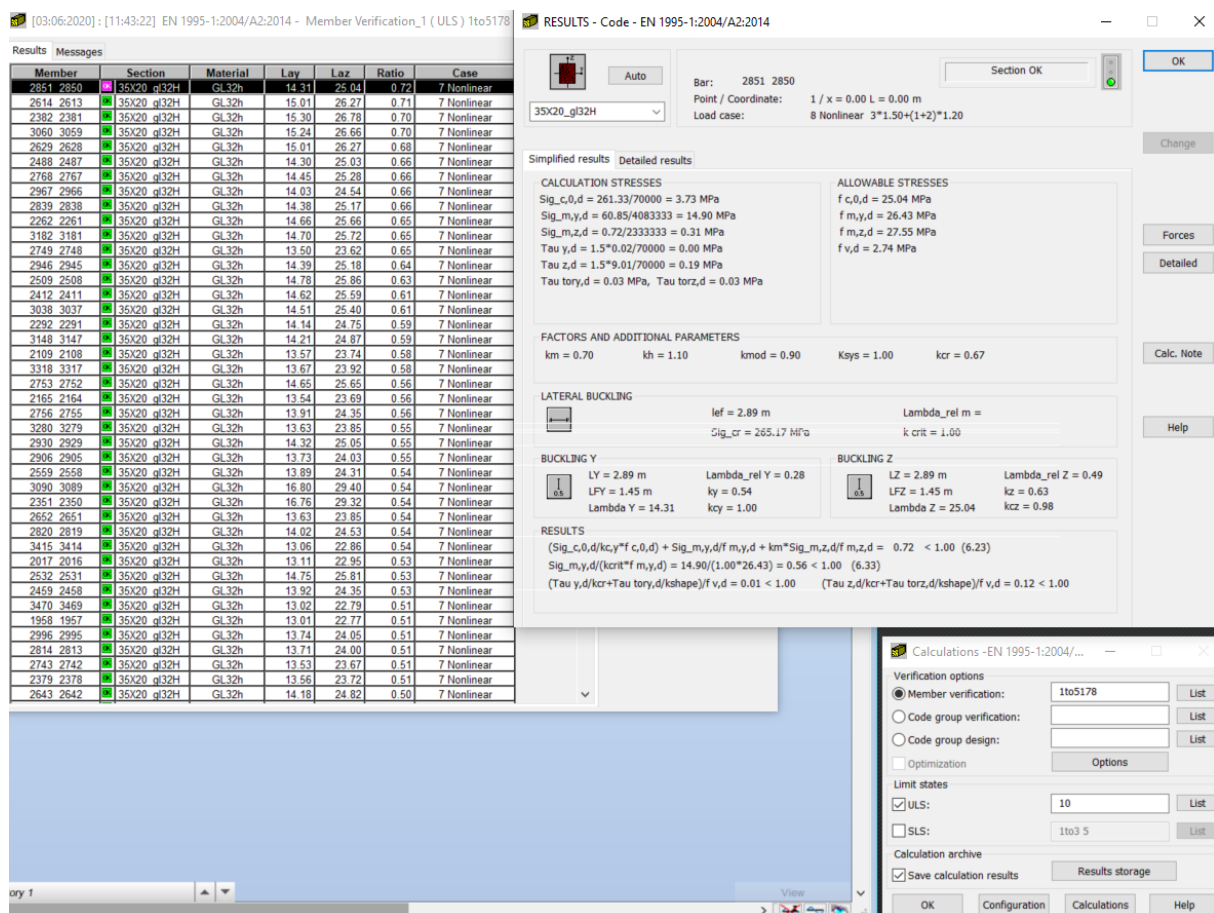
Figure 6.16: Viewport in Robot of timber verification calculations.

6.6 Verification of the parametric workflow

In this section, the gridshell established hitherto in this chapter will be verified by running the structural analysis obtained in chapter 6.4. To get an understanding of how the behaviour of different gridshells, an structural analysis will be done for three different heights (h = 3.0 m, h = 4.5 m and h = 8.0 m), displayed in figure 6.17, and compared to a flat gridshell (h = 0.0 m). In addition to the three different heights, two different connection types, steel and aluminium, will be evaluated based the weight they impose on the structure. The connection types will also be compared to an analysis where the node weight is neglected. Even though this is done as a verification of the parametric workflow obtained in this chapter, trends and patterns from the results will be noted in case they can be used in the case project in chapter 7.

| (a) Gridshell with h = 3.0 m | (b) Gridshell with h = 4.5 m | (c) Gridshell with h = 8.0 m |
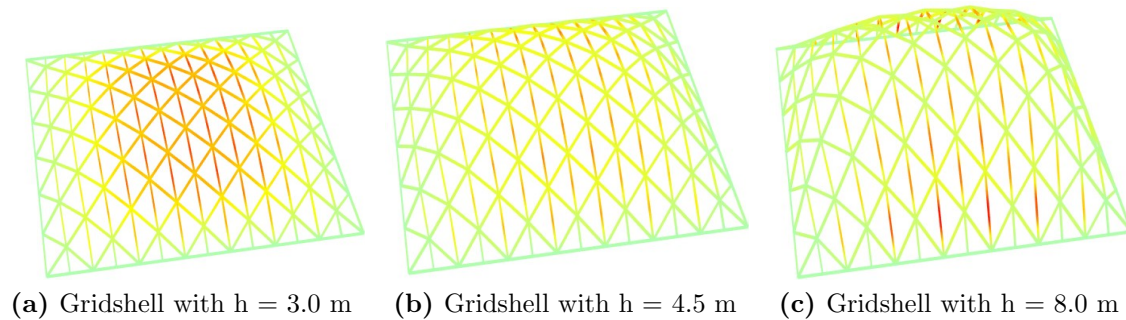
Figure 6.17: Displacement distribution for the three different gridshells.

It is also important to mention that the numbers in the results in this chapter are not obtained for the case of the results themselves. In the same way as the earlier chapters in the parametric workflow, this chapter is made to get the understanding and knowledge of both gridshell structures and the software tools in use. The results will therefore not be of use, except that lessons can be learned from it.

6.6.1 Node weight neglected

As explained in chapter 3.2.1, a structure will be more effective if the transverse loads is carried by normal forces instead of bending and shear action. More of the transverse loads will be carried as membrane actions in a curved structure than in a flat structure like a plate. Table 6.5 displays the results for four gridshells with the same grid structure and with neglected node weight, but different global shapes. The flat gridshell fails to carry the transverse loads in an effective way, and exceeds the material's capacity by 35 % because of the large bending moments and shear forces in the structure.

Table 6.5: Results without node weight.

Gridshell height	h = 3.0 m	h = 4.5 m	h = 8.0 m	h = 0.0 m
Weight	11 360 kg	11 852 kg	13 471 kg	10 932 kg
Max. displacement	1.95 mm	1.65 mm	2.19 mm	108.4 mm
Max. normal force	13.95 kN	12.58 kN	10.82	0 kN
Max. shear force	1.44 kN	1.73 kN	1.93 kN	11.65 kN
Max. bending moment	0.846 kNm	1.06 kNm	1.31 kNm	28.32 kNm
Buckling load factor	34.60	49.76	53.54	-
Utilization	0.158	0.166	0.215	1.35

As already mentioned, one of the main goals for engineers with form finding is to obtain a shape where structure action is exclusively compression forces. With the three heights tested in the parametric workflow in this thesis, all beam elements are in compression. Hence, tension forces do not occur. This, however, would not be the case if the gridshell structure was more complex. Even though the global shape of the gridshell is supposed to contribute to lower the moments and shear forces, the gridshell must be designed in a way such that the capacity is not exceeded. The principle of buckling is discussed in chapter 3.2.2, and as table 6.5 displays, the buckling length factor is adequately above 1.00 for the three gridshells.

Even though it is possible for the material to yield because of shear forces, its more plausible for the connections to yield because of the shear forces in the beam elements. The shear forces tend to peak in the nodes. As explained in chapter 3.2.1, one of the goals with having a curved global shape, is to distribute the forces in a way that causes small moments and shear forces. As can be seen in table 6.5, the flat gridshell has much larger shear forces than the curved ones.

The maximum moments are relatively small for all of the three gridshell heights, compared to the flat gridshell from table 6.5. It can be seen in both the displacements and the BLF that the that these relatively small moments makes an insignificant impact for these gridshells. To find the relation between the gridshell height and maximum moments, multiple different heights were analyzed and the results plotted in the graph in figure 6.18. Table 6.5 displays that for h = 0 m, M_{max} = 28.32 kNm. Hence, when h approaches 0.0, the absolute value of the functions derivative will be greater. It can also be seen from the graph that for h ≤ 0.8, the maximum moment of the gridshell increases when the gridshell height decreases. The function incline here is still relatively small, and thus the maximum moments are not particularly high, even with large values for h.
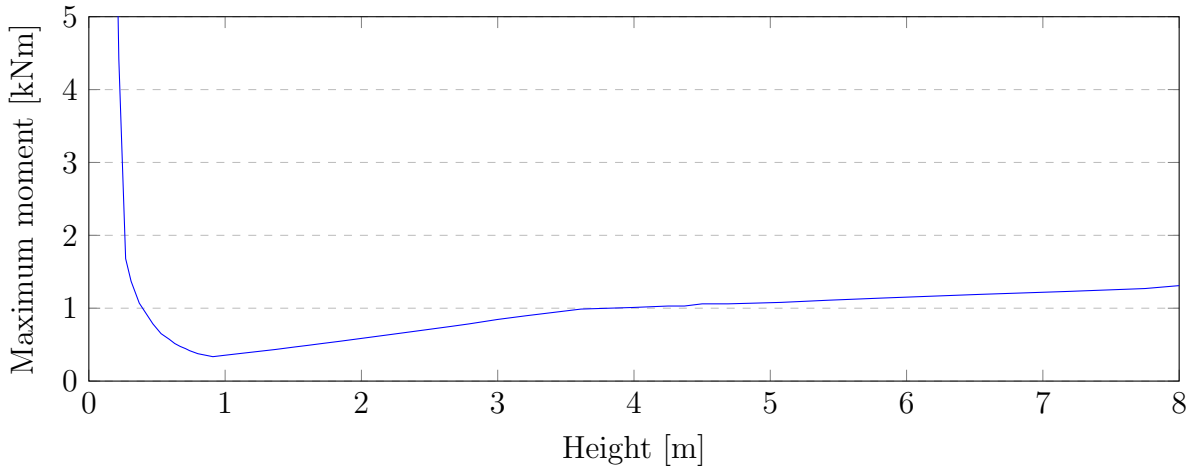
Figure 6.18: Maximum moments for different gridshell heights.

I addition to the maximum displacements, the displacement distribution is interesting for the designer. Figure 6.19 displays how the displacement distribution can be visualized with the Grasshopper script. The figure shows that even though the gridshell with h = 8.0 m has a larger maximum displacement than the gridshell with h = 3.0 m, fewer element has large displacements for the gridshell with h = 8.0 m. The maximum displacements for the gridshell is important. However, the displacement distribution will also be important when designing the structure. As explained in chapter 3.2.2, when the global shape of a structure deflects, it could be less resistant to compression forces, and therefore buckle.
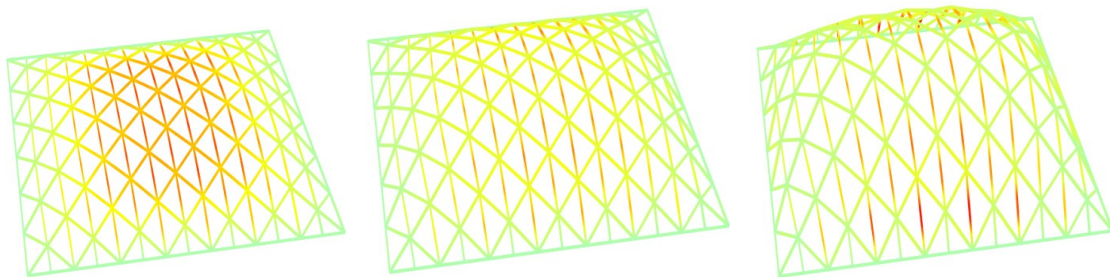
(a) Displacements, h = 3.0 m. **(b)** Displacements, h = 4.5 m. **(c)** Displacements, h = 8.0 m.
Max. displacement = 1.95 mm. Max. displacement = 1.65 mm. Max. displacement = 2.19 mm.

Figure 6.19: The displacement distribution for the three gridshells that is evaluated in this parametric workflow.

6.6.2 Steel nodes included

To evaluate if the node weight should be considered when analyzing a gridshell with steel nodes, the results should be compared to the analysis without node weight. Table 6.6 shows the results for the gridshells with steel nodes. As mentioned in chapter 6.4, the steel nodes can be considered as a point load of 0.846 kN in each node.

Table 6.6: Results with steel nodes.

Gridshell height	h = 3.0 m	h = 4.5 m	h = 8.0 m	h = 0.0 m
Weight	21 014 kg	21 506 kg	23 125 kg	20 586 kg
Max. displacement	2.11 mm	1.73 mm	2.21 mm	121.4 mm
Max. normal force	15.48 kN	13.71 kN	11.61	0 kN
Max. shear force	1.44 kN	1.73 kN	1.93 kN	13.04 kN
Max. bending moment	0.846 kNm	1.06 kNm	1.32 kNm	31.72 kNm
Buckling load factor	31.10	45.53	49.83	-
Utilization	0.173	0.166	0.228	1.52

Changes in forces and displacements

Table 6.7: Percentage change in normal forces in the gridshells.

Gridshell height	h = 3.0 m	h = 4.5 m	h = 8.0 m
Max. normal force	15.48 kN	13.71 kN	11.61 kN
Percentage change	10.97 %	8.98 %	7.30 %
BLF	31.10	45.43	49.83
Percentage change	-10.12 %	-8.70 %	-6.93 %

When adding the point load from the steel nodes, the maximum normal forces in the gridshells are increased, as can be seen in table 6.7. It can be found in the table that the percentage change in the maximum normal force in the gridshell is smaller for the gridshells with a larger global height. Additionally, the BLF is decreasing inversely proportional to the maximum normal forces.

Table 6.6 shows that as opposed to the normal forces, both the shear forces and bending moments has not changed when adding the weight from the steel nodes. This can be explained by the simplex global shape of the gridshell, which makes all of the point loads transfer into compression forces.
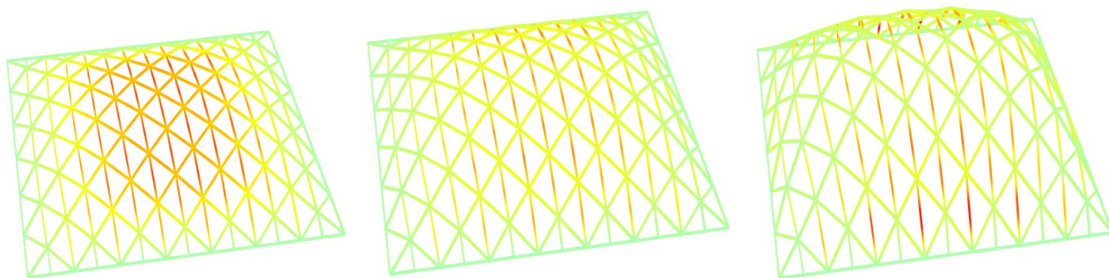
(a) Displacements, h = 3.0 m. Max. displacement = 2.11 mm. **(b)** Displacements, h = 4.5 m. Max. displacement = 1.73 mm. **(c)** Displacements, h = 8.0 m. Max. displacement = 2.21 mm.

Figure 6.20: The displacement distribution for the three gridshells with steel nodes.

Table 6.8: Percentage change in displacements in the gridshells.

Gridshell height	h = 3.0 m	h = 4.5 m	h = 8.0 m
Max. displacement	2.11 mm	1.73 mm	2.21 mm
Percentage change	8.21 %	4.85 %	0.913 %

As is displayed in table 6.8, the maximum displacement increases when steel nodes are included in the analysis. The percentage increase is higher for a gridshell structure with a smaller global height, h. The reason for this could be that the magnitude of the loads are already so large that it does not make a big difference if the point loads from the nodes are added. Table 6.8 also shows that the gridshell with h = 4.5 m is the structure with the smallest maximum displacement. This could be explained by the fact that the global shape of this structure is such that the beam elements is exploited more evenly. Figure 6.20 displays the displacement distribution for the gridshells with steel nodes. Comparing it to figure 6.19, it can be seen that the distribution is basically the same.

Changes in global weight

As described in chapter 6.4, the steel nodes in this case weigh 86.2 kg, which gives a total of 9654 kg for the entire structure. As table 6.9 displays, the nodes increases the global weight of the structure with between 70 - 90 %, depending on the global height of the structure. In this chapter, the snow loads are much larger than these dead loads, which means that even with the loads from the weight of the nodes, snow loads will be decisive when designing the gridshell.

Table 6.9: Percentage change in weight.

Gridshell height	h = 3.0 m	h = 4.5 m	h = 8.0 m	h = 0.0 m
Weight without nodes	11 360 kg	11 852 kg	13 471 kg	10 932 kg
Weight	21 014 kg	21 506 kg	23 125 kg	20 586 kg
Percentage change	84.98 %	81.45 %	71.67 %	88.31 %

If the extra weight from the steel nodes is evenly distributed across the 40 exterior nodes, each exterior node has to carry 241.35 kg, which is equivalent to 2.37 kN. This could make a difference when designing the supports for the gridshells.

6.6.3 Aluminium nodes included

As mentioned in chapter 6.4, the aluminium nodes can be considered as a point load of 0.465 kN in each node. Table 6.10 displays the results for the gridshells with aluminium nodes. The results with aluminium nodes will be compared with the results from the analysis without node weight.

Table 6.10: Results with aluminium nodes.

Gridshell height	h = 3.0 m	h = 4.5 m	h = 8.0 m	h = 0.0 m
Weight	11 360 kg	11 852 kg	13 471 kg	10 932 kg
Max. displacement	2.03 mm	1.69 mm	2.20 mm	121.4 mm
Max. normal force	14.79 kN	13.20 kN	11.26	0 kN
Max. shear force	1.44 kN	1.73 kN	1.93 kN	13.04 kN
Max. bending moment	0.846 kNm	1.06 kNm	1.32 kNm	31.72 kNm
Buckling load factor	32.60	47.34	51.43	-
Utilization	0.166	0.173	0.222	1.52

Changes in forces and displacements

Table 6.11: Percentage change in normal forces in the gridshells.

Gridshell height	h = 3.0 m	h = 4.5 m	h = 8.0 m
Max. normal force	14.79 kN	13.20 kN	11.26 kN
Percentage change	6.02 %	4.93 %	4.07 %
BLF	32.60	47.34	51.43
Percentage change	-5.78 %	-4.86 %	-3.94 %

Much like the steel nodes, the aluminium nodes is not affecting the maximum shear forces and moments in the gridshell. However, the normal forces do increase, and therefore the BLF decrease, as can be displayed in table 6.11.

Table 6.12: Percentage change in displacements in the gridshells.

Gridshell height	h = 3.0 m	h = 4.5 m	h = 8.0 m
Max. displacement	2.03 mm	1.69 mm	2.20 mm
Percentage change	4.10 %	2.42 %	0.457 %

As can bee seen in table 6.12, the maximum displacements increases when aluminium nodes are included in the analysis. However, the increase is not particularly large. It is the gridshell with h = 4.5 m which has the smallest displacements, as it is for both the analysis with steel nodes and analysis without node weight. The distribution is also basically the same as it is for the gridshells where the nodes are neglected and the gridshells with steel nodes. This can be displayed in figure 6.21.
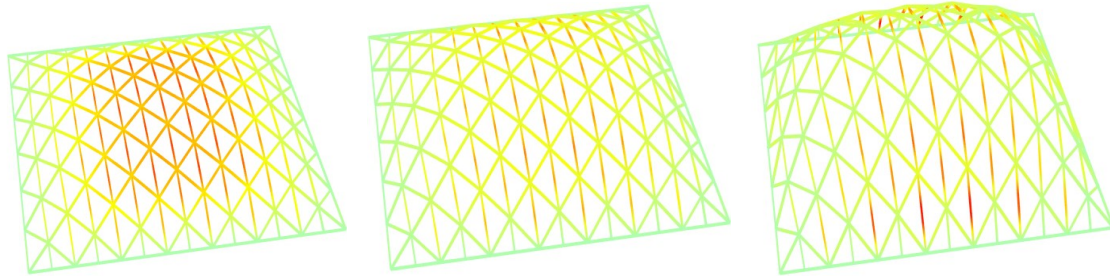
(a) Displacements, h = 3.0 m. **(b)** Displacements, h = 4.5 m. **(c)** Displacements, h = 8.0 m.
Max. displacement = 2.03 mm. Max. displacement = 1.69 mm. Max. displacement = 2.20 mm.

Figure 6.21: The displacement distribution for the three gridshells with steel nodes.

Changes in global weight

As described in chapter 6.4, the aluminium nodes in this case weigh 47.4 kg, which gives a total of 5309 kg for the entire structure. As table 6.13 displays, the nodes increases the global weight of the structure with between 35 - 50 %, depending on the global height of the structure. If the extra weight from the aluminium nodes is evenly distributed across the 40 exterior nodes, each exterior node has to carry 132.73 kg, which is equivalent to 1.30 kN.

Table 6.13: Percentage change in weight.

Gridshell height	h = 3.0 m	h = 4.5 m	h = 8.0 m	h = 0.0 m
Weight without nodes	11 360 kg	11 852 kg	13 471 kg	10 932 kg
Weight	16 669 kg	17 161 kg	18 780 kg	16 241 kg
Percentage change	46.73 %	44.79 %	39.41 %	48.56 %

6.6.4 Comments on the verification of the parametric workflow

The aim of this chapter was not to optimize a gridshell for any one specific criteria, but instead to show how geometry and structural data can be manipulated in a parametric workflow. The setup was created in such a way that it will be easy to change parameters as desired. The method investigated here will therefore serve as a general framework for investigating different design optimization objectives in the case project in chapter 7. This being said, the comparative results obtained through this parametric workflow does provide a definitive description of the interaction between form and structural action for a gridshell structure. The results therefore provides a more explicit comprehension of how adjusting the different parameters affect the system as a whole.

The results show that the weight difference between the different material choice for nodes do have an impact on the forces in the structure. Notably, it materializes as greater displacements and thus a smaller capacity margin. However, the maximum forces in the gridshell, and therefore also the displacements, has not been significantly affected by

including the node weights. Therefore, it has to be decided whether the advantages of using aluminium, as discussed in chapter 3.3, is worth the increase of costs of production. This could depend on the foundations of the structure. The global weight of the structure is carried by the foundations, and the global weight of the structure is the only variable with a significant difference when using steel or aluminum nodes. Alternatively, for an extremely light weight gridshell where the nodes make up the majority of the total weight, the material choice could become more of a consequential structural issue. This would give rise to other issues regarding bearing capacity, however, especially for permanent outdoor structures.

During this chapter many parameters were kept unchanged to form a basis for comparison, but that also means that the results have some limitations. Since the maximum utilization for the members where low in this study, it can be expected that a more effective structure would be more sensitive to the additional loads provided by the inclusion of node weight. In chapter 3.2.1 it was mentioned that unevenly distributed loads and point loads can disturb the effective structural action of shells. It could therefore be expected that using a coarser grid with fewer nodes would distribute the extra loads more unevenly, which in turn would be expected to produce larger relative bending moments and shear force in the members.

6.7   Summary of the parametric workflow

In this chapter a discrete timber gridshell has been constructed using Grasshopper. It has been shown how the global shape of a gridshell can be optimized with dynamic relaxation with regard to various variables. Subsequently, the the parametric workflow was verified by analyzing the structural performance of the gridshell for three different heights. Both steel nodes and aluminium nodes was used in the verification, both to clarify how to change node material in the Grasshopper script, and to get a hint if the node weight makes any difference, which will be investigated more closely in chapter 7.

To verify statements made in chapter 3.2, that curved shell structures obtain better structural performance than flat shell structures, gridshells with a curved global shape was compared to a flat gridshell. As can be read in chapter 6.6, the gridshells with a curved global shape will suffer from much smaller forces acting on them, than if the gridshell would have been flat. Of the three gridshells investigated, the gridshell with an h/b-ratio of 0.225 has the lowest maximum displacements out of the gridshells that have been analyzed, regardless of the node type. This can give an indication of which h/b-ratios will yield the best structural performance in the case study in chapter 7. Even though the design in this chapter is of one specific structure, that is worth noting.

For a timber gridshell to work as desired, the nodes is essential. The weight of the nodes isolated is not very large. However, a timber gridshell is a relatively lightweight structure, which makes the weight of the nodes a large part of the total weight of the structure. Therefore, the node weights should be included in an analysis to examine whether the nodes will make a difference for that specific project. The node weights can also be of great importance to the design of the foundations.

As explained initially in this chapter, the results from the parametric workflow are not important in itself. The chapter is used to illustrate and explain in detail how gridshell structures can be designed in a parametric way, how to obtain a Grasshopper script with the possibilities to optimize based on different parameters and how to get the desired results from a structural analysis. Therefore, an optimization for the different parameters is not done in this chapter. Further, the focus of the case project in chapter 7 can be on the actual results and what they represent.

7   Case project: British Museum

7.1   Introduction of the case project

Chapter 6 provides a framework for design and analysis of gridshells in a parametric environment. A complete design of a new structure including shape, elements and details is outside the scope of this project, but a realistic design task is still needed to study the competing issues of aesthetics, structural performance and manufacturing feasibility. Therefore, the known building of the British Museum Great Court Roof presented in chapter 2.2.2, is selected to provide a specific case for design and evaluation of a gridshell. The steel structure at the British Museum will in this thesis be redesigned into a timber structure, with new generalized node principles facilitated based on chapter 3.3.

Timber has been chosen because it is a cheap, lightweight and sustainable material. Possibly incorporating aluminum connections on top of this, will make for a very lightweight structure. Facilitating cheaper materials and logistics will both support gridshells as a more viable structure of choice in Norway, and at the same time have the construction be sustainable. Since timber gridshells are relative lightweight, snow loads will be significant. To make the case project realistic for Norwegian climate, load actions are selected according to Norwegian design rules, introduced in chapter 4. Snow loads in Trondheim will be significantly greater than that of London. Hence, the actions on the timber gridshell in this case project will be greater than the actions on the actual Great Court Roof in London.

There were restrictions on both global height and glass panel size when the Great Court Roof was designed. The aim of the case project is to investigate the possibilities to improve the shape of the Great Court Roof, without these restrictions, with regard to parameters applied to both structural performance and repetitive building parts.

7.2 Materials and constraints

As in chapter 6, the shell structure evaluated is a discrete segmented timber gridshell, with nodes of either steel or aluminium.

Beam elements

The original Great Court Roof of the British Museum is made out of hollow steel members (RHS). The RHS steel members have all a standard width of 80mm due to the glass support detail. The cross sectional height varies from 80mm to 200mm according to their structural requirements, where the smallest height of 80mm is near the Reading Room and increases towards the outer rectangular perimeter [21].

Based on the results of a previous study done for the British Museum Great Court [44], the conversion to timber will use GL32h members of dimensions 200x350 mm. Table 7.1 show the material properties for GL32h. In the parametric workflow described in chapter 6, GL30h is used as material. It is however, also shown in that chapter how to change the material properties in the Grasshopper script.

Table 7.1: Material properties for GL32h [12].

Material	$E_{0,g,05}$[MPa]	$G_{g,05}$[MPa]	$f_{m,k}$ [MPa]	ρ[kN/m^3]	α_T [1/C°]
GL32h	11 800	540	32	4.4	$5.0\cdot10^{-6}$

In chapter 4.3 the material constraints of timber is described, and there it can be read that when designing in ULS, some factors has to be taken into account. The design strength is obtained as shown in equation 7.1. The factors k_{mod} and γ_M can be found in the National Annex in NS-EN 1995 1-1 [13], and they are displayed in table 7.2. The value for k_{mod} varies and depends on the defined load duration for each loads applied on the structure in the ULS calculations. When only permanent loads is considered, the k_{mod} is set to 0.6. For ULS combinations with snow loads, the k_{mod} factor is set to 0.9 according to the National Annex in EC5, which will be used for this case study. With the new information, the design strength, $f_{m,d}$, equals 25.04 MPa, which is the strength used in the Grasshopper script.

$$X_d = k_{mod} \cdot R_k/\gamma_M \tag{7.1}$$

Table 7.2: The factors k_{mod} and γ_M for glulam [13].

Material	k_{mod}	γ_M
GL 32h	0.9	1.15

Nodes

The nodes are assumed to be rigid. That is, all transitional and rotational degrees of freedom are constrained. Thus, moments can be transferred between the beam elements. Node characteristics and capacity is a large topic, and will not be discussed in detail in this thesis. It will, however, be discussed in the thesis written by Ragnhild Myrnes and Kristin Kilvik Skeide, which is a part of the same project as this thesis. In this thesis it is assumed that the nodes not will yield, and the Great Court Roof will be investigated regarding other parameters.

Supports

The unique structural system of the Great Court Roof of the British Museum is discussed in detail in chapter 2.2.2. The Great Court Roof has many boundary conditions due to the buildings it rests on top of. In this case study the boundary conditions is simplified and all supports are assumed pinned around the boundary to achieve the usual arch effect from a double curved roof. The total weight of the roof is also not considered according to the original conditions.

Displacements

Displacements in a shell structure can be crucial and in the worst case scenario lead to buckling of the structure. Buckling leading a shell structure to collapse is discussed in chapter 3.2.2. The maximum structure span divided by 200 gives the maximum value of displacements. This gives a maximum displacement value of 140 mm for the Great Court Roof [23].

Global displacements and beam deflections in timber beams can change over time due to long term effects as creep. Long span timber gridshells can be prone to creep deformations and decrease the overall structural capacity years after its completion. Deformations due to long term effects is not investigated in this thesis and only instant deflections are considered.

7.3 Loads on the roof

As described in chapter 4.1, design values of loads has to be used. Two formulas, 6.10a and 6.10b is introduced, where the formula that gives the least favourable load combination is the one to be used. In this case project, the snow load are the leading variable action. The snow load is also by far the load working on the roof with the largest magnitude. Thus, the formula 6.10b will give the least favourable results, and therefore 6.10b is used.

7.3.1 Dead laods

Dead loads are the permanent loads that will continously be the same over time. The only dead loads working on the Great Court Roof of the British Museum is weight of the structure it self. It is suitable to separate the dead loads from beam elements, panels and nodes according to their structural action, which is elaborated further. Because of the fact that 6.10b from chapter 4.1 gives the least favourable results, to get the design dead loads, they needs to be multiplied with the factor $\xi\gamma_{\text{Gj,sup}} = 0.89 \cdot 1.35 = 1.20$.

Weight of beam elements

The weight of the beam elements is simply the materials density multiplied with the total volume of beam elements of the structure. Therefore, the weight of beam elements depends on the material used, which in this case project is GL32h, the global shape of the roof, and both shape and density of the grid. These are parameters that is considered when trying to optimize the Great Court Roof.

In chapter 6.4, it can be read about how different loads can be included in the Grasshopper script using Karamba. To implement the weight of the beam elements, a Karamba component with gravity loads has to be used in the Grasshopper script. This is done in the exact same way as in chapter 6. The gravity loads component will depend on the parameters mentioned in the last paragraph, as well as the cross sections in use. To get the design load from the beam elements, however, the gravity load component needs to be multiplied with a factor of 1.20.
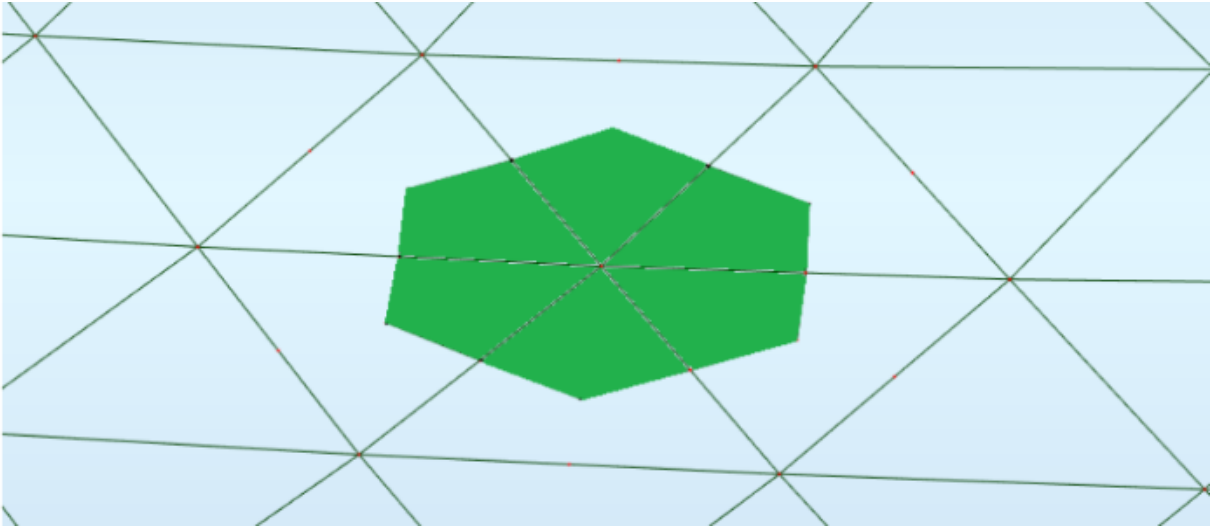
Weight of glass panels

As mentioned in 2.2.2 the gridshell of the British Museum is covered by a layer of double pane glass panels. These are only connected to the gridshell at each node. Since this project do no include any specific node calculations, a suitable way to adapt the glass panel loads in the Grasshopper script, is to convert them to point loads acting on each node. For the original topology of the British Museum gridshell these glass panels are triangulated, like the grid topology. Thus, each of the point loads acting at the nodes is defined by the weight of one third of a nodes adjacent panel area. This is displayed in figure 7.1. The weight of the glass panels is 60 kg/m^2 [21]. This gives:

$$P = m \cdot a = m \cdot g \tag{7.2}$$

$$p_g = 60 kg/m^2 \cdot 9.81 m/s^2 = 588.6 N/m^2 \approx 0.59 kN/m^2$$

The total area of the Great Court Roof and the number of interior nodes can be found in the Grasshopper script. They will depend on the grid pattern and the global shape, which in this case project is changed as a part of the optimization. For the original global shape, however, there are 1566 interior nodes, and the total area of the structure is estimated at 6254.85 m^2.

Figure 7.1: The weight of the glass panels is distributed to the adjacent nodes.

The magnitude of the point load in each node depends on the size of the adjacent glass panels, which for the original topology varies. The point load magnitudes will therefore also vary for each node. To achieve this, the Karamba components *Loads* (see figure 7.3), allow for a uniform mesh load to be divided into point loads which in this case will be the nodes. The weight from the glass panels is distributed as point loads determined by the areas of the adjacent glass panels. This is displayed in figure 7.1.

To get a sense of the magnitude of the point loads, the mean point load from the glass panels is calculated. The mean area per node can be determined as in equation 7.3, which shows that the average node will have to carry the weight from 3.994 m^2 of glass.

$$Area\,per\,node = \frac{6254.85\,m^2}{1566\,nodes} = 3.994\,m^2/node \tag{7.3}$$

And thus, the mean value of the point loads from the glass panels for each node, for the original global shape, is:

$$P_{g,\,mean} = 3.994\,m^2 \cdot 588.6\;N/m^2 = 2350.87\;N \tag{7.4}$$

The mean value however, will not be used in the Grasshopper script, as the *Loads* component makes the distribution more accurate. The load given in equation 7.2 is used in the Grasshopper script to get the results as accurate as possible.

(a) Local   **(b)** Global   **(c)** Global projected to global plane
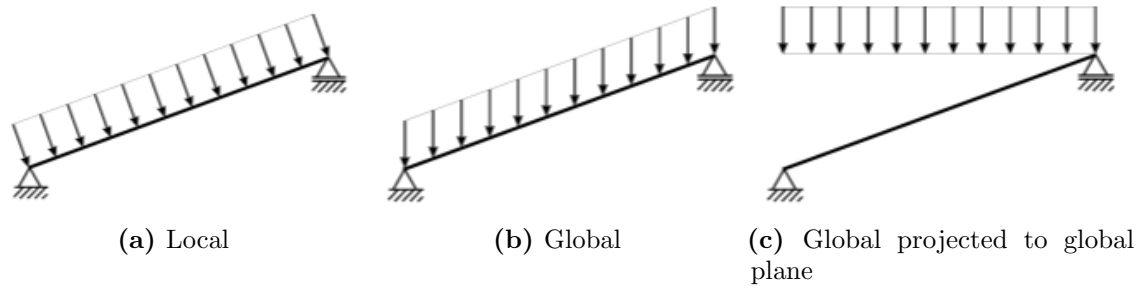
Figure 7.2: The orientation of loads on a mesh using the *Loads* component [10].

Distributed loads, as the loads from the glass panels are, can be considered in one out of three different ways, which is displayed in figure 7.2. The loads from the glass panels is assumed to act on the gridshell, but in the directions of the global coordinate system directions, which is displayed in figure 7.2b.
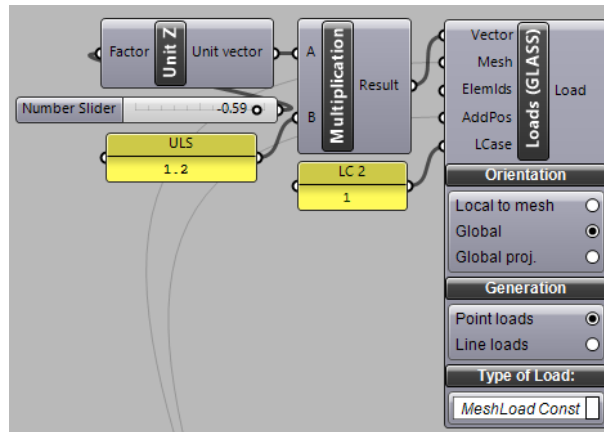
Figure 7.3: Karamba plug-in for loads. Surface loads from weight of the glass is handled as a global projection to the surface and distributed as point loads to the nodes.

As explained earlier in this chapter, to get the design load from the glass panels, $p_{Ed.g}$, the load from the panels p_g, needs to be multiplied with a factor of 1.20. Thus:

$$p_{Ed.g} = 706.3N/m^2$$

Weight of nodes

In this case project, it is investigated there are any structural benefits of using aluminium nodes instead of the cheaper and more common version that is steel nodes. The nodes are described in chapter 6.4, and table 7.3 shows the results from the calculations done for a cross section of 350x200.

Table 7.3: Node properties.

Material	Total node weight	Weight per node	P_n	$P_{Ed.n}$
Steel	155 677 kg	86.2 kg	0.846 kN	1.015 kN
Aluminium	85 604 kg	47.4 kg	0.465 kN	0.558 kN

7.3.2 Live Loads

Live loads are temporary or short term loads. Environmental loads are typical examples for live loads. There are many different environmental loads that could have been examined, such as wind, snow, temperature and seismic loads. In this thesis, however, only snow and wind loads is considered.

Because of the fact that 6.10b from chapter 4.1 gives the least favourable results, to get the design live loads, they needs to be multiplied with the factor $\gamma_Q = 1.50$, if the live load is unfavourable. If the live load is favourable, however, $\gamma_Q = 0$.

Snow loads

In this thesis, all structures is investigated as if they were in Trondheim. This is taken into account in chapter 4.2, where it its discussed how to calculate the snow loads. This can be seen in equation 7.5. C_e and C_t was discussed in chapter 4.2 and they both equal to 1.0. s_k is the characteristic snow load, and is given as $s_k = 4.50$ kN/m^2.

$$s = \mu_4 C_e C_t s_k \tag{7.5}$$

If the conditions are assumed undrifted, the snow load form factor, μ_4 should be set to 0.8, and if not μ_4 has to be calculated for the specific structure. This is done in equation 7.6. The h/b-ratio has to be decided. The specifics of the Great Court Roof is found in table 7.4.

Table 7.4: Specifics for the Great Court Roof.

Height, h	6.786 m
Width, b_1	71.52 m
Width, b_2	$\frac{1}{2} \cdot 95.33$ m $= 47.67$ m.
Design width, b	b $=$ min$\{b_1; b_2\} = 47.67$ m

$$\mu_4 = 0.2 + 10 \cdot h/b \tag{7.6}$$

Using the specifics from table 7.4 and equation 7.6, μ_4 is calculated to be 1.624. Further, the design snow load is calculated for both drifted and undrifted conditions. The results can be found in table 7.5.

Table 7.5: Design snow load, s, for drifted and undrifted conditions.

Condition type	μ_4	s	s_{Ed}
Drifted	1.624	7.31 kN/m^2	10.97 kN/m^2
Undrifted	0.80	3.60 kN/m^2	5.40 kN/m^2

The snow load is distributed the same way the loads from the glass panels are distributed, which is displayed in figure 7.1. To achieve this in the Grasshopper script, the *Loads* component is used in the same way as for the glass panels. The snow load however, is not working on the gridshell in a global coordinate system. The snow load is distributed on the area that results from projecting the gridshell to global coordinate planes, which is displayed in figure 7.2c [10].

Evaluation of the effect from snow loads is done with both undrifted and drifted conditions. Snow loads can give asymmetric loading when it's not evenly distributed, as for the drifted case. Unevenly distribution of loads for shell structures is not ideal and a comparison of the undrifted and drifted condition can be relevant to investigate how the structure behaves.

Wind loads

Wind loads are short term loads acting unevenly on a exposed surface, giving both pressure and uplift forces. Wind tunnel test done over the Great Court roof showed that the outer perimeter of British Museum separates the wind flow and decreases potential wind loads on the roof [21]. The test gave only small forces and consistently negative pressure (uplift). From their calculations, the fifty year uplift force does not exceed 0.3 kN/m^2 which is well below the total weight of the roof.

In chapter 4.1, it is explained that the factor γ_Q, that should be multiplied with accompanying variable actions, should equal to 0 if the action is favourable. This means that the wind loads not will be taken into account in this chapter.

7.4 Results for the original shape

The original shape of the Great Court Roof of the British Museum can be seen in figure 7.4. The shape and grid pattern is the same as the original construction, but will be analysed using the constraints and material presented in chapter 7.2. In this subsection, the analysis and evaluation criteria developed through chapter 5 & 6 will be tested on the original shape of the Great Court Roof. The results obtained will be used as a basis for comparison with the optimized shapes presented further on in this chapter.
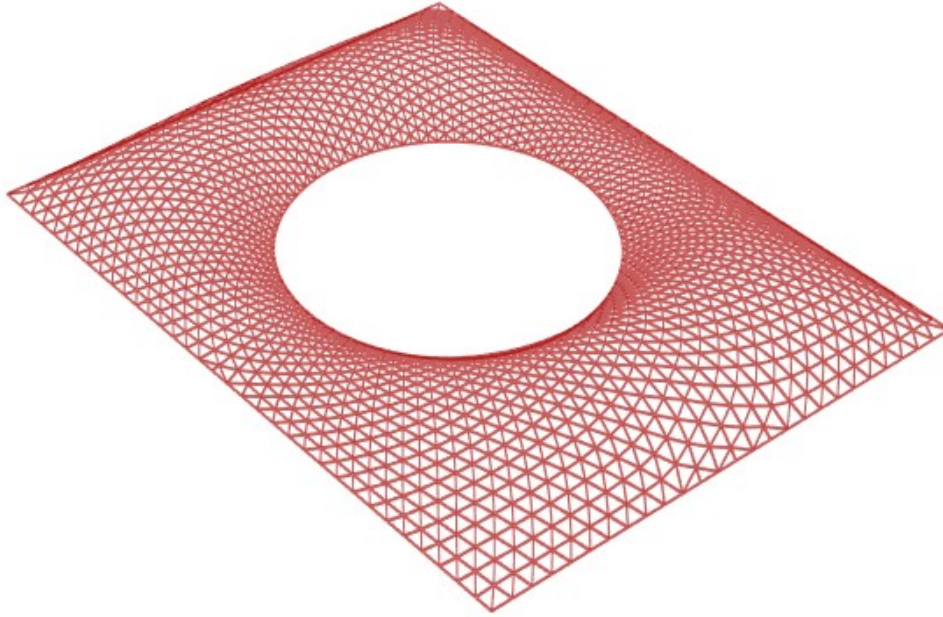

Figure 7.4: The original global shape and grid pattern of the Great Court Roof of the British Museum.

Table 7.6: Structural data for the original shape of the Great Court Roof.

Node type	Nodes neglected	Aluminium nodes	Steel nodes
Weight of beam elements	331 802 kg	331 802 kg	331 802 kg
Weight of nodes	0 kg	85 604 kg	155 677 kg
Total weight	331 802 kg	417 406 kg	487 479 kg
Max. displacement	128.82 mm	131.30 mm	133.35 mm
Max. compression force	472.78 kN	481.75 kN	489.13 kN
Max. tension force	152.65 kN	156.59 kN	159.82 kN
Max. shear force	18.35 kN	18.71 kN	19.00 kN
Max. bending moment	67.13 kNm	68.34 kNm	69.33 kNm
Min. BLF	6.56	6.44	6.35
Utilization (EC5)	0.75	0.77	0.78

Table 7.6 displays the structural data from the analysis of the original shape of the Great Court Roof. The results are for steel nodes, aluminium nodes and for the gridshell where

the weight of the nodes is neglected. It can be seen in table 7.6 that variations in results are relatively small. The global displacement pattern is also distributed similarly for the three different cases tested. This is displayed in figure 7.5, where it can be seen that there are barely a difference in the displacement distribution for the three node types. It can be noted that due to the Reading Room (circular boundaries) being off centered by 5 m towards north, the displacements is largest for the longest span.

(a) Node weight neglected.   **(b)** Aluminium nodes.   **(c)** Steel nodes.
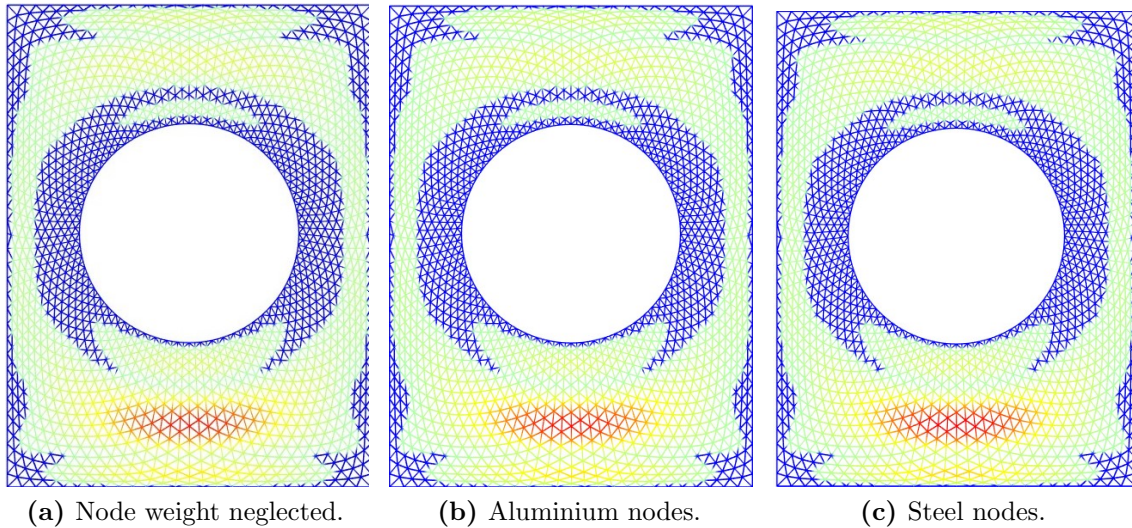
Figure 7.5: Distribution of displacements for the different node conditions. Red colour displays highest values of displacements, while blue has zero or small values of displacements.

Repetitive nodes

Investigating repetitive building parts for the original shape of the British Museum was done using the custom developed Angler component, described in chapter 5.

(a) No tolerance   **(b)** +/- 1 degree   **(c)** +/- 1.5 degrees
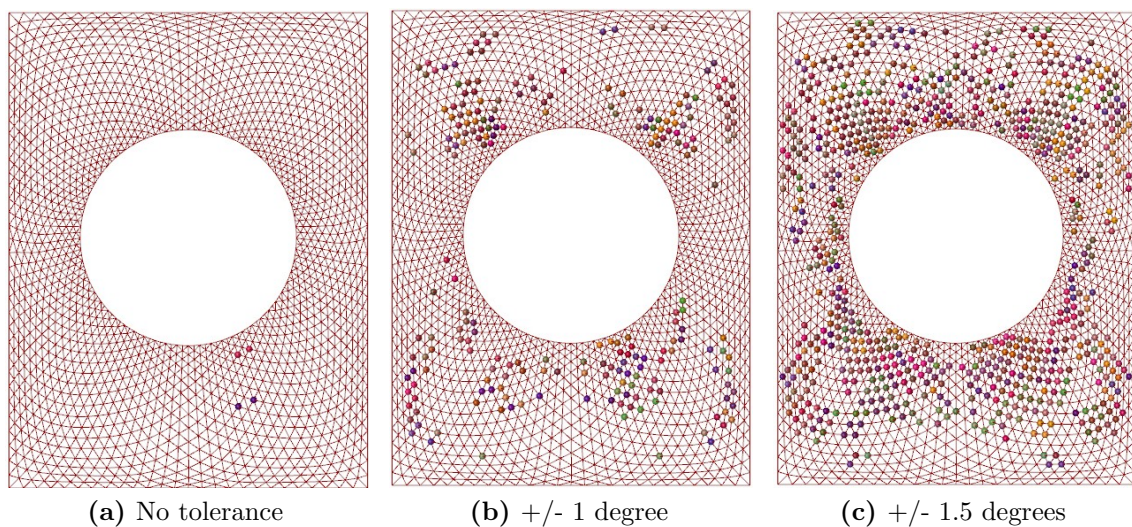
Figure 7.6: Similiar node groups distribution for different angle tolerances.

Since Grasshopper allows for completely precise angle calculations, having no tolerance between identical node angles is not particularly insightful for investigating identical building parts for this particular structure. Comparing figure 7.6b and 7.6c, however, it can be seen that small changes in tolerance has a significant impact on the amount of similar nodes identified by the component. Having used rigid connections as a basis for modeling, means that the reliance on tolerance should be kept to a minimum. However, promoting a generalized approach in regard to any specific node designs, a tolerance of +/- 1 degrees for all angles defining a specific nodes geometry will be used as a basis for comparison between the different shape and topology optimizations. As can be seen in table 7.7, for the original shape of the British Museum this results in 100 different groups of 219 identical nodes.

Table 7.7: Identical nodes and group size. +/- 1 degree of tolerance.

Number of identical nodes	Number of groups
6	1
4	3
3	9
2	87
Identical nodes total	Groups Total
219	100

Excluding supports, the total number of nodes in the Great Court is 1566. This means that with the tolerance used, there are still 1347 unique node configurations that must be fabricated individually. Proceeding, the term *repetitive nodes* will refer to all groups containing one or more identical nodes. This represent the same number as *identical nodes total* in table 7.7. This will be set in comparison to the total number of nodes, and the number of unique node configurations in a particular gridshell model for evaluation.

7.5 Optimization of the shape

The aim of this case project is to investigate and optimize the global shape and topology of the Great Court Roof gridshell, with respect to repetitive nodes and the structural performance. This is done in accordance to the procedure introduced in the parametric workflow in chapter 6 and information obtained earlier in this chapter.

7.5.1 Global shape optimization

The global shape of the Great Court Roof was originally designed so that it would not be able to be seen from the ground level outside. The optimization in this chapter will investigate what global shape give the most structurally efficient configuration of the gridshell if this height restriction is neglected. Several parameters needs to be taken into account for this, such as maximum displacement, total weight and the buckling load factor.

The original height of the Great Court Roof is 6.786 m, which gives a h/b-ratio of 0.142. Compared with the models examined in chapter 6 that had h/b-ratios 0.150, 0.225 and 0.400, respectively, gives an indication that a ratio of 0.142 is relatively low, and probably not optimal with respect to the structural efficiency. A greater h/b-ratio can therefore be expected to make the structural performance better. The Great Court Roof is a much more complex structure than the gridshell investigated in the parametric workflow. Therefore, it will not necessary behave exactly in the same way. However, it can be expected to be similarities to that behaviour in terms of stress distributions. The global shape of the Great Court Roof will therefore be changed in order to investigate which global height give the best results in terms of structural performance, and to whether or not changing the shape affect the amount of repetitive nodes of the structure at all.

The load case in this optimization attempt will be applied as discussed in chapter 7.3, with assumed undrifted conditions for the snow load. The node weight is neglected in this part of the case project, as it was shown in chapter 7.4 that the additional loads imposed from node weight is not significant for the performance of this structure. If an improved shape is found, however, the node weight can be added for validating results.

Form finding, by the use of dynamic relaxation, will be used to investigate improved shapes for the British Museum gridshell. As already mentioned in 5.2, the custom developed Dynamic Relaxation component will not be used in this chapter due to limitations in computing power. Kangaroo, discussed in chapter 3.5.2 and exemplified in the parametric workflow of chapter 6 will be used instead. The gridshell will be investigated for heights between 6.79 m and 15.24 m, to get a better understanding of the global shape influence on structural behavior for this structure, and to investigate if the number of repetitive nodes are affected by the h/b-ratio. Figure 7.7 displays the investigated height range, where figure 7.7a displays the lowest height, which is the height of the original shape of the Great Court, and figure 7.7b displays the largest height investigated.
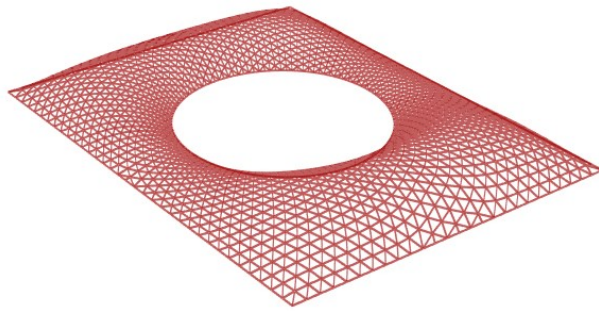
**(a)** The original shape of the Great Court Roof.
h = 6.79 m.
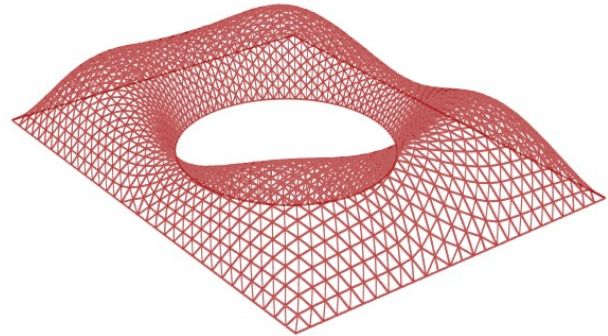
(b) The largest height investigated.
h = 15.24 m.

Figure 7.7: The lowest (a) and largest (b) heights investigated in this chapter.
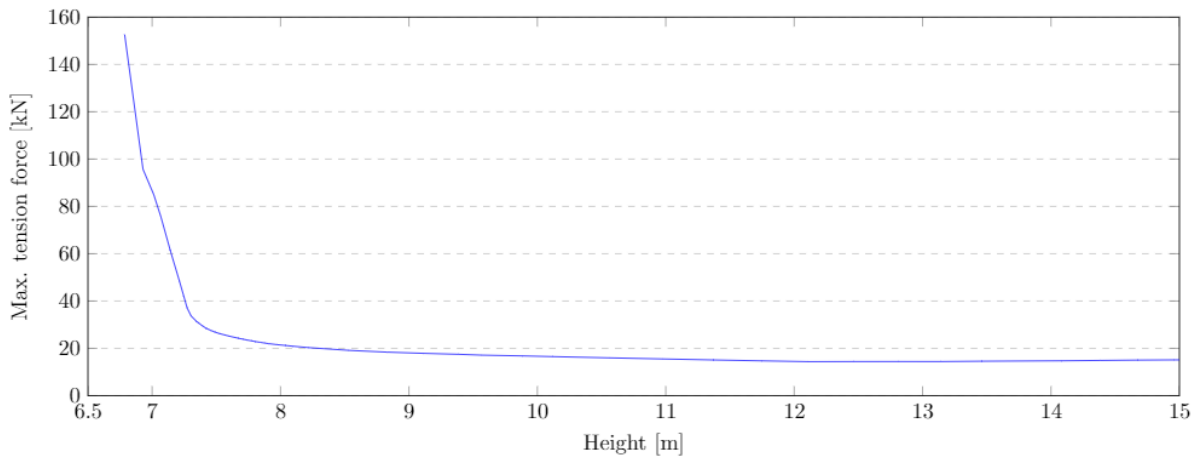
Maximum forces

The distribution of forces can give a good indication on how efficient the structural performance of a gridshell is. As explained throughout chapter 3, shell structures have excellent capacity when their curvature allow them to carry loads primarily through membrane action. Tension and bending moments should therefore be kept to a minimum, particularly when the material in use is timber. Table 7.6 from chapter 7.4 show that there are tension forces in the Great Court Roof, with the maximum being relatively high. By changing the global shape, and thus the h/b-ratio, the structural performance can be improved by minimizing the tension and bending moments originating from the relatively flat original design.

The graph in figure 7.8 displays the maximum moment in the gridshell for different global shapes, where the global shape is differentiated by its global height. The graph shows that the maximum moments in the structure decreases as the h/b-ratio increases. The graph also shows that the decrease is much greater at first, until h ≈ 7.3 m, which gives a h/b-ratio of 0.153, and that it evens out at h ≈ 9.1 m, which gives a h/b-ratio of 0.191.
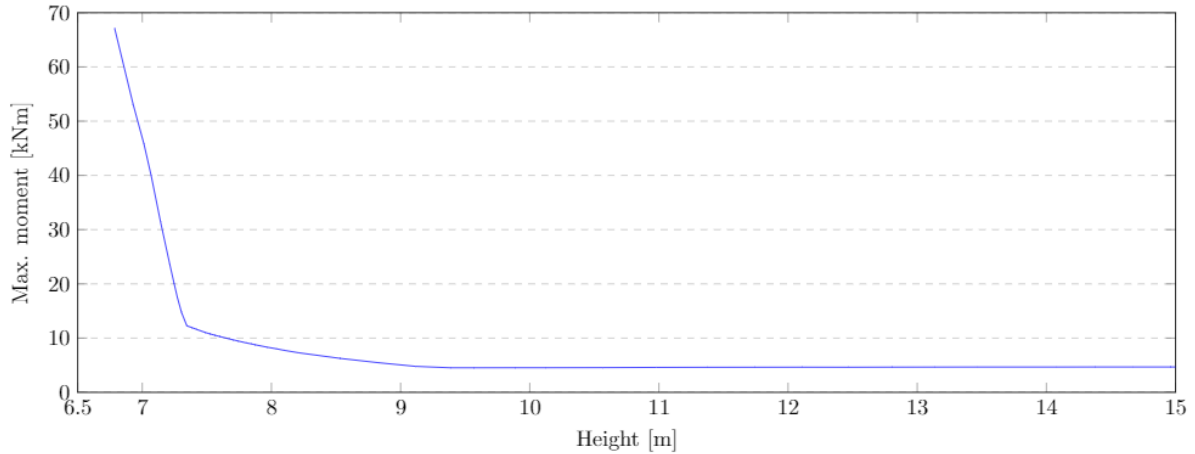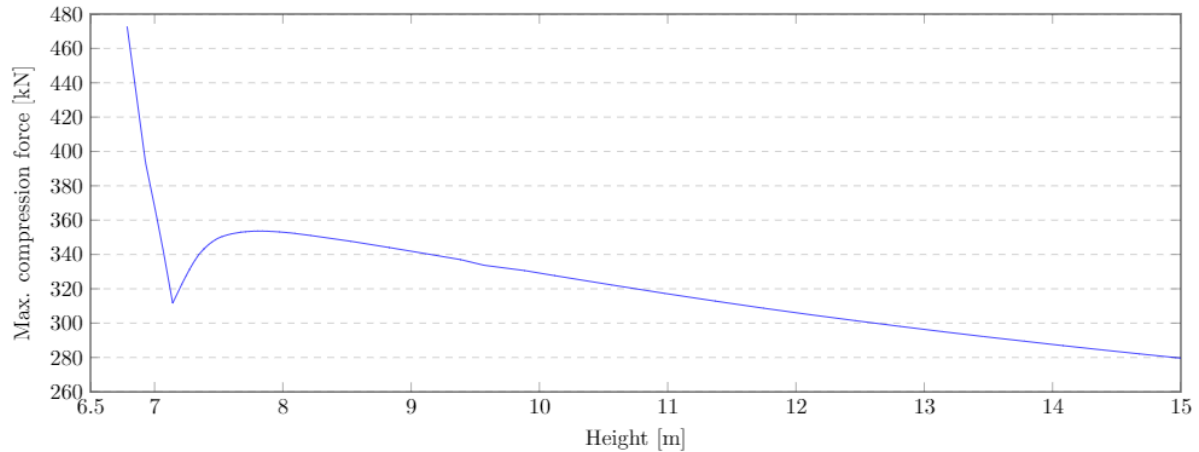
Figure 7.8: The maximum moment in the Great Court Roof depending on the global shape, which is differentiated by its height.

The graph in figure 7.9 displays the difference in maximum tension for the different global shapes. The maximum tension force in the structure decrease rapidly when changing from the original shape one with a height of h ≈ 7.4 m, which gives a h/b-ratio of 0.155. The maximum tension keeps decreasing steadily, but with a much lower rate for a h/b-ratio larger than 0.155.

Figure 7.9: The maximum tension force in the Great Court Roof depending on the global shape, which is differentiated by its height.

Comparing the two graphs above, the behaviour for maximum moment and maximum tension seem almost perfectly correlated for the changes in height. Both are rapidly decreasing before the h/b-ratio of approximately 0.15 is reached. After that the derivative of both graphs tend to zero.

The graph in figure 7.10 displays that the maximum compression force in the structure has a trough for the h/b-ratio in the interval between 0.147 and 0.153 (7.0 m < h < 7.3

m). In addition to the trough, the maximum compression force will be lower than the trough for the h/b-ratios of 0.231 and higher (h ≥ 11 m). Compared to the original shape however, the maximum compression forces are relatively low for all h/b-ratios above 0.147.


Figure 7.10: The maximum compression in the Great Court Roof depending on the global shape, which is differentiated by its height.

In chapter 3.4 it is explained that one of the goals of form finding is to obtain the shape with the least amount of moment and tension forces. However, large maximum compression forces in a structure is not necessarily desired, and can lead to buckling. In chapter 3.2.2 it is explained that an efficient shell structure would still need to handle bending action to avoid this. The distribution of forces is also an important issue, and lowered maximum forces is a sign of better distribution overall.

Structural performance

The structural performance cannot be based on maximum forces and moments alone, even though they can provide an indication. The buckling load factor, BLF, has to be calculated separately. This is especially important for the structural validity of gridshells. The concept of global buckling and the buckling load factor is discussed in both chapter 3.2.2 and chapter 6.13. A system will collapse due to global buckling if the BLF ≤ 1.0, but due to the complexity of the gridshell structures it can be desired to achieve a BLF as high as possible. As can be seen in figure 7.11, there will not be a collapse due to global buckling for the global shapes that has been investigated. However, the graph peak at the h/b-ratio at 0.147 (h = 7.0 m). The peak can be explained with figure 7.8 and figure 7.9, which shows the graph for respectively maximum moments and tension forces. The minimum BLF decreases for the same h/b-ratios the maximum moment and tension forces decreases. This can be explained by the length of each beam element being increased when the h/b-ratio is increased. However, as explained, and which can be seen by the graphs in figure 7.8, 7.9 and 7.10, the forces is more evenly distributed with a larger

h/b-ratio. Moreover, the magnitude of the BLF is relatively large for all the global shapes investigated.
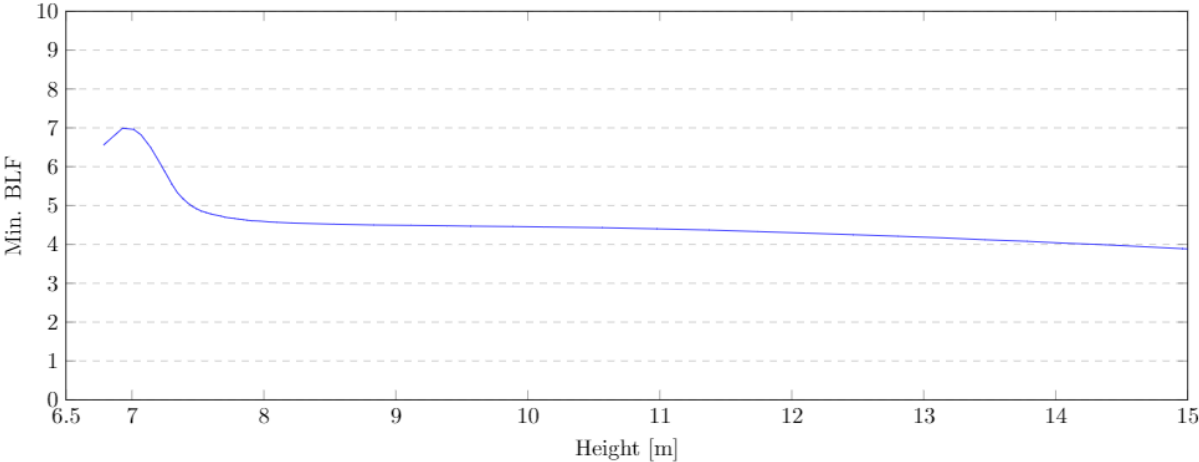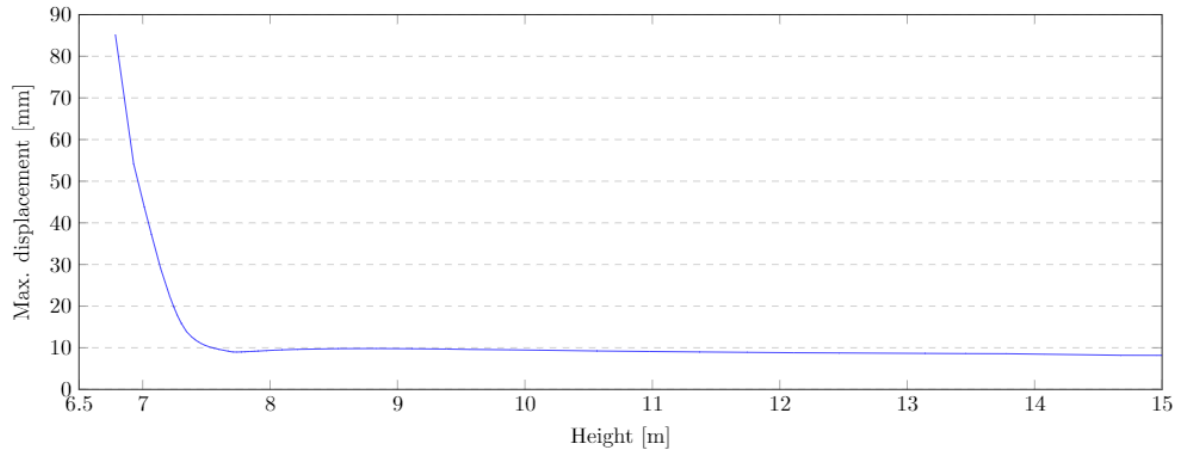

Figure 7.11: The minimum buckling load factor in the Great Court Roof depending on the global shape, which is differentiated by its height.
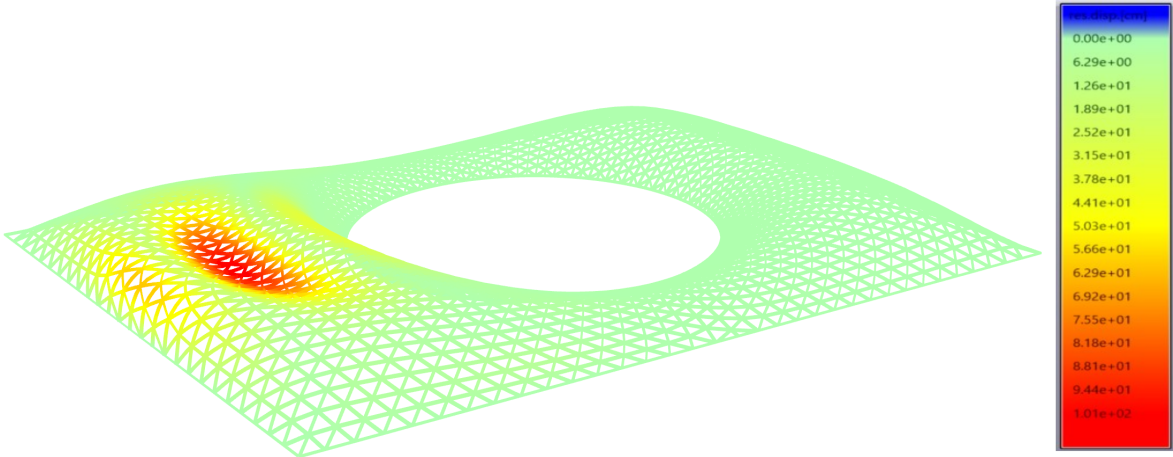
Figure 7.12: The first buckling mode of the original shape in the Great Court Roof. Colour legend values in cm.

Figure 7.12 displays first buckling mode for the original shape. The longest span is most vulnerable to global buckling where the members will undergo tension for the given buckling mode.

When optimizing a gridshell for structural efficiency, displacements need to be taken into account. Large displacements can alter the distribution of forces, contribute to increased moments and ultimately decrease structural capacity. Figure 7.13 display the development of the maximum displacement for changes in global shape. It can be seen that the displacements also correlates closely with the changes in maximum moment and tension, as displayed in figure 7.8 and 7.9, respectively.

Figure 7.13: The maximum displacement in the Great Court Roof depending on the global shape, which is differentiated by its height.

Once again, not only the maximum displacement, but also the distribution of the displacements should be taken into account. Figure 7.14 displays the displacement distribution for four different h/b-ratios; 0.147, 0.162, 0.212 and 0.275. The first one was decided based on the trough of the maximum compression force, displayed in figure 7.10. The second was chosen from the peak of minimum BLF, displayed in figure 7.11. The last two were chosen arbitrarily for comparison.
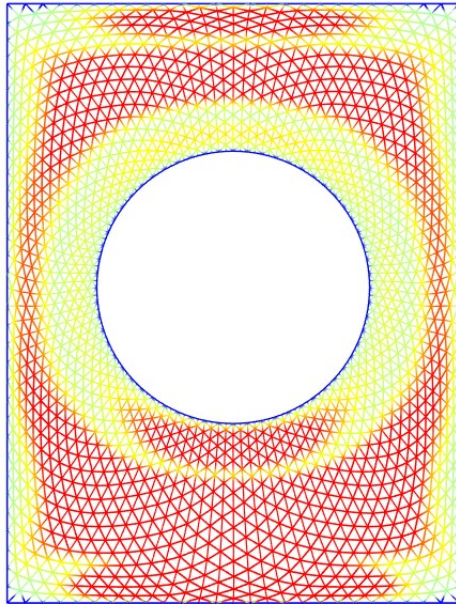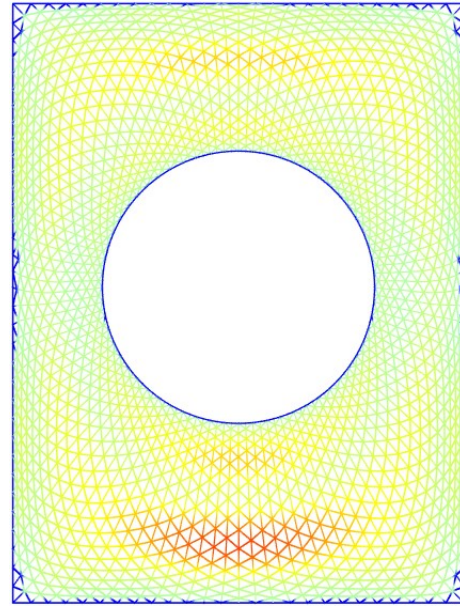
(a) h/b = 0.147.
h = 7.0 m.
Max. displacement = 43.79 mm.
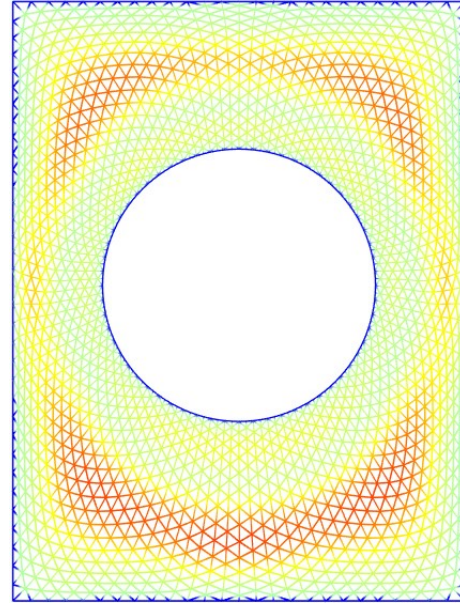
(b) h/b = 0.162.
h = 7.7 m.
Max. displacement = 8.99 mm.
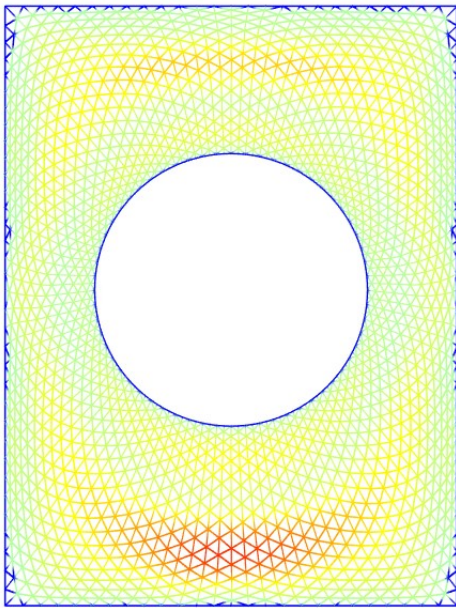
(c) h/b = 0.212.
h = 10.1 m.
Max. displacement = 9.42 mm.

(d) h/b = 0.275.
h = 13.1 m.
Max. displacement = 8.65 mm.

Figure 7.14: The distribution of displacements for four different global shapes.

Figure 7.14a displays the gridshell with an h/b-ratio of 0.147. As displayed, there are relatively big displacements distributed on a large region of the gridshell, which is not ideal. The gridshell with an h/b-ratio of 0.162, in figure 7.14b, has a similar displacement distribution. Even though the displacements are much smaller, there are still relatively big displacements in a large parts. Even though the maximum displacement in the gridshell in figure 7.14b is approximately the same as for the gridshells in figure 7.14c and figure 7.14d,

the distributions differ. The gridshell with the lowest h/b-ratio has bigger displacements over a much larger area than the gridshells in figure 7.14c and figure 7.14d. This can be explained by forces being more evenly distributed for the latter two.

The utilization of the members are not investigated at the same extent as the BLF and displacements. This is because it could not be done with Karamba, and a completely different software, Autodesk Robot, had to be used instead. Therefore, the utilization is a factor only investigated for specific h/b-ratios. However, based on the behaviour of the maximum forces, displacements, BLF and the utilization found for the original shape, it can be safe to say that the different shapes investigated should be approved for EC5 capacity. The utilization for the h/b-ratio of 0.168 can be seen in table 7.9, which substantiates this claim.

Supports

Increasing the h/b-ratio will increase the total weight of the structure nearly linearly, as figure 7.15 displays. After investigating the structural performance, it is clear that the total weight of the structure is less significant than the global shape, and therefore the structural performance can be improved with a heavier structure. However, the total weight of the structure will have an impact on the supports of the structure. The supports of the gridshell will also have a capacity, and heavier structures will need sturdier supports.
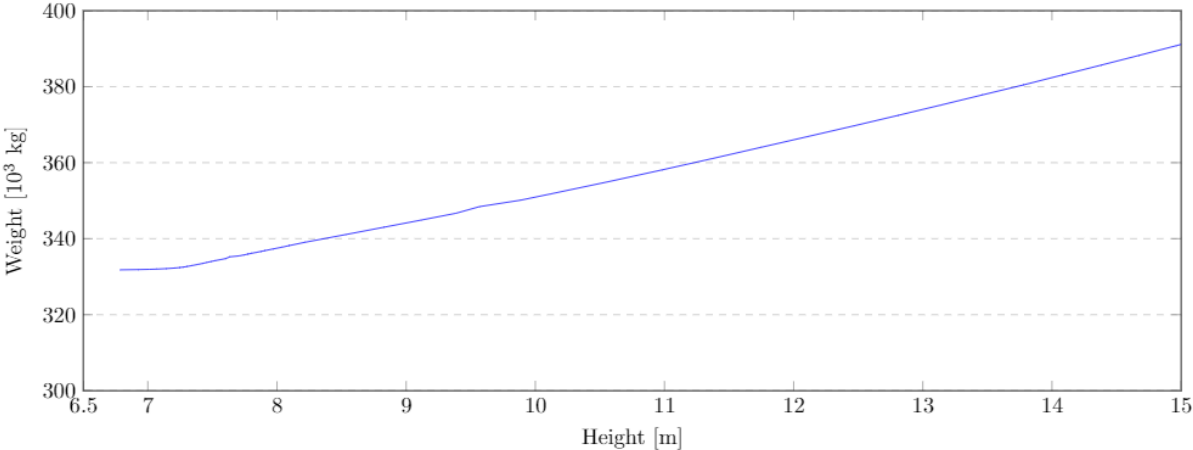
Figure 7.15: The weight of the Great Court Roof depending on the global shape, which is differentiated by its height.

93
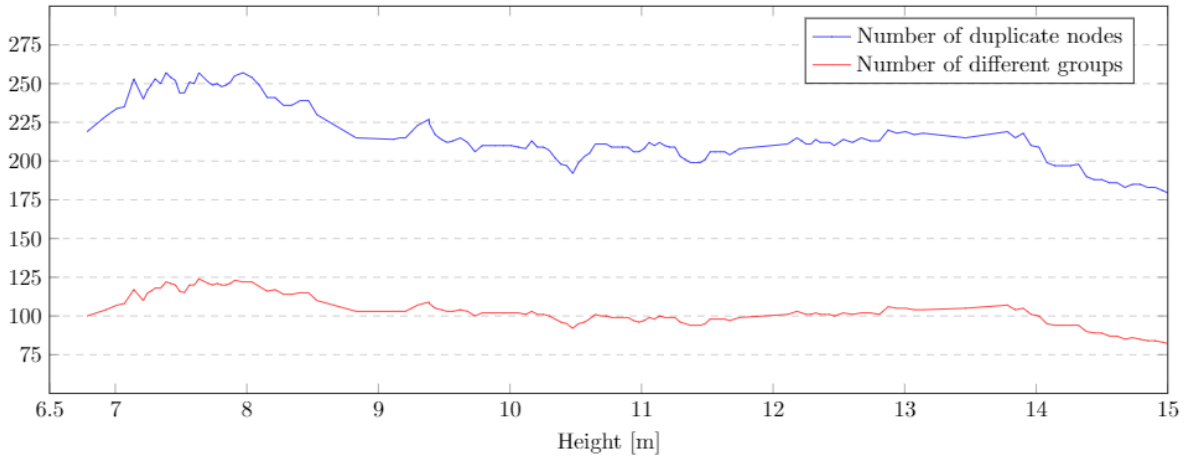
Repetitive nodes

Figure 7.16: The number of repetitive nodes and the number of different groups, depending on the global shape. +/- 1 degree of tolerance used.

Figure 7.16 displays how the amount of repetitive nodes are affected by the changes in height for the original grid pattern of the British Museum. There seems to be no clear correlation between the global shape of the structure and the general repetitiveness. Having verified a design for structural performance, however, this analysis could be used to tweak the h/b-ratio a bit to provide the most beneficial result in terms of repetitive nodes.

**Table 7.8:** Results for the gridshells in figure 7.17.

h/b-ratio	Total number of nodes	Number of repetitive nodes	Number of groups	Percentage repetitive nodes	Number of unique nodes
0.159	1566	257	124	16.41%	1309
0.168	1566	257	122	16.41%	1309
0.212	1566	208	101	13.28 %	1358
0.275	1566	218	104	13.92%	1348

Table 7.8 displays the number of repetitive nodes and the number of groups of repetitive nodes for four different global shapes. Figure 7.17 displays the distribution of the repetitive nodes for the global shapes mentioned. The global shapes in figure 7.17a and 7.17b is examined because they represent the peaks at the graph in figure 7.16. The table shows that the gridshell in figure 7.17b, with an h/b-ratio of 0.168 will be a better choice in terms of repetitive nodes. This is because the gridshell with an h/b-ratio of 0.168 has a smaller amount of groups with repetitive nodes, and therefore a smaller amount of nodes has to be produced for this h/b-ratio.
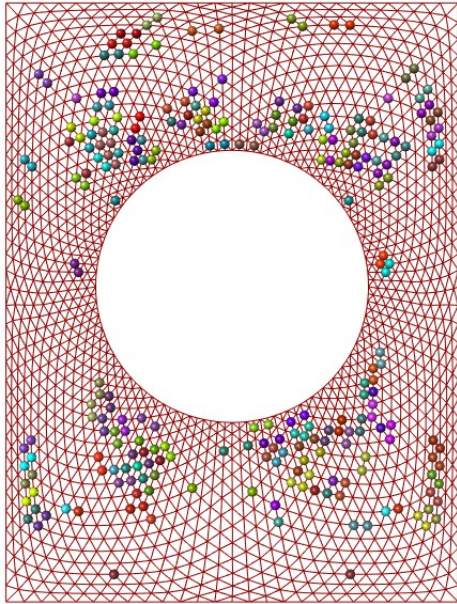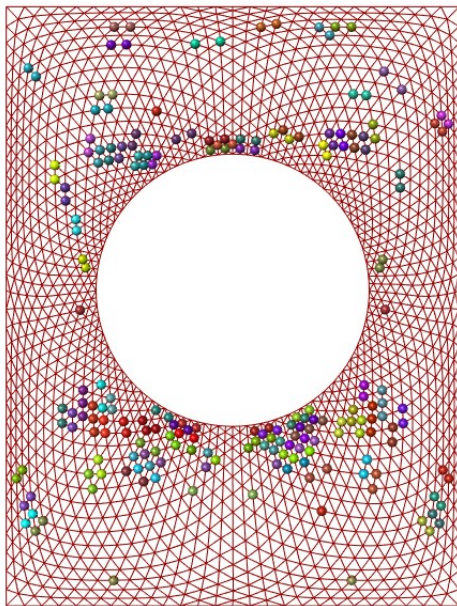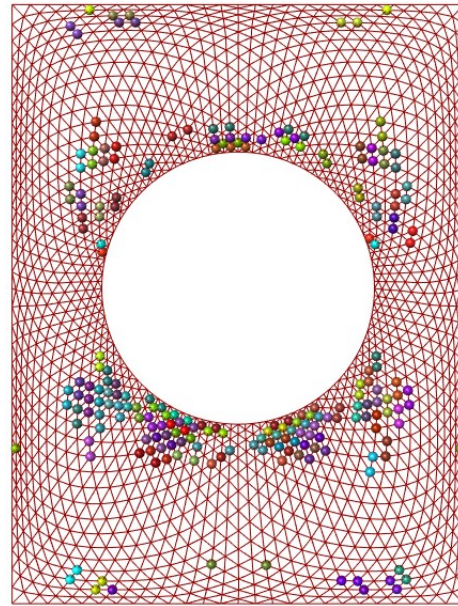
(a) h/b = 0.159.
h = 7.6 m.
Number of repetitive nodes = 257.
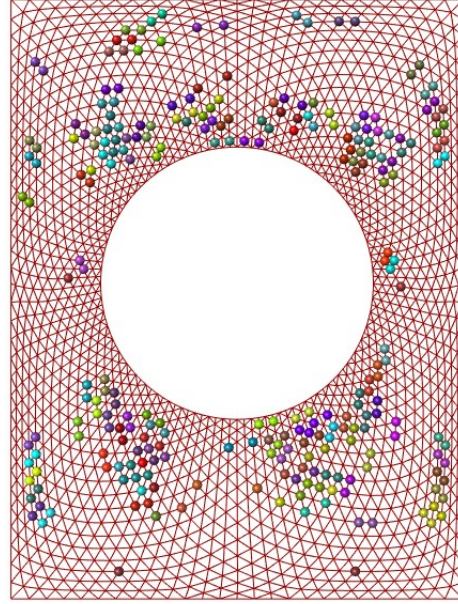
(b) h/b = 0.168.
h = 8.0 m.
Number of repetitive nodes = 257.

(c) h/b = 0.212.
h = 10.1 m.
Number of repetitive nodes = 208.

(d) h/b = 0.275.
h = 13.1 m.
Number of repetitive nodes = 218.

Figure 7.17: The distribution of the similar nodes for four different global shapes. +/- 1 degree tolerance used.

Previously, displacements were discussed and figure 7.14c (h/b-ratio of 0.212) and 7.14d (h/b-ratio of 0.275) displays two gridshells with approximately the same displacement pattern and maximum displacement. The distribution of repetitive nodes of the same two gridshells can be seen respectively in figure 7.17c and 7.17d. Table 7.8 shows that with respect to repetitive nodes, the gridshell with an h/b-ratio of 0.275 will be a better choice

than the gridshell with an h/b-ratio of 0.212, but the difference is not significant.

Shape optimization summary

This subsection has shown that the structural performance of the Great Court Roof can be greatly improved by using dynamic relaxation to change its global shape. A relatively small increase in the h/b-ratio can have a significant impact on the structural capacity. This means that the structure could be made much more efficient, and economically viable, by using less material in terms of smaller cross sections and less dense grid patterns. When the structural performance is improved, it gives the opportunity to design with respect to other criteria. Fabrication and installation of nodes in have been discussed throughout this thesis as a large source of complexity and cost of construction for gridshells. Figure 7.14 and figure 7.13 shows that larger heights will be beneficial in terms of minimizing displacements. On the other hand, figure 7.16 and table 7.8 shows that smaller h/b-ratios, still within the margin of improved structural performance, could be beneficial in terms of achieving a higher amount of repetitive nodes. Hence, a h/b-ratio could be chosen based on maximizing the number of repetitive nodes without compromising the structural performance much. The impact this would have on the viability of construction is probably minuscule though, when taking the total number of unique node configurations in to account. In any case, the results serve as a basis for comparison with the complete topological redesign of the following chapter.

Table 7.9: Results for the Great Court Roof with an h/b-ratio of 0.168.

Node type	Nodes neglected	Aluminium nodes	Steel nodes
Weight of beam elements	337 310 kg	337 310 kg	337 310 kg
Weight of nodes	0 kg	85 604 kg	155 677 kg
Total weight	337 310 kg	422 914 kg	492 987 kg
Max. displacement	9.33 mm	9.37 mm	9.40 mm
Max. compression force	353.13 kN	358.31 kN	362.56 kN
Max. tension force	21.58 kN	22.10 kN	22.53 kN
Max. shear force	4.05 kN	4.06 kN	4.06 kN
Max. bending moment	8.31 kNm	8.33 kNm	8.34 kNm
Min. BLF	4.60	4.53	4.47
Utilization	0.23	0.23	0.24

Table 7.8 shows that the best results in terms of repetitive nodes is given for the gridshell with an h/b-ratio of 0.168. The results for this gridshell is shown in table 7.9. Compared to the results for the original global shape, which can be seen in table 7.6, the tension forces, shear forces and bending moments is much lower, both for aluminium nodes, steel nodes and when the nodes are neglected. The new global shape distributes the forces in a better way than the original global shape. Therefore, the utilization and maximum displacement will also be much lower.

Table 7.10: Maximum displacement compared for the original global shape and for the gridshell with an h/b-ratio of 0.168 compared.

| Node type	Max. displacement original shape	Max. displacement h/b = 0.168	Reduction of max. displacement
Nodes neglected	85.17 mm	9.33 mm	89.05 %
Aluminium nodes	87.02 mm	9.37 mm	89.23 %
Steel nodes	88.55 mm	9.40 mm	89.38 %

Table 7.10 compares the maximum displacement for the original shape with the maximum displacements for the gridshell with an h/b-ratio of 0.168. The displacements is reduced by almost 90 % regardless of the node type. Table 7.10 also shows that the difference in displacements for the different node types are minimal.

7.5.2 Topology optimization

The original structure of the Great Court Roof may seem like a repetitive structure at first glance. In chapter 7.5.1, however, this was proven not to be the case. The aim of this section is to investigate if it is possible to change the original mesh of the roof in order to obtain a greater amount of identical node networks. To investigate this, the grid pattern of the British Museum will be completely redesigned by the Grasshopper plugin Lunchbox, as presented in chapter 6.2.

The new grid patterns were generated by projecting the original mesh onto the global xy-plane, keeping the outer rectangle and inner circular boundaries in place. Guide lines for the new mesh was defined from the corners of the rectangle and to the middle of the inner circle, as shown on figure 7.18, separating the surface into four. In this section, a new triangulated mesh and a quadrilateral mesh will be investigated. Examples can be seen in figure 7.19. With Lunchbox, values of u and v will determine the amount and grid lines generated on the surface, and hence, the density of the mesh. Due to the inner and outer boundary lines, the grid become more dense closer to the inner circle.
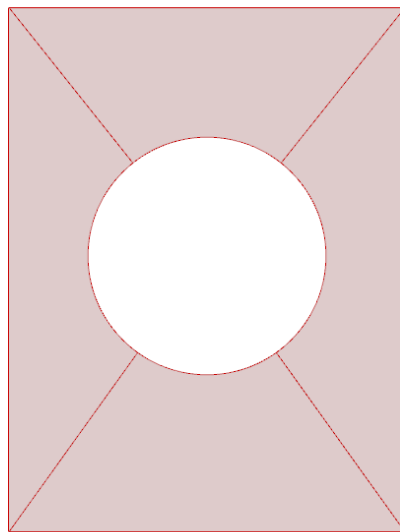
Figure 7.18: Projected surface from original mesh onto the xy-plane, with the diagonal guidelines.
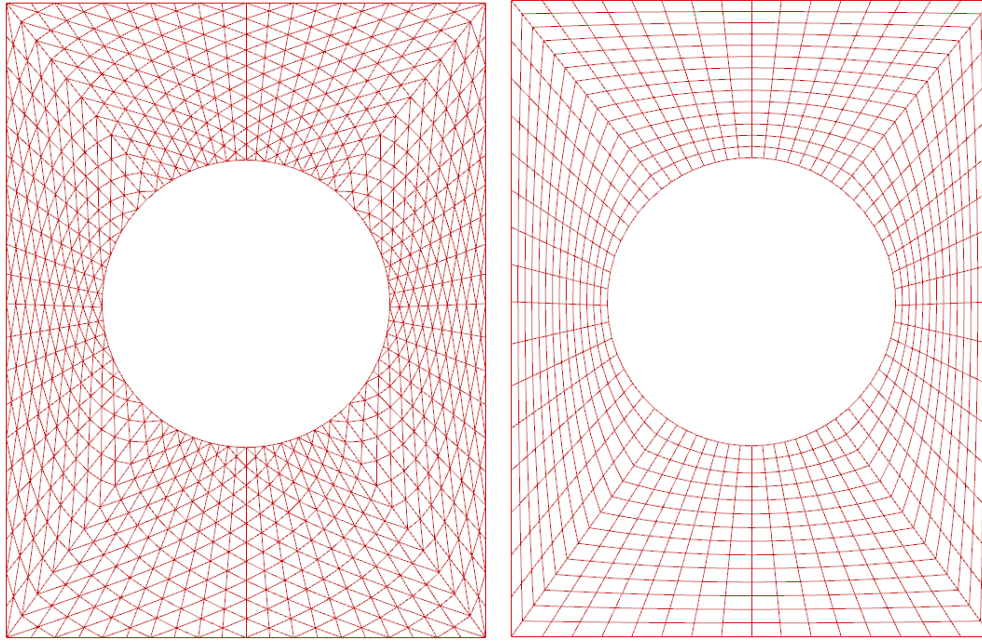
(a) Triangulated mesh   (b) Quadrilateral mesh

Figure 7.19: New mesh generated onto flat surface.

The flat meshes were form found using Kangaroo to obtain doubly curved gridshell models. The h/b-ratio of 0.168, which had favorable results for both structural performance and repetitive nodes in chapter 7.5.1, was chosen to simplify comparison between the different meshes.

Mesh 1: Triangulated grid patterns

The original mesh of the Great Court Roof is already triangulated, but is not symmetric due to placement of the inner circular boundary within the outer rectangle one. A more symmetrical triangulated grid will be generated with the help of the guidelines shown in figure 7.18. This could have an impact on the amount of repetitive nodes, whilst keeping the general aesthetic similar to the original. Three different meshes are investigated. The length and amount of members is determined by the values given for u and v division on the flattened surface, as explained in the start of this chapter.

The most dens mesh was chosen to generate approximately the same amount of nodes as the original grid. The coarser meshes was generated arbitrarily as a basis for comparison, but also to lessen the total amount of nodes. Details for the two meshes are given in table 7.11. The shape of the outer rectangular boundary and inner circle have a big impact on the mesh topology by making the grid much denser closer to the inner circle than closer to the outer boundary when generating the grid this way. As seen in table 7.11, there are big variations in length between members for both meshes, which is not favorable for a repetitive structure. However, both meshes have the same amount of supports on the

outer rectangle as on the inner circle, similarly to the original structure.

Table 7.11: Details triangulated mesh.

Triangulated mesh	Mesh 1.1 (coarse)	Mesh 1.2	Mesh 1.3 (dense)
u, v division	20, 20	26, 22	28, 28
Nodes	920	1300	1736
Number of beams	2440	3692	4760
Beam length	1.37 m - 9.34 m	1.41 m - 8.43 m	0.97 m - 7.4 m
Glass area	1.58 m^2 - 13.38 m^2	1.16 m^2 - 9.46 m^2	0.78 m^2 - 7.67 m^2
Surface area	6823.1 m^2	6893.9 m^2	6713.5 m^2

Figure 7.20 shows the colour display of the similar nodes for the three triangulated meshes. It can be seen from both figure 7.20 and table 7.12, that the number of repetitive nodes is the largest for mesh 1.3. Mesh 1.2 has a higher percentage repetitive node than mesh 1.1, however, the number of unique nodes that has to be manufactured is higher for mesh 1.2 than the other two.

(a) Triangulated mesh 1.1　　**(b)** Triangulated mesh 1.2　　**(c)** Triangulated mesh 1.3
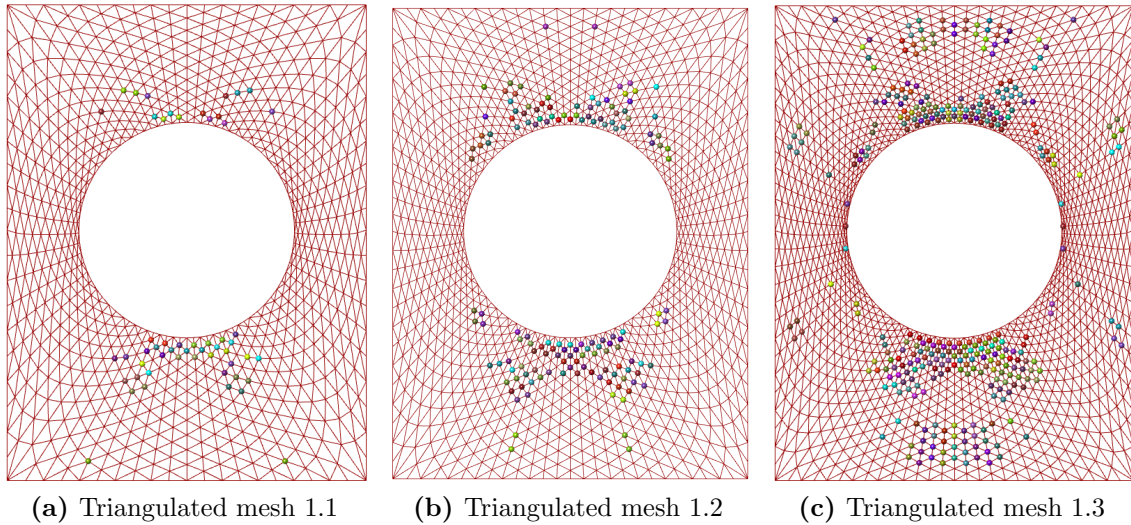
Figure 7.20: Repetitive node groups distribution for the triangular meshes.

Table 7.12: Results for the gridshells in figure 7.20.

Mesh	Total number of nodes	Number of repetitive nodes	Number of groups	Percentage repetitive nodes	Number of unique nodes
1.1	920	53	26	5.76%	867
1.2	1300	143	65	11.00%	1157
1.3	1736	325	137	18.72%	1046

Mesh 1: Structural analysis and evaluation

Table 7.13 displays the maximum values obtained from the structural analysis with Karamba and Robot. Mesh 1.2 has an overall better structural performance than both the coarser mesh 1.1 and the denser mesh 1.3. Additionally, mesh 1.1 has an utilization-ratio of 0.98, which is not acceptable considering the weight of the nodes was neglected in the analysis. Mesh 1.1 will therefore not be evaluated further. The redesigned triangulated meshes are both experiencing greater stresses than the mesh from chapter 7.5.1 with the same h/b-ratio. For these geometries, the largest ULS design utilization from EC5 was given by local buckling checks (eq. 6.23 in EC5 [13]).

Table 7.13: Results for new triangulated mesh

Triangulated mesh	Mesh 1.1	Mesh 1.2	Mesh 1.3
Weight	252 086 kg	302 890	343 530 kg
Max compression	597.0 kN	418.8 kN	445.3 kN
Max tension	122.2 kN	50.5 kN	86.8 kN
Max shear	30.7 kN	16.1 kN	19.6 kN
Max bending	71.5 kNm	38.0 kNm	45.1 kNm
Max utilization	0.98	0.59	0.66
Max displacement	50.9 mm	27.4 mm	36.7 mm
Min. BLF	3.19	4.53	3.90

Based on table 7.12, only mesh 1.3 has a higher percentage of repetitive node networks than the original Great Court Roof. Mesh 1.2, which has a better structural performance than 1.3, is doing worse than the both the original mesh and mesh 1.3 for percent-wise repetitiveness. However, the total amount of unique nodes that must be manufactured for construction is lower both for mesh 1.2 and mesh 1.3, than for the original roof. These redesigns are therefore both an improvement on the original in this regard.

Mesh 2: Quadrilateral grid patterns

This pattern is less complex than the triangulated mesh pattern, and each node only have four connected members instead of six. The orientation of each panel was rationalized to obtain planar surfaces, which is important for facilitating glass panels on a quad mesh. As explained in chapter 3.4.2, any triangulated mesh will have planar surfaces by default, so for the other models this have not been an issue. Planar surfaces can be achieved in Grasshopper by sorting all points to it is respective four corners and using the *CoPlanar* component in Kangaroo. As for the triangulated meshes, the grid is more dense close to the inner circle than it is to the outer boundary. The variation of the beam lengths and glass surface area can be seen in table 7.14, which are overall much better than for any of the triangulated grid patterns tested.

Table 7.14: Details quadrilateral mesh.

Quadrilateral mesh	Mesh 2.1	Mesh 2.2	Mesh 2.3
u. v	16, 14	24, 18	30, 22
Nodes	960	1824	2760
Number of beams	1856	3552	5400
Beam length	1.19 m - 6.50 m	0.88 m - 4.41 m	0.75 m - 3.56 m
Glass area	3.50 m^2 - 14.40 m^2	1.60 m^2 - 7.73 m^2	1.21 m^2 - 6.07 m^2
Surface area	6529.0 m^2	6543.4 m^2	6910.2 m^2

Figure 7.21 shows the colour display of the repetitive nodes of the different quadrilateral meshes investigated. Both figure 7.21 and table 7.15 shows that the percentage of repetitive nodes is increasing as the mesh get more dense. This was also the case for the triangulated mesh.

(a) Quad mesh 2.1   (b) Quad mesh 2.2   (c) Quad mesh 2.3
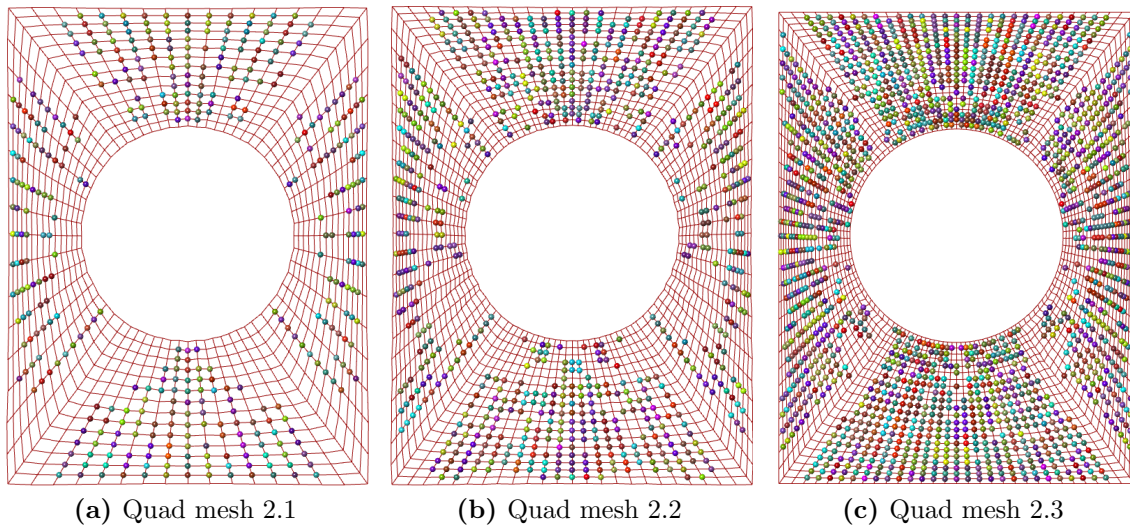
Figure 7.21: Repetitive node groups distribution for quadrilateral meshes.

Table 7.15: Results for the gridshells in figure 7.21.

Mesh	Total number of nodes	Number of repetitive nodes	Number of groups	Percentage of repetitive nodes	Number of unique nodes
2.1	960	406	153	42.29%	554
2.2	1824	784	302	49.28%	1040
2.3	2760	1714	512	62.1%	1046

Mesh 2: Structural analysis and evaluation

Structural analysis reveal that the performance of these structures are not sufficient, only mesh 2.3 did not exceed a maximum utilization ratio of 1 from EC5 design verification for its members. Once gain node weight were not included in this analysis, therefore the

utilization ratio of 0.94 is dangerously high. Maximum displacements are also much worse then for any of the other grid configurations, but mesh 2.3 is within the tolerance of 140 mm.

Table 7.16: Results for new quadrilateral mesh

Quadrilateral mesh	Mesh 2.1	Mesh 2.2	Mesh 2.3
Weight	169 448 kg	229 021 kg	285 238 kg
Max compression	3279 kN	529.5 kN	381.0 kN
Max tension	1663.7 kN	56.0 kN	190.4 kN
Max shear	942.0 kN	156.2 kN	82.2 kN
Max bending	2483 kNm	182.5 kNm	60.5 kNm
Max utilization	-	2.68	0.94
Max displacement	925 mm	236 mm	122 mm
Min BLF	0.98	1.40	2.05

All quadrilateral meshes exhibit a substantially larger amount of repetitive nodes compared to that of the triangular grid meshes. In addition to having by far the highest percent of repetitiveness than any of the triangular configurations, all of them had the same or fewer amount of unique node configurations as well. Mesh 2.3, which was the only, arguably, structurally adequate alternative, have a substantially higher amount of total nodes than any other configuration tested, though.

7.5.3 Comparison of the results from the optimizations.

In table 7.17, the results obtained in chapter 7.5.1 and 7.5.2 is compared. It can be seen from the table that the structural performance of mesh 2.1 and 2.2 is inadequate. Mesh 1.3 and 2.3 is arguably insufficient as well, considering node weight were not included in the analysis. As mentioned earlier in this chapter, 140 mm was set as a limit for the maximum displacement, and both mesh 2.1 and 2.2 exceed this. Additionally, both of these meshes have utilization ratios above 1, and the BLF for mesh 2.1 is below 1. In contrast, the original mesh, mesh 1.2 and mesh 1.3 all have sufficient structural performance. Mesh 1.1 and mesh 2.3 is in a gray area.

Table 7.17: Comparison of some key results for the different meshes investigated. All of the gridshells has an h/b-raio of 0.168 m.

Mesh	Max. displacement	Min. BLF	Max. utilization	Total number of nodes	Number of repetitive nodes
Original mesh	9.33 mm	4.60	0.23	1566	208
Mesh 1.1	50.90 mm	3.19	0.98	920	53
Mesh 1.2	27.4 mm	4.53	0.59	1300	143
Mesh 1.3	36.7 mm	3.90	0.66	1736	325
Mesh 2.1	925 mm	0.016	-	960	406
Mesh 2.2	236 mm	1.40	2.68	1824	784
Mesh 2.3	122 mm	2.05	0.94	2760	1714

The results from the structural analysis reveals that the use of a triangulated grid is beneficial due to its structural stiffness compared to the quadrilateral alternative. On figure 7.22 the two most dense mesh alternatives is illustrated.

(a) Mesh 1.3   (b) Mesh 2.3
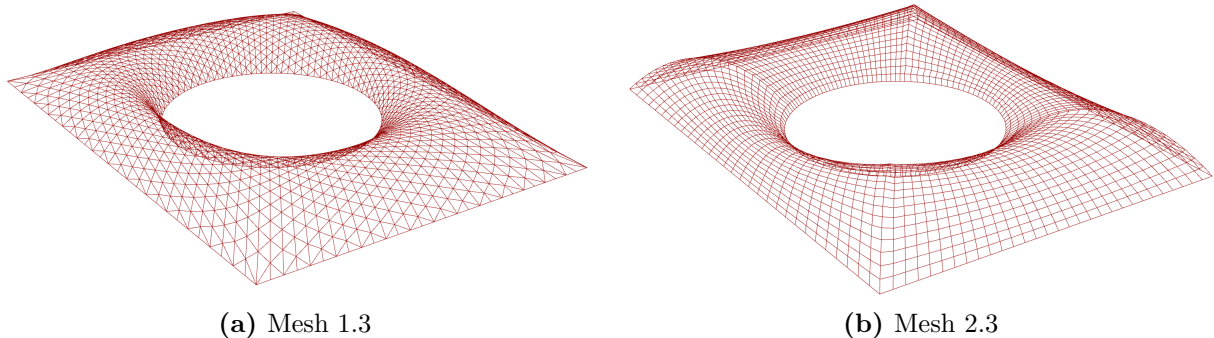
Figure 7.22: Perspective view of mesh 1.3 and mesh 2.3

When it comes to repetitive nodes, they should be compared with number of unique node configurations fr that mesh. This is because even though the percentage of identical nodes can be high for one particular gridshell, the number of different nodes that has to be

manufactured total can still be very high. Table 7.18 displays the number of different nodes in each of the different mesh patterns tested in the case project.

Table 7.18: Number of nodes that has to be manufactured compared for the gridshells with sufficient load bearing capacity.

Mesh	Total number of nodes	Number of repetitive nodes	Percentage repetitive nodes	Number of unique nodes
Original	1566	208	16.41 %	1358
1.1	920	53	5.76 %	867
1.2	1300	143	11.00 %	1157
1.3	1736	325	18.72 %	1411
2.1	960	406	42.29%	554
2.2	1824	784	49.28%	1040
2.3	2760	1714	62.10 %	1046

It can be seen that in general, the quadrilateral meshes are performing much better than any of the triangular alternatives in terms of repetitive node networks. These were, however, not performing adequately structurally. Only mesh 2.3 was arguably performing well enough, but the total amount of nodes in this configuration make it hard to argue for this configuration over the triangular ones.

7.6 Discussion

There are three parameters that makes the most sense to change when optimizing the structural efficiency of the Great Court Roof: the global shape, the grid pattern topology and cross sections dimensions. Of the three parameters mentioned, cross sections are the least complicated.

With uniformly sized members for the whole structure, the performance of a gridshell will behave almost linearly with changes in cross sections dimensions. Larger cross sections give better load bearing capacity, but also more weight. The boundary conditions and constraints will in this case affect the behaviour of the structure to a greater extent when changing the global shape or the topology. If cross sections of varying sizes were included, however, this would probably not be the case. Cross sections of varying size is discussed more in chapter 7.7, but was not included in the case project. Therefore, the different gridshells have only been investigated for different global shapes and topologies.

If the aim of the case project was to conclude with one definite design proposal for the Great Court Roof, optimizations regarding global shape and topology would have had to be done first. Cross sections could then have been changed to get the ultimate utilization and buckling load factor. The cross sections could also be optimized for each beam member to get an even better structural performance. This was, however, beyond the scope of this thesis, but would generally improve the results from the structurally analyses.

Steel versus aluminium nodes

Table 7.6 in chapter 7.4 display the structural analysis results for the original shape of the Great Court Roof, redesigned as a timber gridshell. The analysis were done with node weight neglected, aluminium nodes and steel nodes. The table shows that the difference in the results for the three are minimal, even though the additional weight is a substantial part of the total. This claim is supported by the results of the parametric workflow in chapter 6. Therefore, if node materials is chosen by node capacity and costs, steel should be preferred, even though aluminium is lighter. In chapter 3.3, some arguments for choosing aluminum instead of steel is discussed.

Global shape optimization

The optimization of the global shape in chapter 7.5.1 provides an indication of which h/b-ratios provide the best structural performance for the Great Court Roof. The h/b-ratio greatly affects the structural performance, which can be seen by the maximum displacements in the structure. The original global shape of the Great Court Roof, which has an h/b-ratio of 0.142, has a maximum displacement of 85.17 mm. This is below the limit of 140 mm. However, with large displacements the possibility of both local and global buckling will increase. By increasing the h/b-ratio to 0.159, the maximum displacement

will be below 10 mm with the original mesh. This can be explained in the distribution of forces. The graphs in chapter 7.5.1 displays that the maximum moments, tension forces and compression forces are decreasing as the h/b-ratio is increased from the its original value, and therefore, the displacements also decrease. Hence, the force distribution in the gridshell improves when the original h/b-ratio is increased. This effect appears to diminish and flatten out as a h/b-ratio of around 0.159 is reached, which is a height of around 7.6 m.

The graph in figure 7.16 displays that the number of repetitive nodes is somewhat affected by the h/b-ratio, but there does not seem to be a clear relationship between the two. If the topology was to be kept as it is, figure 7.16 could be used to maximize the amount of repetitive nodes in a definite design. The h/b-ratios between 0.159 and 0.315 all have similarly sufficient structural performance, and therefore the peaks in the graph of repetitive nodes within these h/b-ratios could be used to choose the global shape of the structure. This would need to be weighed against the extra material needed for the increased member lengths of larger h/b-ratios, however, as the difference is small. It is, in any case, not a huge difference considering the amount of unique nodes that would still have to be produced for the topology of the original Great Court Roof. Since the original shape did not facilitate repetitive nodes in the design, this could be expected. The reason for this could be that the design constraints affecting it in terms of height and boundary conditions, demanded other considerations to be taken in to account instead. It can also be that the unique outer and inner boundary condition, not being symmetrical, did not facilitate repetitive node networks while simultaneously not compromising on aesthetics and structural performance.

Topology optimization

By facilitating repetitive node networks in the design, manufacturing and construction costs for discrete gridshells can decrease significantly. Especially in Norway where the cost of labour is high, this will be an important aspect for the feasibility of building these structures. The amount of repetitive node configurations were not hugely impacted by the shape optimization, as could be expected. Changing the grid pattern topology, however, provided opportunities to increase this number significantly. Having already improved the structural performance of the gridshell in terms of shape, repetitive nodes could be further examined on different grid patterns. Thus, by using an h/b-ratio with considerable better structural performance than the original global shape, there should be greater opportunities to increase the number of repetitive nodes. In chapter 7.5.2 different grid patterns were investigated with the aim of increasing the amount of repetitive nodes networks, while at the same time have the designs be structurally viable.

For the triangulated grids, both the coarser mesh 1.1 and mesh 1.2 were favourable in regard to having less total nodes, and less unique node configurations than the original Great

Court Roof. However, mesh 1.1 was not structurally viable. Mesh 1.3 was comparable with the original with regard to the nodes, with a small increase in percentage of repetitiveness, but also in the number of unique nodes. Mesh 1.2 had the best structural performance of the three tested, and was almost on par with the original. Even though it had a lower percentage of repetitive nodes than the original, it has both a lower total number of nodes, and a lower number of unique node configurations. Mesh 1.2 should therefore be a cheaper alternative to construct than the original mesh, while keeping a similar aesthetic.

The structural performance of the quadrilateral meshes investigated, is as expected not nearly good as the triangluar meshes. Table 7.17 shows that the mesh 2.3 is the only of the three meshes with an arguably adequate structural performance. Mesh 2.3 is also the mesh with the best percent-wise results regarding repetitive nodes. With 62.1 % repetitiveness, it is leagues ahead any of the triangulated alternatives. On the other hand, mesh 2.3 is so dense, that even though the percentage of repetitive nodes is very high, the total number of nodes is also very high. Any benefit from the repetitive node networks would likely be outweighed by the fact that there are so many nodes in total. All the quadrilateral meshes were, however, producing much better results in terms of repetitive node networks than any of the triangulated ones. The structural performance of these meshes could have been better with for example steel bracings in the most vulnerable areas, as its done for the Mannheim Multihalle gridshell presented in chapter 2.2.1. Changing the cross sections could possible also be enough. Neither of these options were investigated further in this thesis.

Without a thorough cost estimation where everything from manufacturing, installation to labour is included, a definite answer cannot be given on which gridshell will be the least expensive and complicated to build. However, the redesigned mesh 1.2 *should* facilitate a cheaper fabrication and construction process than the original Great Court Roof while simultaneously perform nearly as well structurally. The parametric workflow environment developed for this case project, shows that both analysis and redesign can be carried out quickly and effectively. Which of the investigated gridshells yields the best results, depends on which parameter is considered the most important.

7.7 Concerns and uncertainties regarding the case project

In this thesis, some assumptions and simplifications has been made. There are some work that could have been done, but are not, or simply could have been done differently. The following list contains some bullet points on some of the concerns and uncertainties regarding the procedure, assumptions and results presented in this chapter:

- In this thesis the joints are assumed to be fixed. In reality, the joints will be categorized as semi-fixed rather than fully fixed. The results would differ somewhat if the correct stiffness for some specific node case were used instead. However, the whole case project require that any node design used is sufficiently rigid to transfer shear and bending moments.

- Timber structures under long-term exposure of loads will experience creep deformations. Creep can contribute to a different loading situation, making moments in the structure larger. This is not taken into account in this thesis.

- A way to obtain a larger load bearing capacity for a gridshell structure with quadrilateral meshes, is to use shear-braces to increase the gridshells stiffness. Brace members in steel or aluminium can be welded to the node connections, and therefore not affect the number of repetitive nodes for the gridshells. This could have made the structural performance of the quadrilateral gridshell 2.1 and 2.2 acceptable. In any case, a larger cross section would have proven beneficial for the less dense grids in general.

- The cross sections of the Great Court Roof varies in the original structure, increasing in size toward the outer rectangular boundary and the corners. This was not implemented in models for this case project. However, the most utilized members were appearing consistently in the corners, as could be expected based on the original design. It could be that a gridshell spanning the irregular boundaries imposed by the British Museum does not lend itself very well for a uniform cross section distribution. In any case, the utilization ratio was the main reason behind the insufficient structural performance for some of the different quad grid pattern topologies examined. Introducing cross sections of varying size for these topologies, could therefore be important to obtain a sufficient structural performance and also minimizing the number of different nodes that has to be manufactured as well.

- Gridshells are relatively lightweight structures, and therefore the snow loads used in this thesis constitute a majority of the loads acting on the structures. Hence, if only self weight was considered, the results would have been different. This applies especially to the h/b-ratio, as the h/b-ratio recommended probably would be smaller without the snow loads.

- The same h/b-ratio was used for all the different grid pattern topologies examined in

chapter 7.5.2. However, the different densities of the patterns tested also presented a substantial variation in the self weight of the structures (170 000 kg - 340 000 kg). The most efficient h/b-ratio for gridshells will in large part be determined by the magnitude and distribution of the loads, which in these cases varied due to the self weight. The large contribution from the snow load used in the case project *can* have made this less of an issue overall, but it is still expected that it would have an impact on the structural performance of these models.

- Generating grid pattern topologies where the variations in each member were minimized, would have been expected to make the most favorable designs in terms of repetitive nodes. This would have been interesting to compare with the original grid pattern of the British Museum Great Court. The parametric workflow developed for the case project did not facilitate this approach, however. Instead the node comparisons were done for more generalized patterns.

- The tolerance allowed for identical nodes were set as a constant +/- 1 degrees throughout the case project. This was as mentioned chosen arbitrarily because the precision of the geometrical framework of Rhino and Grasshopper means that no identical nodes would have been identified outside completely symmetrical models. The degree to what one can expect to rely on these tolerances is complicated, and should therefore be evaluated as a basis for comparison instead of definite for the designs. It is explained in chapter 2.2.3, that the Pods Sport Academy did not allow for tolerances in the design even though they optimized for repetitive node networks. Due to the design and manual assembly of the nodes on sight, they had no problems incorporating tolerances during construction. Hence, the issue of tolerance should be investigated in depth for more definite designs.

- Designing checks according to EC5 is not implemented as a component in Karamba and it was found convenient to use well tested structural analysis software as Robot which the Karamba model can be exported to. However, this can be time consuming when analysing several of structures. Considering this, it could be beneficial to make own developed components for Eurocode validation with structural analysis in Karamba.

8 Conclusion

8.1 Closing comments

Throughout this thesis, it has been shown that a parametric design environment can make the tasks of architects and engineers both easier and more efficient, particularly for complex building projects where close collaboration between the two are paramount. Establishing the visual scripts of the parametric models were found to be quite time consuming and convoluted, but correspondingly easy to use when established. Not knowing how to do an operation can be frustrating, and some specific operations can be essential to the whole script. The potential of the parametric workflow was found even greater with easy implementation of custom written code and specialized components. Even though it took some time to program the components used in this thesis, it was imperative to the study that it was done.

Design and construction of gridshells is a very complicated issue. The relationship between the shape, grid pattern topology and cross sections are very closely intertwined, which means that changing one parameter warrants a change in another, and so on. This promotes a sort of 'looping' quality to gridshells structural response, which means designing in a parametric environment is almost mandatory. Combined with the opportunity of real-time analysis and evaluations, the parametric environment will make complex and abnormal structures both easier to design and affordable to build. This could make a big impact on both the building industry and the urban environment of the future.

Through the case project, it has been shown that the choice of aluminium as a node material for timber gridshells cannot be argued based on the structural performance. The weight of the nodes should, however, be included in a structural analysis. Timber is strong but lightweight, so the nodes will end up representing a significant amount of the total weight of the structure. This can be critical for the supports and foundation, and should therefore be included. The effect of the additional weight from nodes on structural behaviour was less noticeable for optimized h/b-ratios of the curvature.

The curvature of a gridshell affects its structural performance to a great extent, and it was found that the Great Court Roof is not optimized for structural efficiency. By increasing the h/b-ratio from 0.142 to 0.159, which is equivalent to increasing the height of the structure with 0.81 m, the structural performance of the gridshell is significantly improved. The increased structural performance opens up for the opportunity of both using less material and optimize regarding other criteria, such as repetitive building parts.

Generating a grid that supported a high percentage of identical node networks, seemed to also compromise on the structural integrity to at least some extent. The quadrilateral redesigns seemed promising as an improvement over the original mesh in regard to repetitive nodes, but were either not structurally adequate, or had to many nodes in total to be

considered a notable improvement in this regard. This could be expected to not be the case, however, if either bigger cross sections or stiffeners had been included for the coarser meshes. The triangular meshes worked much better structurally, but had less repetitive node networks. However, mesh 1.2 were found to be almost as efficient as the original Great Court Roof, and having less unique nodes in the design. In general, it can be thought that minimizing the total number of nodes might be more important than incorporating repetitive node networks for this structure, as the boundaries are not symmetrical.

8.2 Further work

Exploring gridshells in a parametric environment opens up opportunities to do optimizations with respect to desired parameters. In the case project it was shown that small changes in some parameters can make a big difference in the results. It could therefore be interesting to investigate several types of gridshells with different boundary conditions to find connections between the structural performance and height, width and grid density. Such a study can contribute to get a better understanding of gridshells in general. Comparing the ratio between height, width and grid density to repetitive building parts may be the next step in making gridshells a more common structure to build. This could also be transferred to other shell structures.

The custom components developed for this thesis worked mostly as intended. In hindsight, there are definitely potential for further development:

- The Dynamic Relaxation component was not very efficient with computing power, which made it slow to implement in larger Grasshopper scripts. It also only used a fictitious mass / stiffness ratio, which means that the shape obtained must be manually changed to fit the specific material and load case applied to it. A more direct response to actual loads and material data would make the component, and form finding in general, more time-effective. This will not be straight forward to implement in this component, but would have been an interesting addition for gridshell design.

- The Angler component was limited to being a geometrical analysis tool in this thesis, used to evaluate repeating node networks in a given gridshell design. For a more in depth look at nodes and fabrication, the geometrical data through the U-, V- and W-angle outputs could be exported to support a generative method for specific node designs, which could further be incorporated in the model of a gridshell. Chapter 3.4.2 explains that a unique node geometry is defined by three different angles and a normal vector. During the case project the normal vectors were decided from mesh geometry, but this does not have to be the case. Rotating certain normal vectors either manually or by genetic algorithm could probably yield a few more identical nodes. Alternatively, it could be attempted to for example to change normal vectors to only minimize to torsion between nodes.

- To avoid using Robot, a Grasshopper component that calculated the design checks for all beam elements of a Karamba model, could have been developed. This would have made cross section validation much easier, and the parametric workflow environment even better.

If further work were to be done in the case project, it could have been interesting to propose a new shape for the Great Court Roof. The global shape and the topology could

be analyzed and optimized for repetitive nodes, while the structural performance still is as good as possible. To implement this, the global shape optimization and topology optimization has to be combined with an optimization of cross sections. This kind of optimization will be more natural to perform as an iterative loop. Thus, the operations done in this thesis, and a cross sections optimization in addition, could be done multiple times until the results converges and one shape is found. This could have been an interesting addition to this study, both regarding generally optimization of discrete timber gridshells, and optimization of the particular boundary conditions the Great Court Roof of the British Museum has. The proposal of a new shape for the Great Court Roof could also include a cost analysis, which should include costs of manufacturing of nodes and beam elements. In this way more tangible proof could be presented about which gridshell will be the least costly to manufacture.

References

[1] Wikipedia. *Pantheon, Rome.* 2014. [Digital photography]
   URL: `https://en.wikipedia.org/wiki/Pantheon,_Rome`
   Accessed: March 3, 2020.

[2] S. Labonette-Weber. *The Trondheim Holzbau Pier.* 2014. [Digital photography]
   URL: `https://www.ntnu.edu/kt/research/csdg`
   Accessed: March 1, 2020.

[3] Wikipedia. *An upside-down force model of the Colònia Güell, Sagrada Família Museum.* 2009. [Digital photography]
   URL: `https://en.wikipedia.org/wiki/Antoni_Gaud%C3%AD#/media/File:Maqueta_funicular.jpg`
   Accessed: February 14, 2020.

[4] *Mannheim Multihalle - Architecture.* 2020.
   URL: `https://mannheim-multihalle.de/en/architecture/`
   Accessed: March 5, 2020.

[5] Foster + Partners. *Great Court at British Museum.* 2020. [Digital photography]
   URL: `https://www.fosterandpartners.com/projects/great-court-at-the-british-museum/`
   Accessed: March 11, 2020.

[6] R. Harris, B. Gusinde, and J. Roynon. *Design and construction of the Pods Sport Academy, Scunthorpe, England.* 2012.

[7] Norwegian University of Science and Technology. *Conceptual Structural Design.* 2020.
   URL: `https://www.ntnu.edu/kt/research/csdg`
   Accessed: March 2, 2020.

[8] Standard Norge. *Eurocode: Basis of structural design.*
   URL: `https://www.standard.no/no/Nettbutikk/produktkatalogen/Produktpresentasjon/?ProductID=814830`
   Accessed: May 1, 2020.

[9] Standard Norge. *Eurocode 1: Actions on structures, Part 1-3: General Actions Snow Loads.*
   URL: `https://www.standard.no/no/Nettbutikk/produktkatalogen/Produktpresentasjon/?ProductID=974831`
   Accessed: March 11, 2020.

[10] C. Preisinger. *Welcome to Karamba3D.* 2013.

URL: https://manual.karamba3d.com/
Accessed: March 3, 2020.

[11] Kartverket. *Norgeskart*.
URL: https://www.norgeskart.no/#!?project=norgeskart&layers=1002&zoom=4&lat=7197864.00&lon=396722.00
Accessed: March 11, 2020.

[12] Standard Norge. *NS-EN 14080 Trekonstruksjoner, Limtre og limt laminert heltre, Krav*.
URL: https://www.standard.no/nettbutikk/sokeresultater/?search=+NS-EN+14080
Accessed: March 18, 2020.

[13] Standard Norge. *Eurocode 5: Desgin of timber structures, Part 1-1: General Common rules and rules for buildings*.
URL: https://www.standard.no/no/Nettbutikk/produktkatalogen/Produktpresentasjon/?ProductID=436137
Accessed: March 03, 2020.

[14] *Colonia Güell History*. 2020.
URL: http://gaudicoloniaguell.org/en/history/
Accessed: February 14, 2020.

[15] R. Hooke. *A description of helioscopes, and some other instruments*. Royal Society, London, 1676.

[16] M. Carpo. *Parametric Notations*. John Wiley & Sons Ltd., 2016.

[17] J. Craven. *House Style of the Future? Parametricism*. 2012.
URL: https://www.thoughtco.com/house-style-of-the-future-parametricism-177493
Accessed: February 2, 2020.

[18] L. Mark. *Schumacher and Beigel pay tribute to 'profound' architect Frei Otto*. 2015.
URL: https://www.architectsjournal.co.uk/news/schumacher-and-beigel-pay-tribute-to-profound-architect-freiotto/8679982.article?fbclid=IwAR2S1sGaQmI1WMvkzKjrBznwzPwTh_qrmbVsPl4pfKymfYGtt4-UneVOJ3o
Accessed: March 5, 2020.

[19] E. Schling. *Repetitive Structures : Design and construction of curved support structures with repetitive parameter*. ResearchGate, 218.

[20] The Trustees of the British Museum. *Architecture*. 2020.
URL: https://www.britishmuseum.org/about-us/british-museum-story/

```
architecture
```
Accessed: March 11, 2020.

[21] S. Brown. Engineering the British Museum Great Court Roof. In M. Barnes(ed.) and M. Dickson(ed.). *Widespan Roof Structures*, pages 283–268. Thomas Telford Publishing, 2000.

[22] C.J.K. Williams. *The Analytical and numerical definition of the geometry of the British Museum Geat Court Roof.* Deakin University, 2000.

[23] J. Sisckha. Engineering the construction of the Great Court Roof for the British Museum. In M. Barnes(ed.) and M. Dickson(ed.). *Widespan Roof Structures*, pages 199–207. Thomas Telford Publishing, 2000.

[24] S. Adriaenssens, P. Block, D. Veenendaal, and C. Williams. *Shell Structures for Architecture - Form Finding and Optimization.* Routledge, 2014.

[25] K. Bell. *An engineering approach to Finite Element Analysis of linear structural mechanics problems.* Akademika Publishing, 2013. p. 499.

[26] W. Flügge. *Stresses in Shells.* Springer, 1973. 2nd edition.

[27] S.H. Dyvik. *Engineering the construction of the Great Court Roof for the British Museum.* 2019.

[28] R. Mesnil, Y. Santerre, C. Douthe, and O. Baverel. *Generating high node congruence in freeform structures with Monge's Surfaces.* ResearchGate, 2015.

[29] D.S. Wakefield. *Engineering analysis of tension structures: theory and practice.* 1999.

[30] A. Kilian and J. Ochsendorf. *Particle-spring systems for structural form finding.* 2005.

[31] S. Adriaenssens, L. Ney, E. Bodarwe, and C. Williams. *Finding the Form of an Irregular Meshed Steel and Glass Shell Based on Construction Constraints.* Journal of Architectural Engineering, 2012.

[32] H. Schober. *Transparent Shells - Form, topology, structure.* Ernst & Sohn, 2015.

[33] AGC Glass Europe. *MyZeil.* 2010. [Digital photography]
URL: `https://www.flickr.com/photos/64121389@N05/9077034190/l`
Accessed June 8, 2020.

[34] Archdaily. *Chadstone Shopping Centre / CallisonRTKL + The Buchan Group.* 2017. [Digital photography]
URL: `https://www.archdaily.com/804275/chadstone-shopping-centre-callisonrtkl-plus-the-buchan-group`
Accessed: June 8, 2020.

[35] S.H. Dyvik, M. Luczkowski, J.H. Mork, A. Rønnquist, and B. Manum. *Design of freeform gridshell structures - Simplifying the parametric workflow.* IABSE Symposium, 2019.

[36] Robert McNeel & Associates. *Rhinoceros 3D.*
URL: `https://www.rhino3d.com/resources/`
Accessed: March 2, 2020.

[37] D. Piker. *Kangaroo Physics.* 2020.
URL: `https://www.food4rhino.com/app/kangaroo-physics`
Accessed: March 3, 2020.

[38] C. Preisinger. *Linking Structure and Parametric Geometry. Architectural Design, 83: 110-113.* 2020. DOI: 10.1002/ad.1564.

[39] Robert Mcneel & Associates. *Karamba3D.* 2020.
URL: `https://www.food4rhino.com/app/karamba3d`
Accessed: March 3, 2020.

[40] N. Miller. *LunchBox.* Robert Mcneel & Associates.
URL: `https://www.food4rhino.com/app/lunchbox`
Accessed: March 4, 2020.

[41] GeometryGym. *Geometry Gym.* 2020.
URL: `https://geometrygym.wordpress.com/`
Accessed: April 5, 2020.

[42] Autodesk Inc. *Robot Structural Analysis.* 2020.
URL: `https://www.autodesk.com/products/robot-structural-analysis/overview`
Accessed: April 4, 2020.

[43] Autodesk Inc. *Non-linear Static Analysis.* 2020.
URL: `https://knowledge.autodesk.com/support/robot-structural-analysis-products/learn-explore/caas/CloudHelp/cloudhelp/2021/ENU/RSAPRO-UsersGuide/files/GUID-FB3C86D3-0E30-43A6-82D6-6C50F429FA0D-htm.html`
Accessed: May 4, 2020.

[44] H. Brun. *British Museum grid shell analysis.* Specialization Project. Norwegian University of Science and Technology, Department of Structural Engineering, 2019.

[45] G. Piacentino. *Weaverbird.* 2020.
URL: `http://www.giuliopiacentino.com/weaverbird/`
Accessed: March 3, 2020.

A Attachments

Files containing Grasshopper and C# scripts will be delivered in a zip-file, together with this thesis. The following is a list of the files contained in the zip-file:

- DynamicRelaxation folder - contains the complete C# script for the Dynamic Relaxation component.

- Angler folder - contains the complete C# script for the Angler component.

- Normal folder - contains the complete C# script for the Normal component. Only used to showcase vector generation in chapter 5.

- Custom_components_test_arena.gh - Grasshopper script that showcase the custom components working together.

- Parametric_workflow_script.gh - Grasshopper script used to obtain the parametric workflow environment in chapter 6, which also is visualized in appendix B.

- BM_new_global_shape.gh - Grasshopper script used in chapter 7, which also is visualized in appendix C.1.

- BM_nodes.gh - Grasshopper script used in chapter 7, which also is visualized in appendix C.2.

- BM_new_mesh.gh - Grasshopper script used in chapter 7, which also can be found visualized in appendix C.3.

It is important to note, that in the Grasshopper-files, at least one component will be disabled. This is because the program is running too slow if for example Kangaroo and Karamba components is working simultaneous. For all of the Grasshopper files, Kangaroo needs to converge before the all components is enabled for the script to work in a reasonable speed.

B Grasshopper script for the parametric workflow
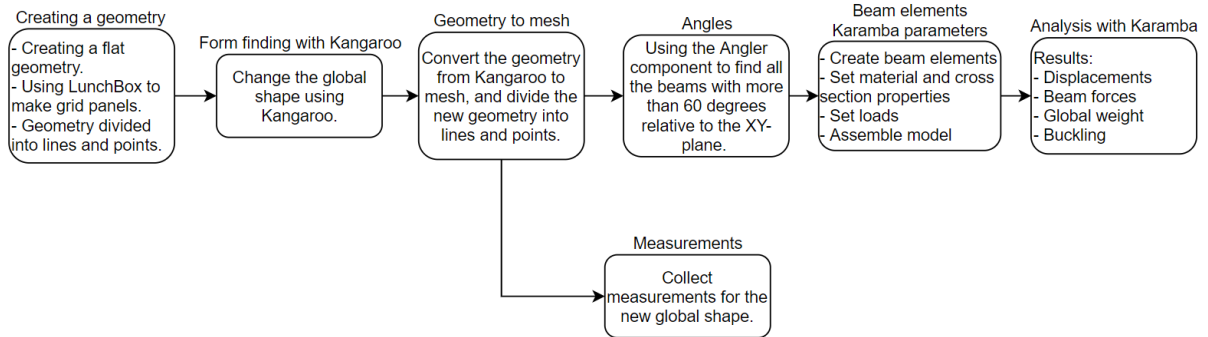
Figure B.1: Step by step how the code works.
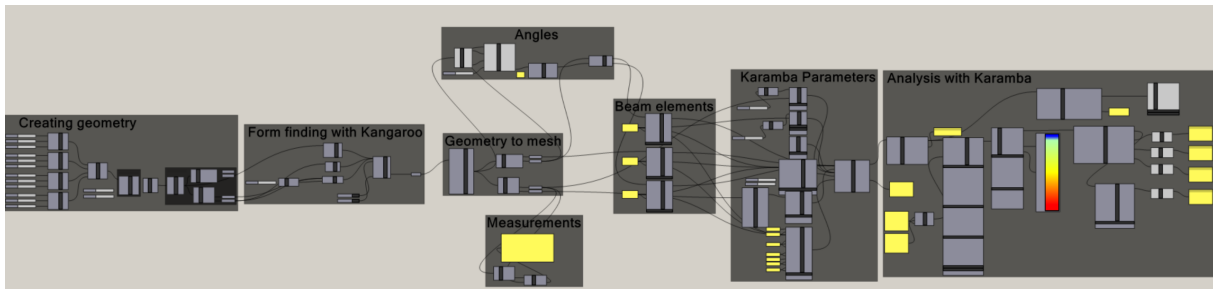
Figure B.2: The entire script used in the parametric workflow.
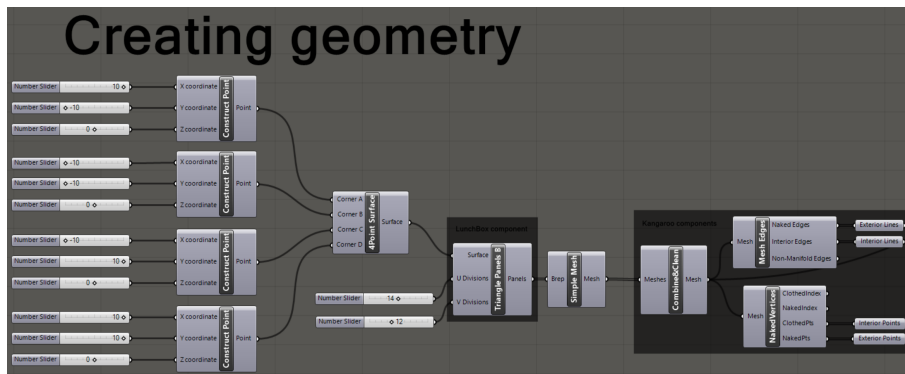
Figure B.3: Creating the geometry...
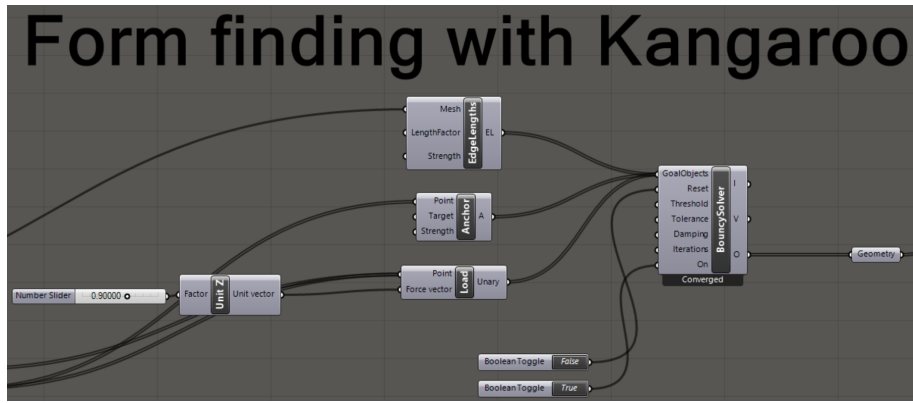
Figure B.4: Using Kangaroo's BouncySolver to change the global shape.
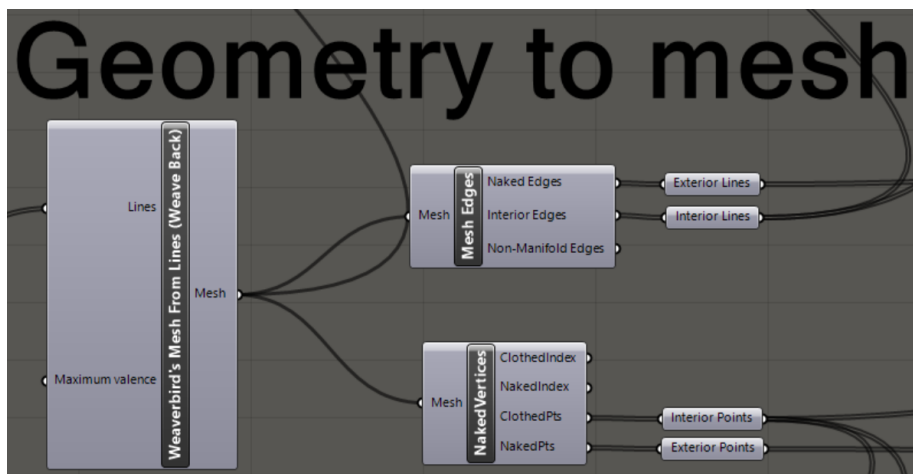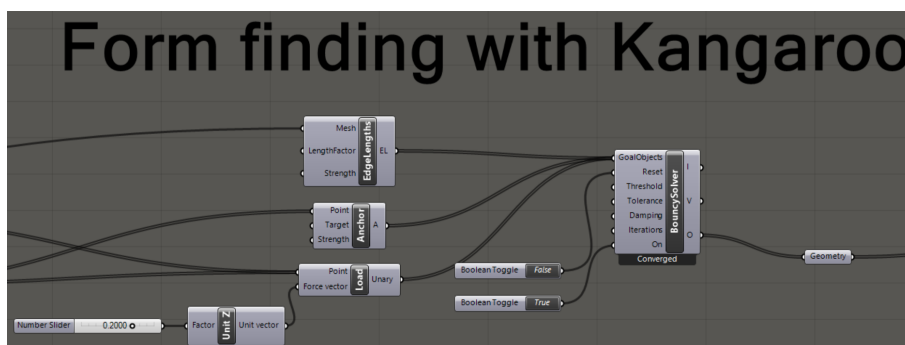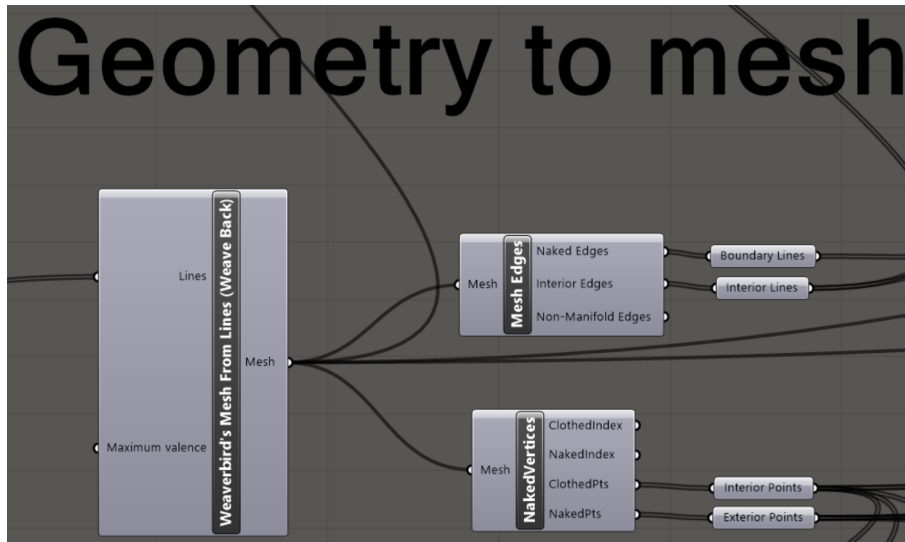

Figure B.5: Converting the new geometry from Kangaroo to a mesh. Then the mesh is divided into lines and points.
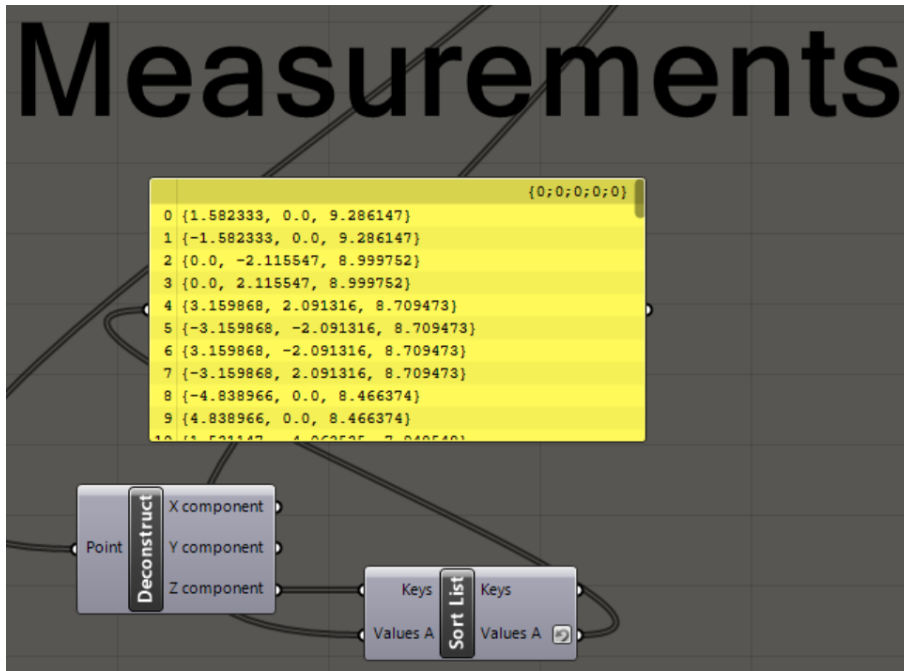
Figure B.6: This part is used to collect the measurements for the new global shape. The new height is particularly important.
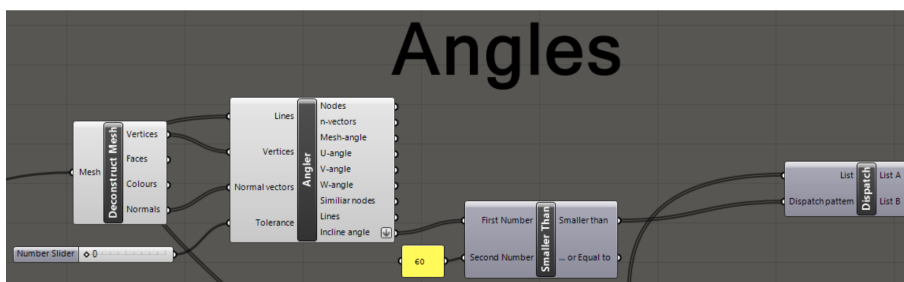
Figure B.7: Using the Angler component to find all the beams with more than 60 degrees relative to the XY-plane. This is used to determine which nodes to have snow loads.
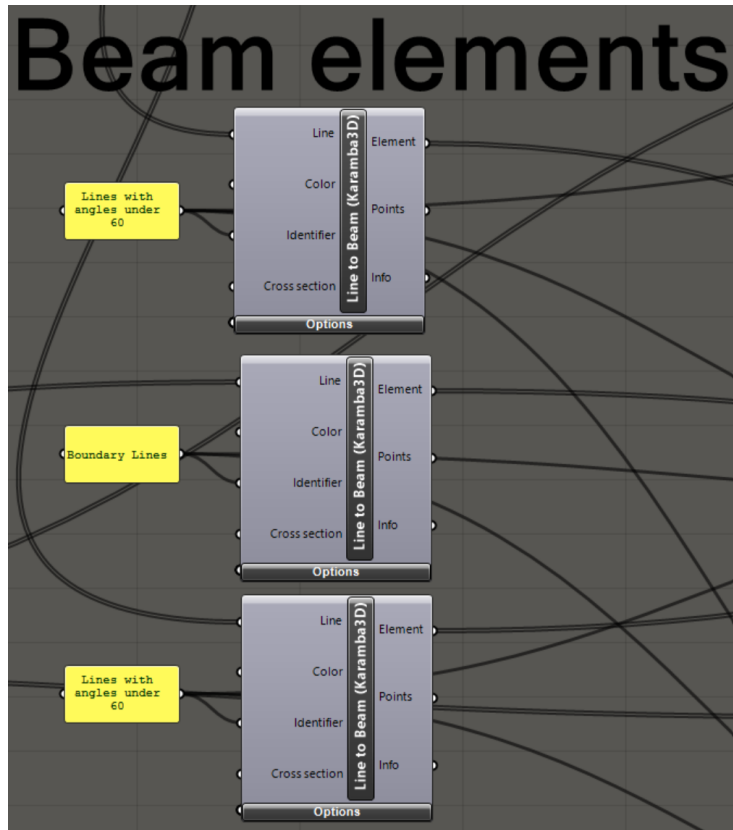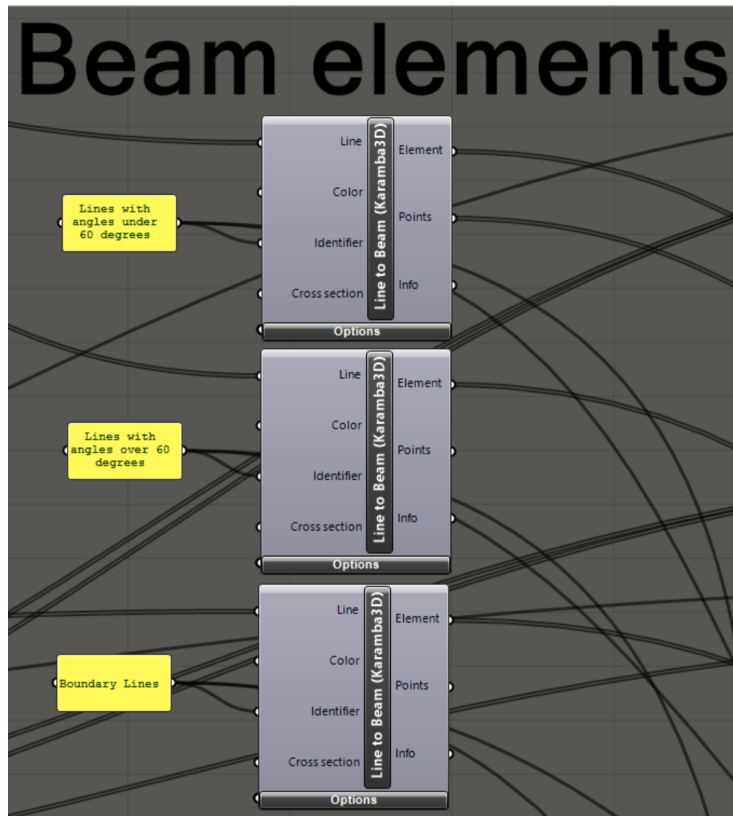
**Figure B.8:** Making the lines to Karamba beam elements.
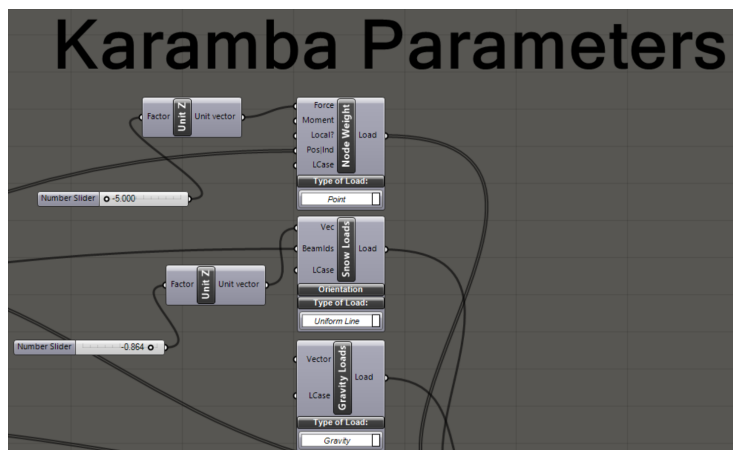
**Figure B.9:** All the loads used in the parametric workflow is set.
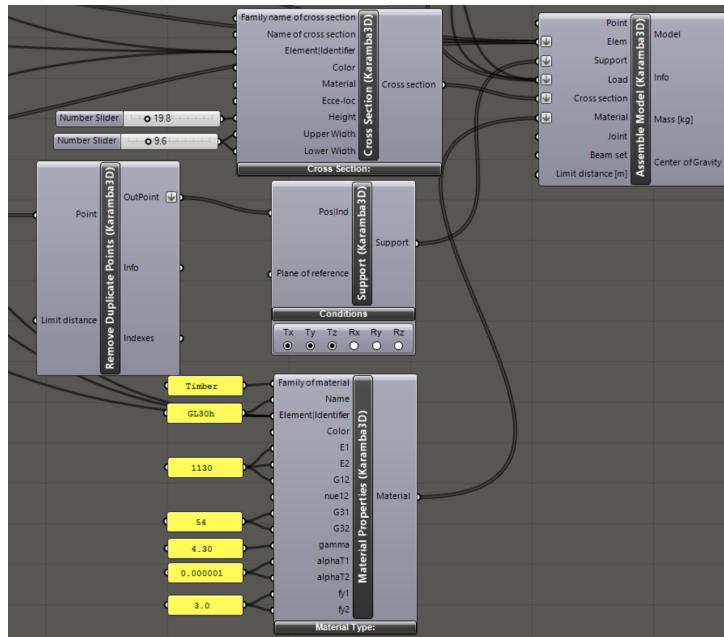
Figure B.10: The rest of the Karamba parameters, as material properties, supports and cross sections. All of the Karamba parameters is assembled in the *Assemble Model* component.
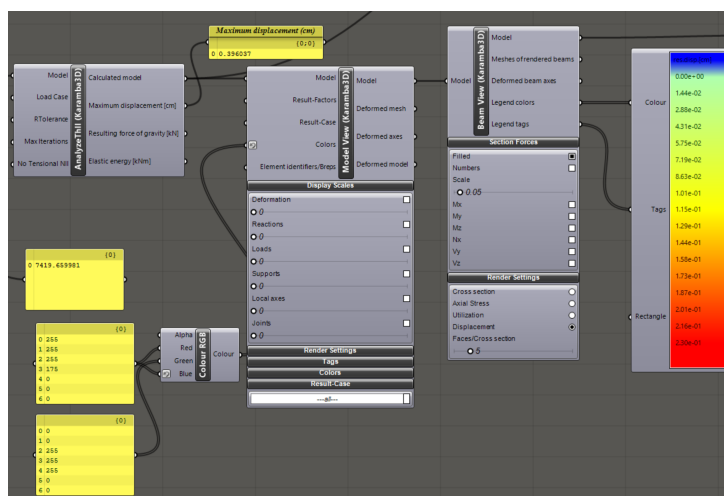
Figure B.11: *AnalyzeThII* analyses the model assembled in figure B.10. Beam view is for visualization in the Rhino view port.
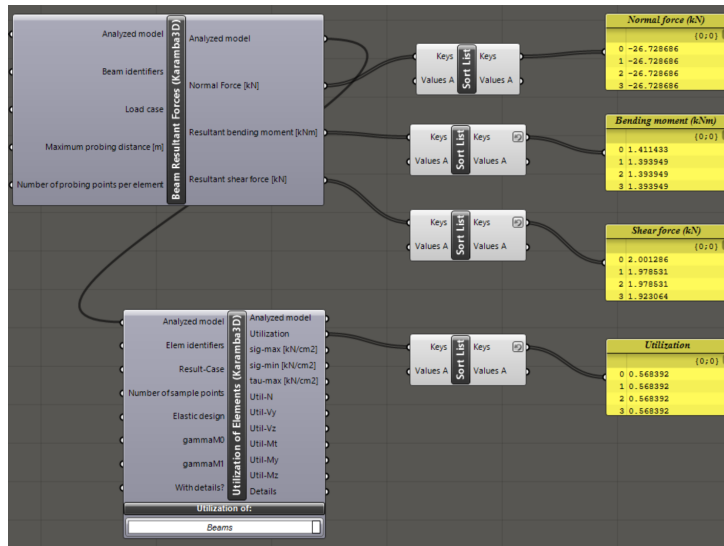
Figure B.12: The forces working in the structure can be displayed after the model is analysed.
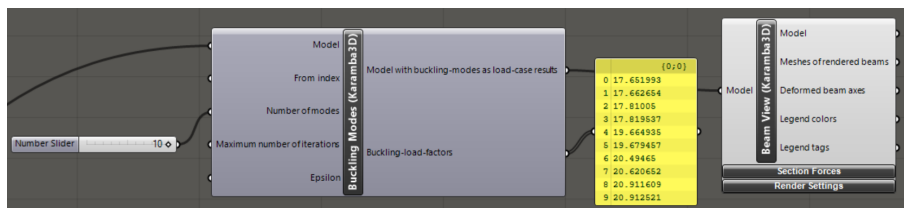
Figure B.13: There must be a separate analysis for buckling.

126

C   Grasshopper script for the case study

C.1   Analysis of the Great Court Roof
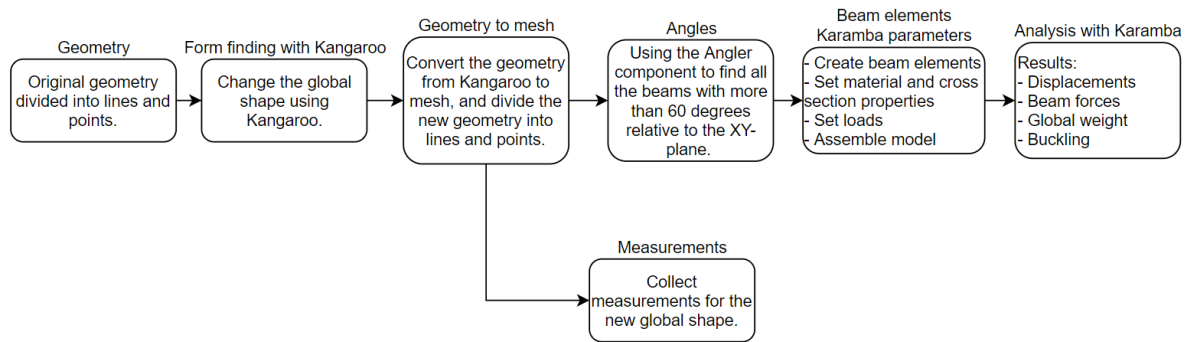
Figure C.1: Step by step how the code works.
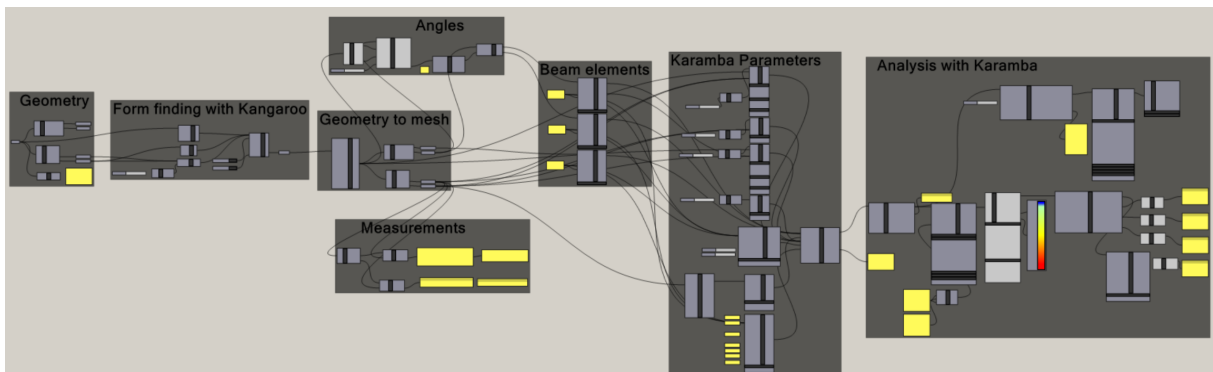
Figure C.2: The entire script used to analyse the Great Court Roof for different global shapes.
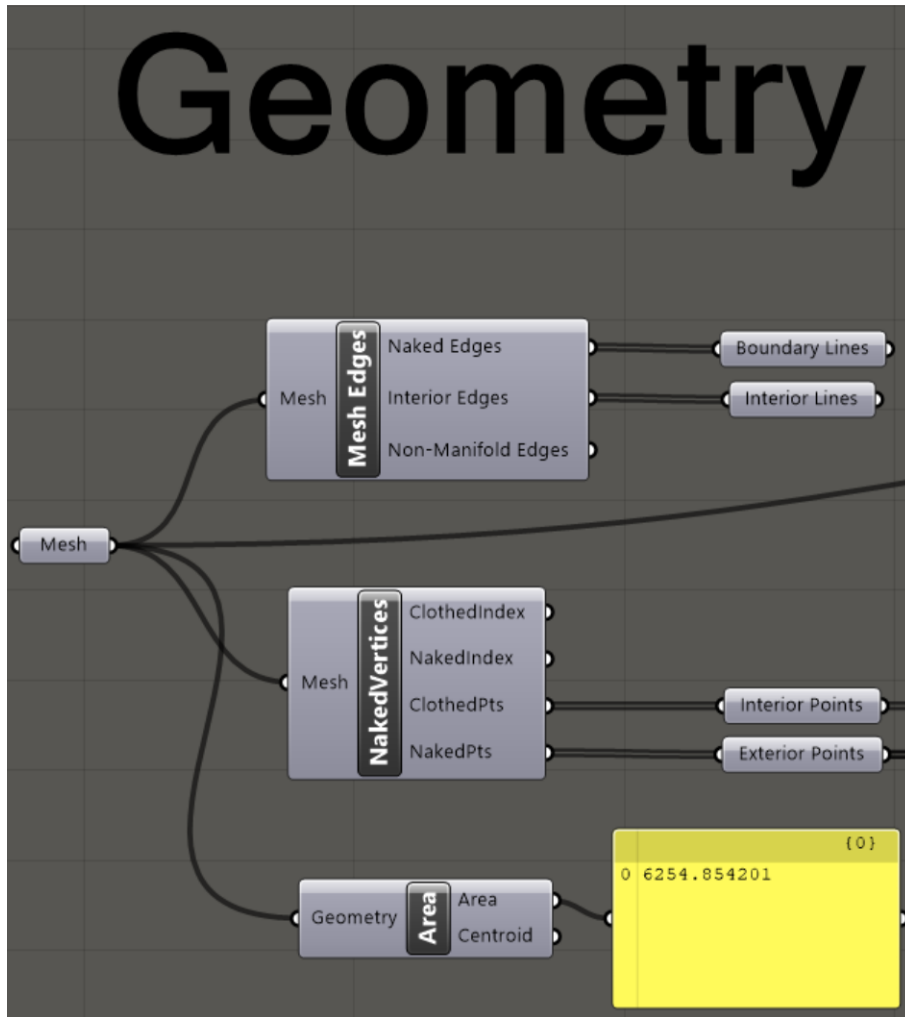
Figure C.3: The original geometry is divided into lines and points.

Figure C.4: Using Kangaroo's BouncySolver to change the global shape.

Figure C.5: Converting the new geometry from Kangaroo to a mesh. Then the mesh is divided into lines and points.
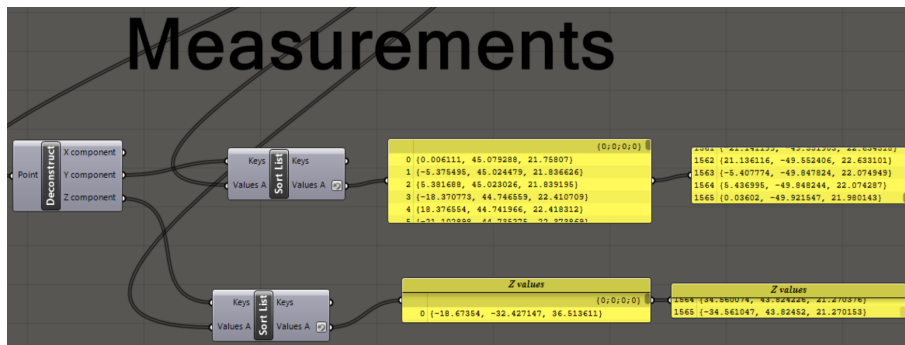
Figure C.6: This part is used to collect the measurements for the new global shape. The new height is particularly important.
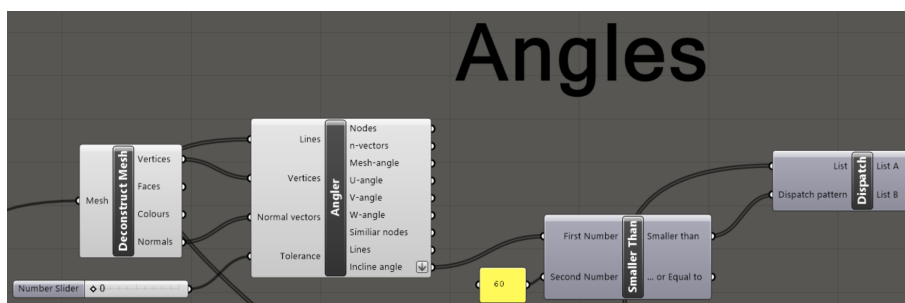
Figure C.7: Using the Angler component to find all the beams with more than 60 degrees relative to the XY-plane. This is used to determine which nodes to have snow loads.

Figure C.8: Making the lines to Karamba beam elements.
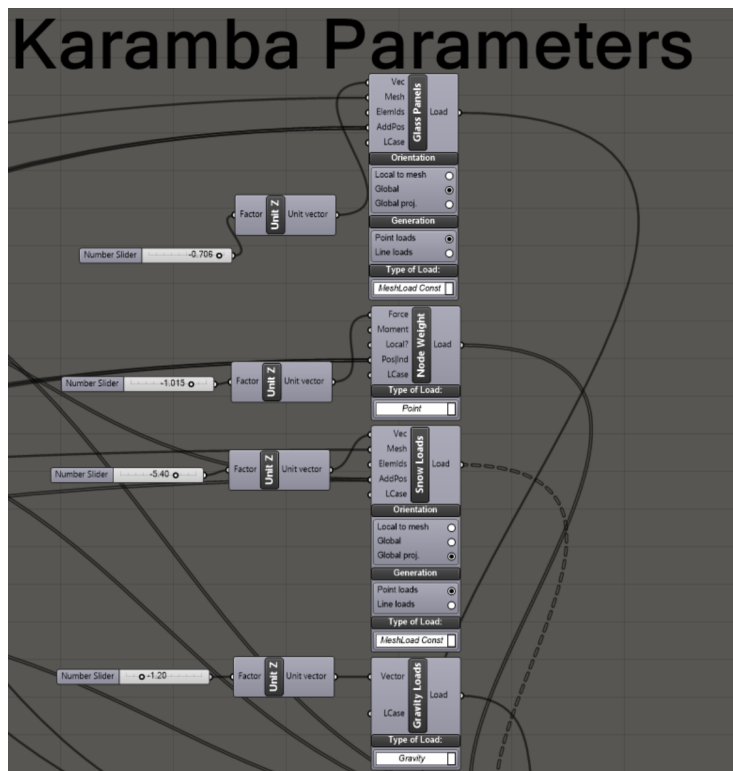
Figure C.9: All the loads working on the Great Court Roof.
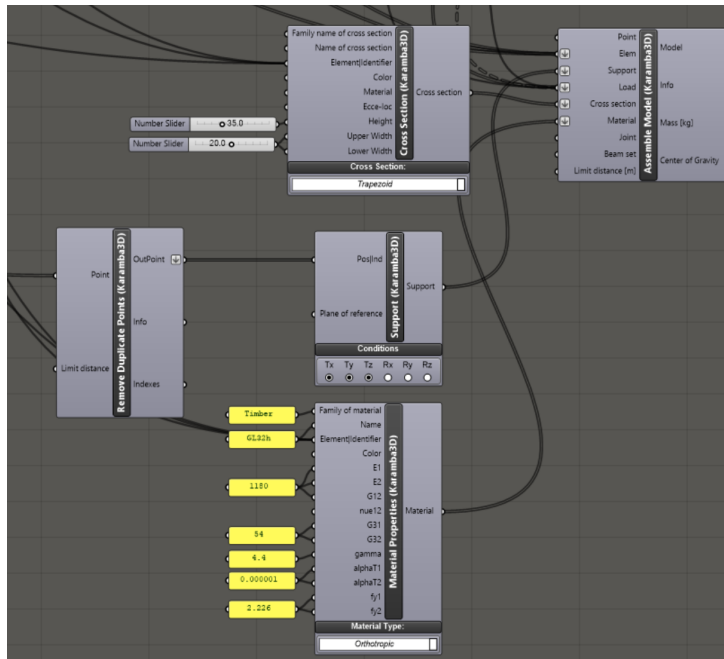
Figure C.10: The rest of the Karamba parameters, as material properties, supports and cross sections. All of the Karamba parameters is assembled in the *Assemble Model* component.
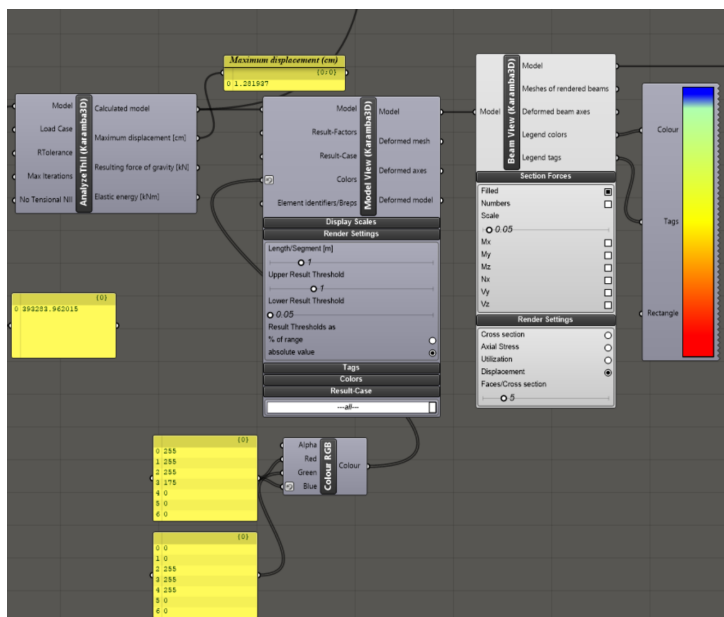
Figure C.11: *AnalyzeThII* analyses the model assembled in figure C.10. Beam view is for visualization in the Rhino view port.
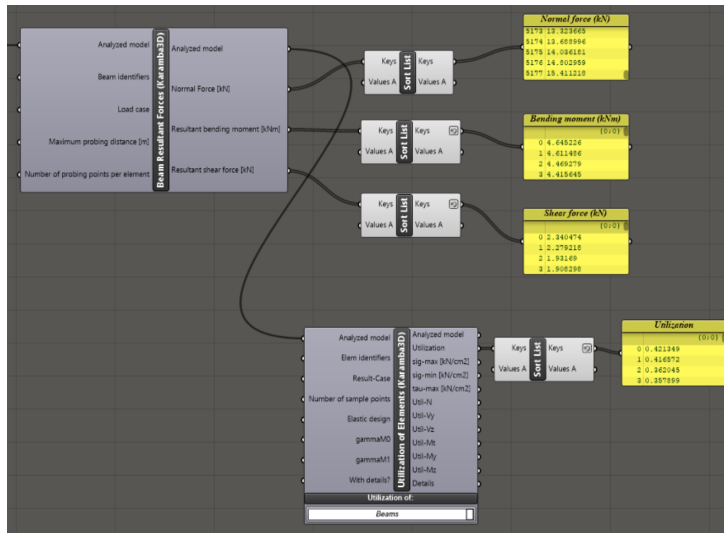
Figure C.12: The forces working in the structure can be displayed after the model is analysed.
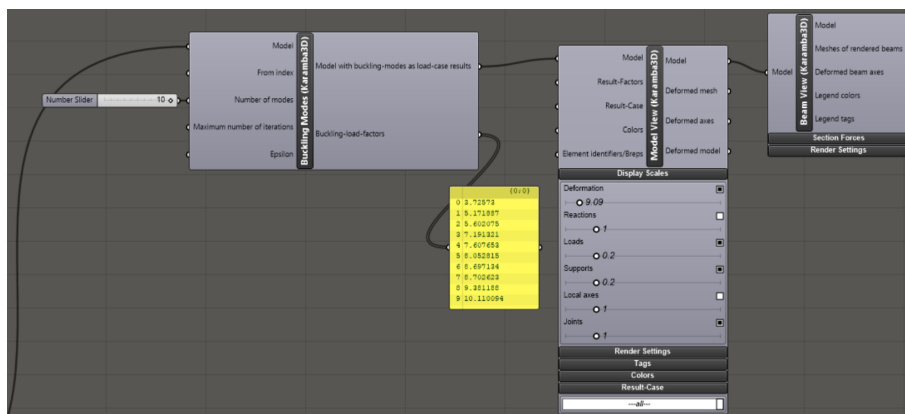
Figure C.13: There must be a separate analysis for buckling.

C.2 Repetitive nodes in the Great Court Roof
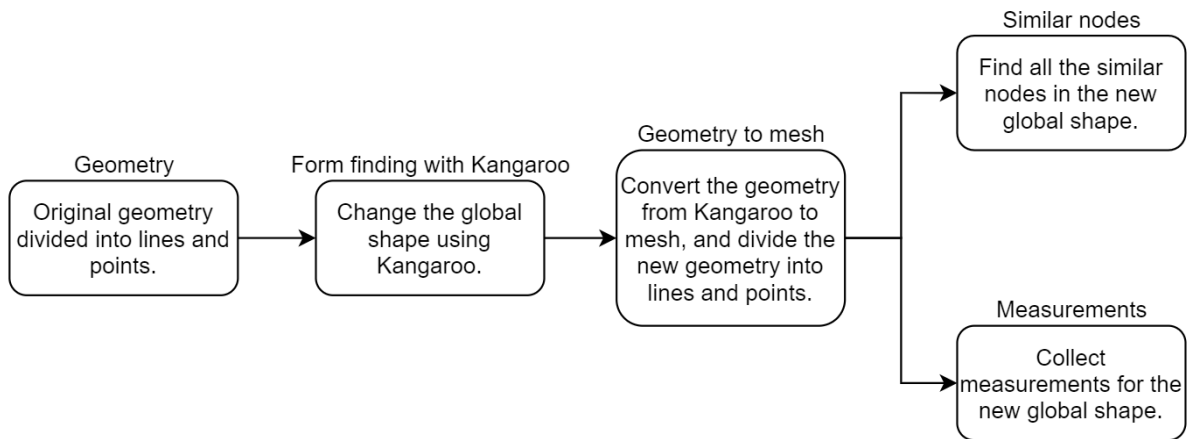
Figure C.14: Step by step how the code works.
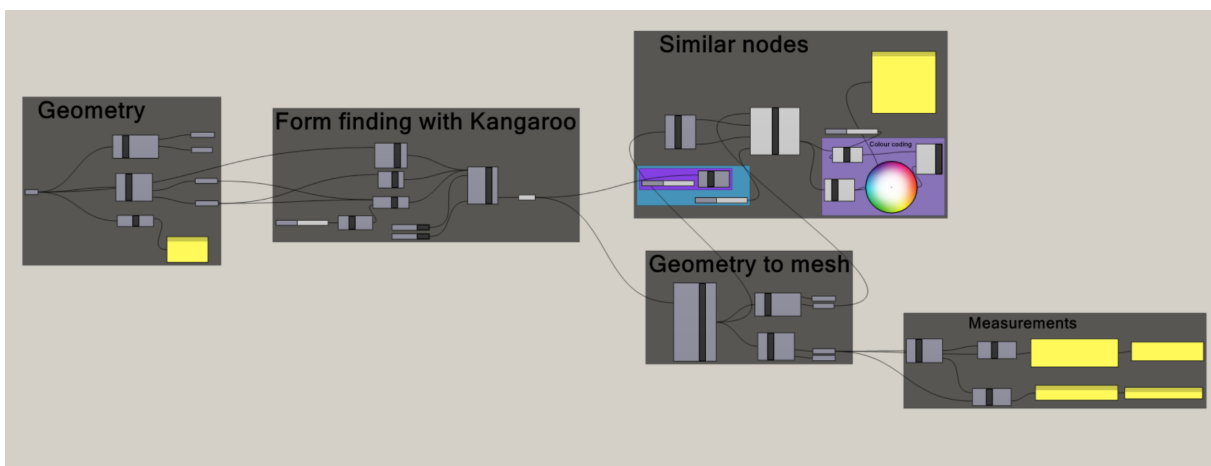
Figure C.15: The entire script used to find repetitive nodes in both the original shape and for other global shapes.
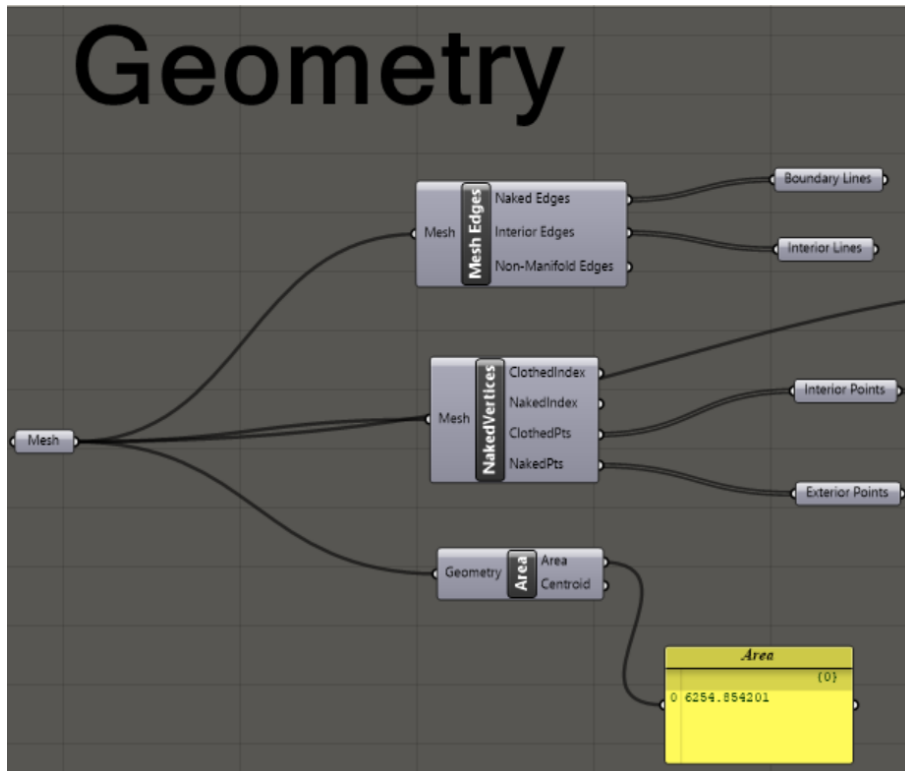
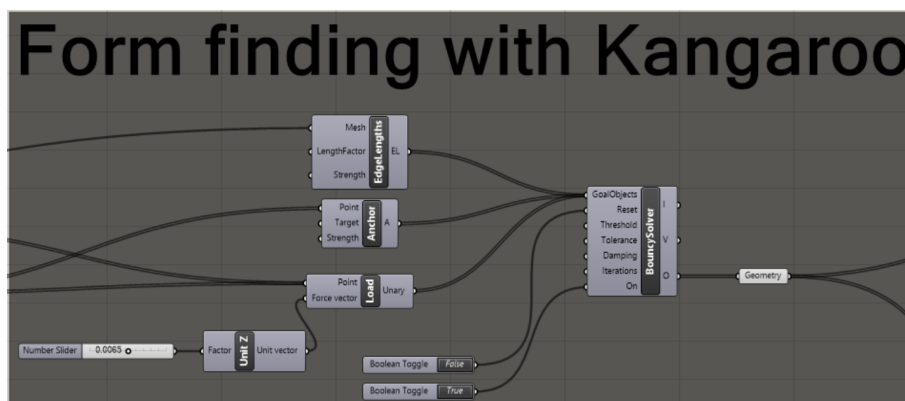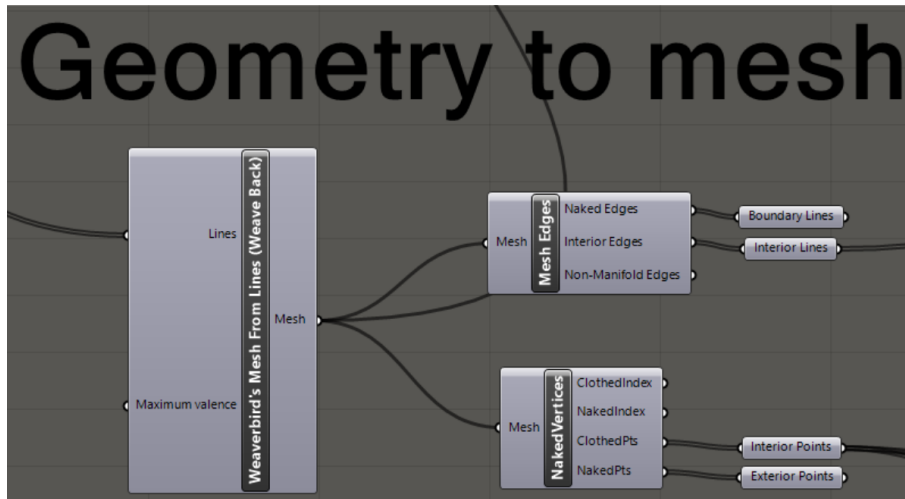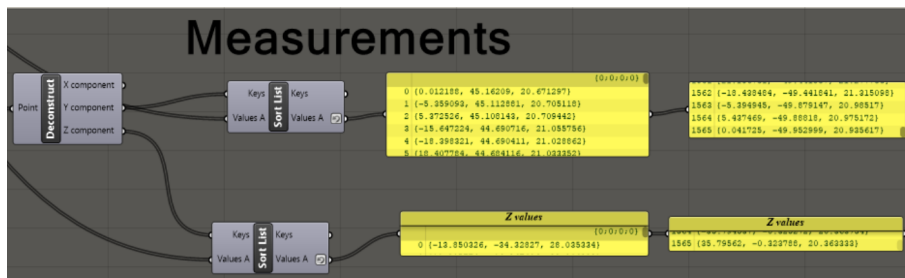**Figure C.16:** The original geometry is divided into lines and points.

Figure C.17: Using Kangaroo's BouncySolver to change the global shape.
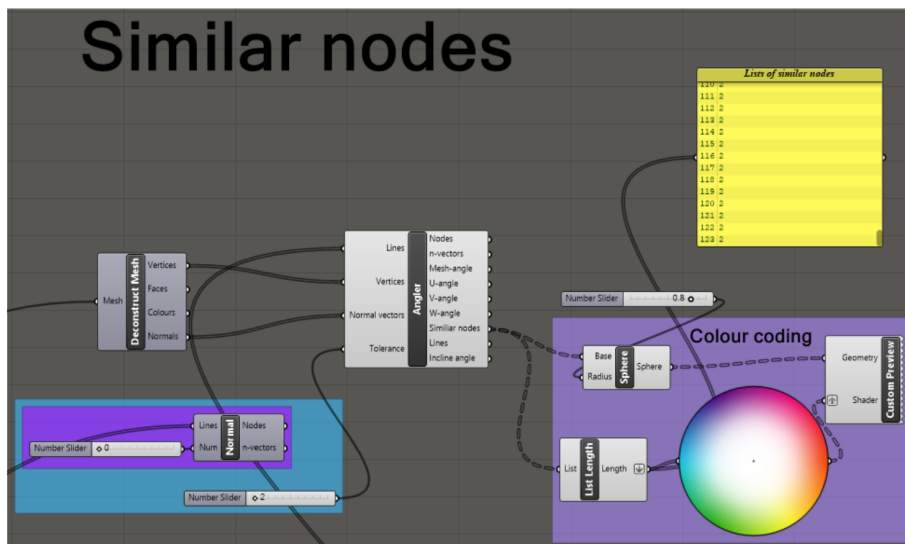
Figure C.18: Converting the new geometry from Kangaroo to a mesh. Then the mesh is divided into lines and points.

Figure C.19: This part is used to collect the measurements for the new global shape. The new height is particularly important.

Figure C.20: Finding all the repetitive nodes in the structure. The colour coding is for visualization in the Rhino view port.

C.3   Generating new mesh for the Great Court roof
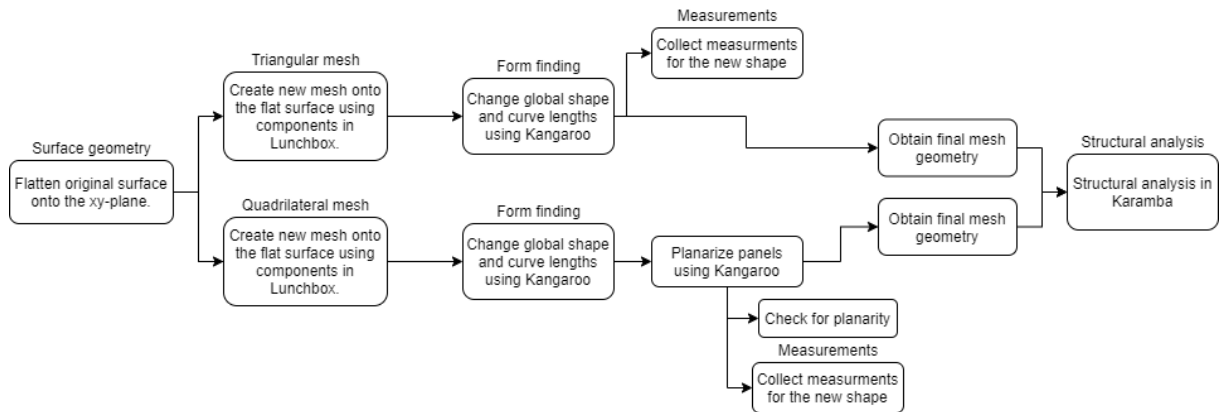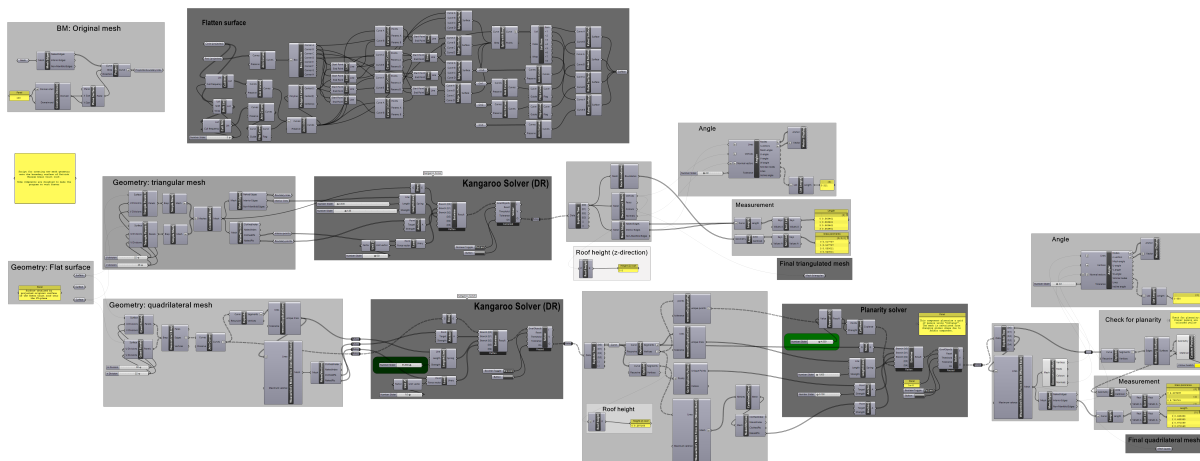

Figure C.21: Step by step how the code works

Figure C.22: The entire script of creating new mesh geometry onto the projected surface of the Great Court Roof.
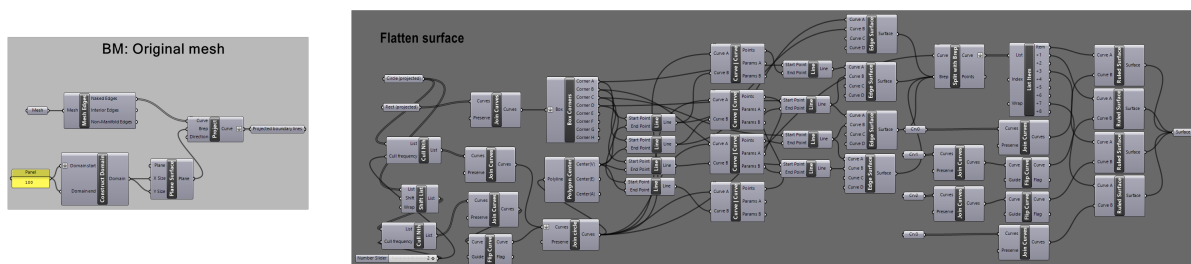

Figure C.23: Projection of the boundary lines of the Great Court Roof and creation of new surface inside, split by diagonal guidelines
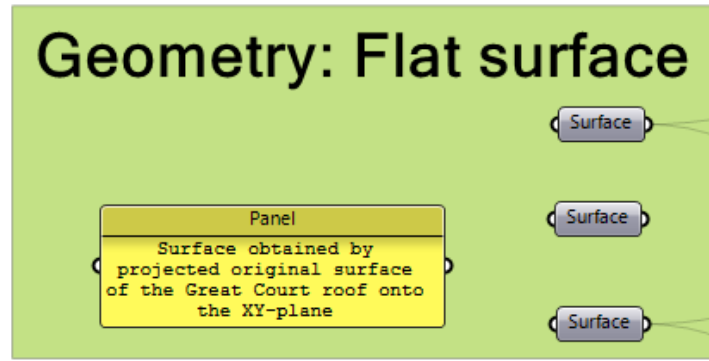
Figure C.24: The flat surface geometry of the Great Court Roof.
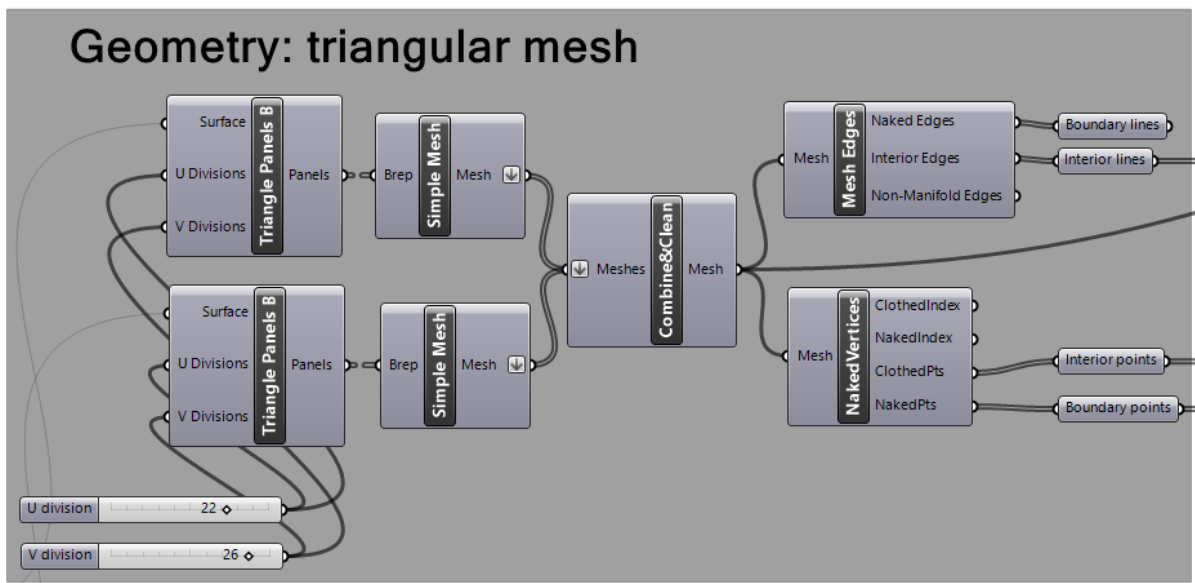
Figure C.25: Creating triangulated lines onto the flat surface by the u- and v parameters in the Lunchbox component.
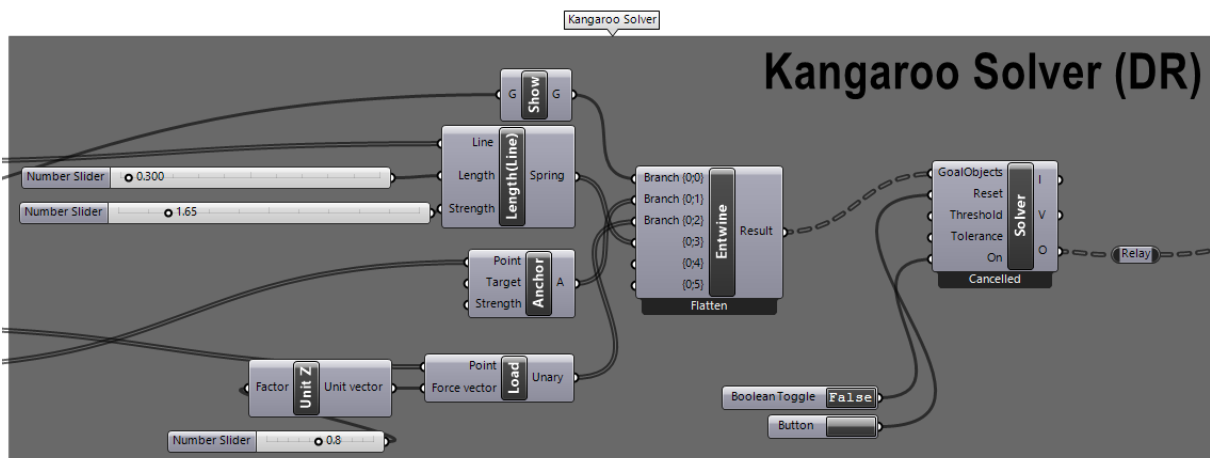
Figure C.26: Form finding using Kangaroo's solver and member length constraints component.

Figure C.27: Measurments of the final shape. Global height and the output of similar nodes is checked.
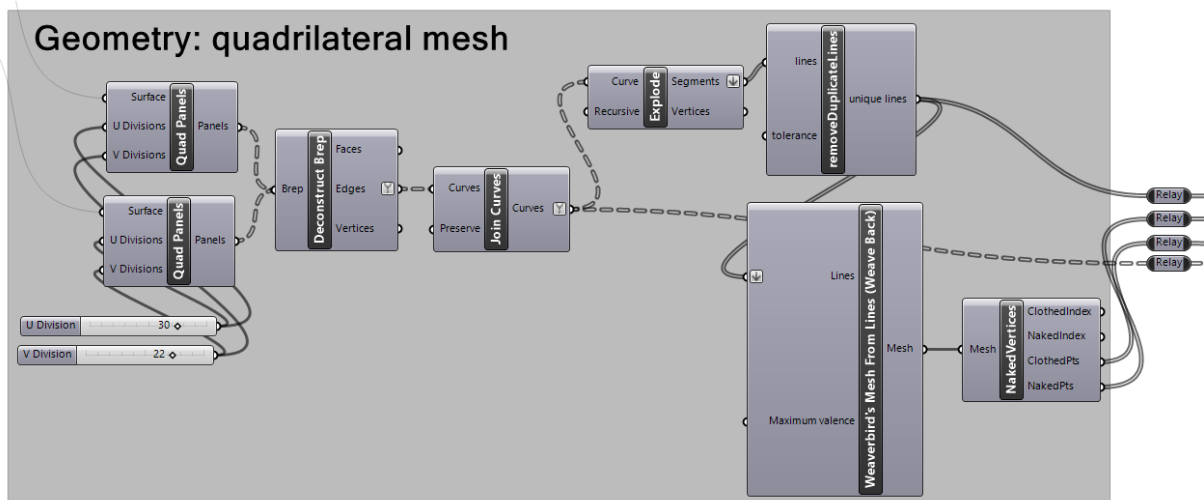
Figure C.28: Creating quadrangular panels on the flat surface by the u- and v parameters in the Lunchbox component *Quad Panels*
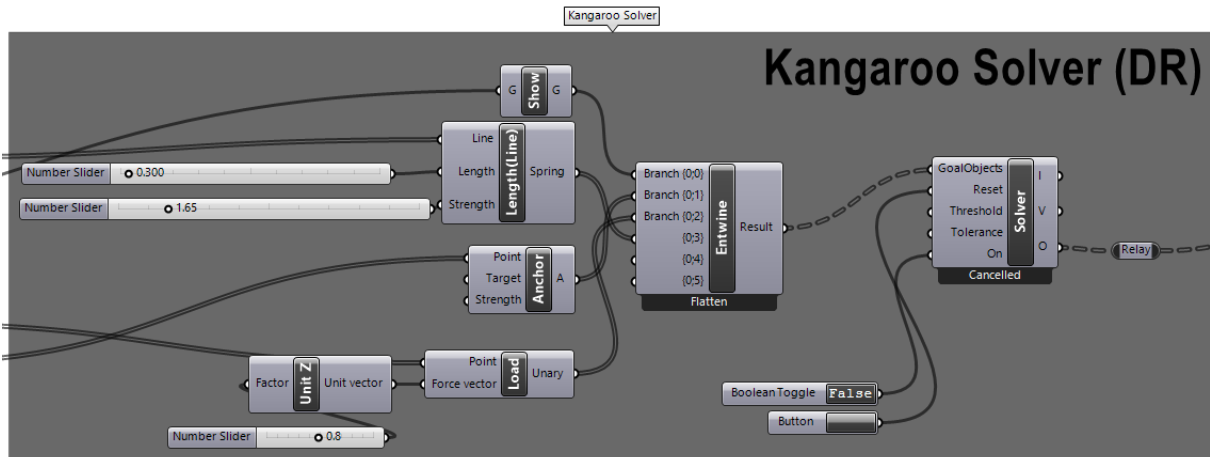
Figure C.29: Form finding using Kangaroo's solver and member length constraints component.
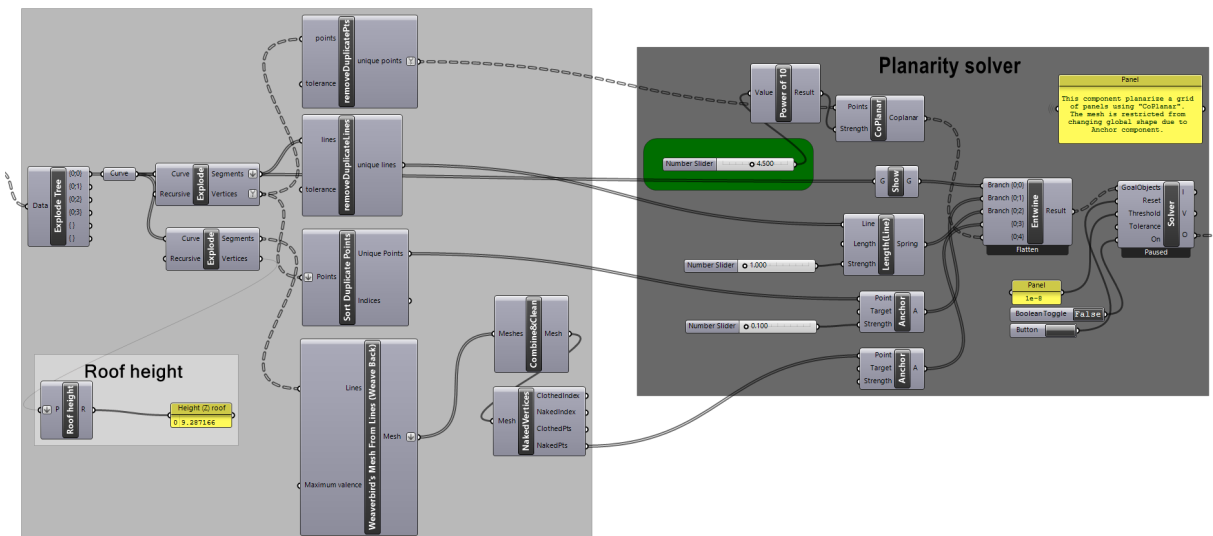
Figure C.30: Using Kangaroo component *CoPlanar* to planarize the quadrangular panels.
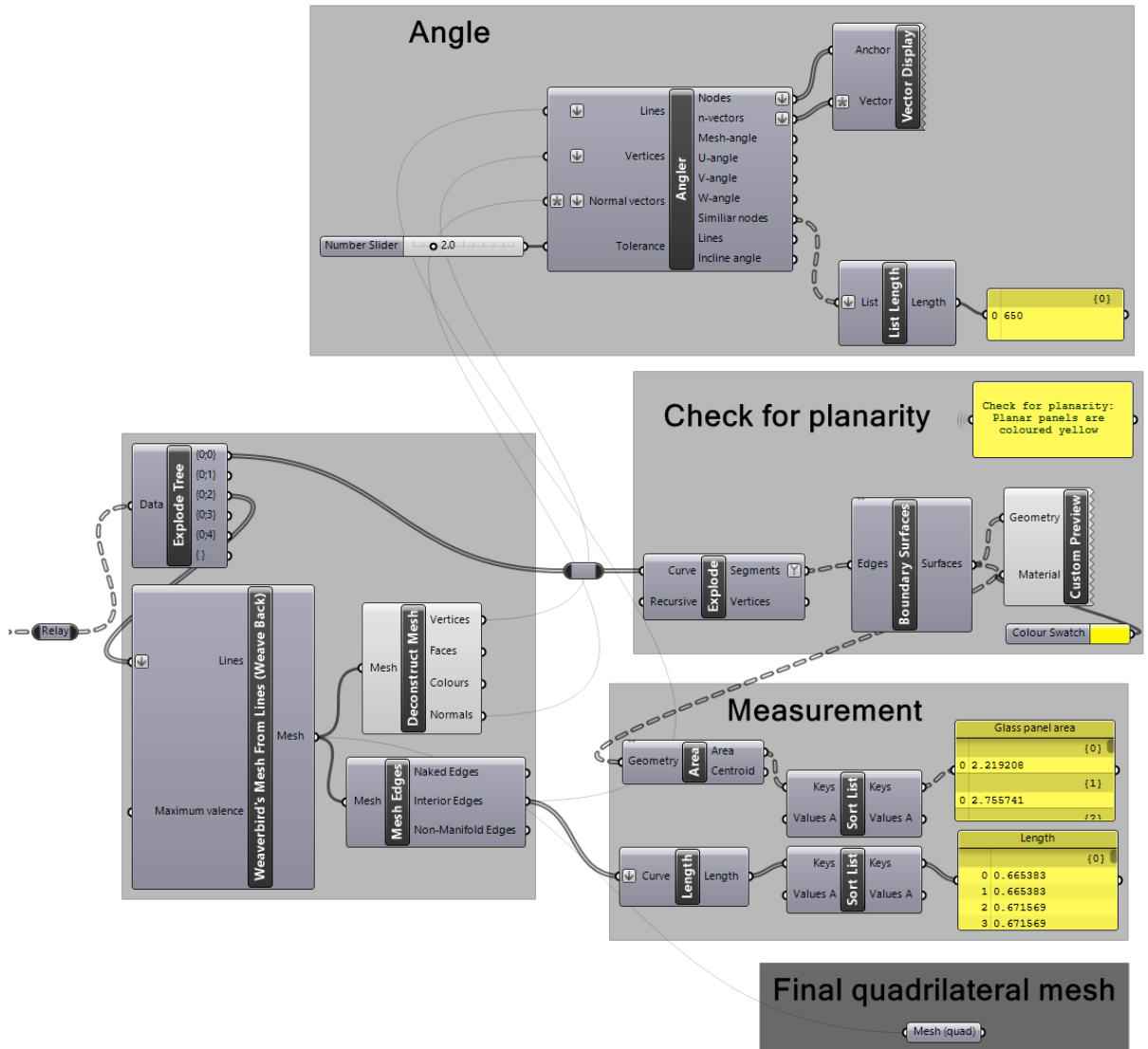
Figure C.31: Measurements of the final mesh. Planarization is checked by the *Boundary Surface* component. The *Custom Preview* component colors the planar panels yellow.

C.4 Required plugins to run Grasshopper scripts

In order to run the Grasshopper scripts provided in addition to this thesis, some plugins must be downloaded and ready to use. The required plugins is listed as following:

- Kangaroo 2.0 [37]

- Karamba3D 1.3.3 [38]

- LunchBox 2017.8.1 (For Rhino 5) [40]

- LunchBox 2018.8.11 or 2018.11.16 (For Rhino 6) [40]

- Weaverbird 0.9.0.1 [45]

- DynamicRelaxation (self made component introduced in chapter 5.2)

- Angler (self made component introduced in chapter 5.3)

- Normal (self made component introduced in chapter 5.3)

- Dynamic Relaxation (self made component introduced in chapter 5.3)

I addition to the plugins above, to export geometry from Rhino Grasshopper to Robot, the following plugins must be used:

- Geometry Gym, ggRhino6Robot v1.2.21 [41]

D Node data

The node data was provided by Kristin Kilvik Skeide and Ragnhild Myrnes, which they have calculated for their own master's thesis.

Capacity of steel connection with laterally loaded bolts + weight calculation

	A	B	C	D	E	F	G	H	I	J	K
1						Capasity of connection with laterally loaded bolts + weight calculation					
2							Yield moment	M_y,Rk	76745,4	Nmm	
3							Embedment strength:	f_h,k:	28,9	N/mm^2	
4		Parameters	Value								
5		d	12	mm							
6		t metal plate	20	mm		Thick cross-section	Outer members:	F_v,Rk,(c):	24245,8	N	
7		rho_k (GL32c)	400	kg/m^3		(Johansens eq.)	(single shear)	F_v,Rk,(d):	11559,9	N	(rope effect neglected)
8		t_1	70	mm				F_v,Rk,(e):	11858,3	N	(rope effect neglected)
9		t_2	180	mm							
10		d_0	13	mm			Inner members:	F_v,Rk,(l):	31173,1	N	
11		rho_steel	7850	kg/m^3			(double shear)	F_v,Rk,(m):	11858,3	N	(rope effect neglected)
12		f_t,0,k	19,5	N/mm^2							
13		k_mod	0,8				One bolt:	F_v,Rk:	46836,3	N	
14		gamma_m	1,3					F_v,Rd:	28822,4	N	
15		# rows	2				Necessary # of bolts:	5,12	6		
16	bolt 4.8:	f_ub	400	N/mm^2			# bolts in one row:	3			
17		A_bolt	113,1	mm^2							
18		f_v,k	3,5	N/mm^2							
19		Shear planes	4			Shear resistance:	Fv,Rd:	72382,29	N		
20		t_ef (d)	30,11	mm		(one bolt)	Necessary # of bolts:	2,038482	4		
21		L_net,t	48	mm			# bolts in one row:	2			
22		L_net,v	648	mm							
23		n	5			Splitting || grain:	Fv,ef,Rd:	193236,6	N		
24		n_ef	3,352			(all bolts)					
25		A_net,t	3360	mm^2			# bolts in one row:	4			
26		A_net,v (inner)	45360	mm^2							
27		A_net,v (outer)	35061,9	mm^2		Block Shear:	Fv,Rd:	174113,9	N		
28		A_net,v (tot)	115483,7	mm^2		(all bolts)					
29							# bolts in one row:	5			
30		F_v,Ed	147550	N							
31		b_wood	120	mm							
32		h_wood	350	mm			bolt resistance, all	723822,9	N		
33		b_steel	62,4	mm							
34		l_steel	145,6	mm		Spacings:	Wood part:	a1:	60	mm	
35								a2:	48	mm	
36		Final steelplate dimension:						a3,t:	84	mm	
37		b_min	129	mm				a4,c:	36	mm	
38		l_min	271,2	mm							
39		V bolts:	39584,1	mm^3			Steel part:	e1:	15,6	mm	
40		V steel plate:	699696,0	mm^3				e2:	15,6	mm	
41		V hexagonal:	864691,7	mm^3				p1:	28,6	mm	
42		V total:	10521576,1	mm^3				p2:	31,2	mm	
43		m total:	82,59	kg							

Figure D.1: Steel nodes

Capacity of aluminium connection with laterally loaded bolts + weight calculation

	A	B	C	D	E	F	G	H	I	J	K
1							Capasity of connection with laterally loaded bolts + Weight calculation				
2							Yield moment:	M_y,Rk:	59477,7	Nmm	
3							Embedment strength:	f_h,k:	28,9	N/mm^2	
4		**Parameters**	**Value**								
5		d	12	mm							
6		t metal plate	20	mm		**Thick cross-section:**	Outer members:	F_v,Rk,(c):	24245,8	N	
7		rho_k (GL32c)	400	kg/m^3		(Johansens eq.)	(single shear)	F_v,Rk,(d):	11224,2	N	(rope effect neglected)
8		t_1	70	mm				F_v,Rk,(e):	10439,4	N	(rope effect neglected)
9		t_2	180	mm							
10		d_0	13	mm			Inner members:	F_v,Rk,(l):	31173,1	N	
11		rho_alu	2700	kg/m^3			(double shear)	F_v,Rk,(m):	10439,4	N	(rope effect neglected)
12		f_t,0,k	19,5	N/mm^2							
13		k_mod	0,8				One bolt:	F_v,Rk:	41757,4	N	
14		gamma_m	1,3					F_v,Rd:	25696,9	N	
15		f_v,k	3,5	N/mm^2							
16		# rows	2				Necessary # of bolts:	5,74	6,0		
17		alpha_v	0,5				# bolts in one row:	3			
18		f_ub	310	N/mm^2							
19		A_bolt	113,1	mm^2		**Shear resistance:**	Fv,Rd:	56096,3	N		
20		gamma_m2	1,25			(one bolt)	Necessary # of bolts:	2,63	4		
21		t_ef (d)	29,86	mm			#bolts in one row	2			
22		L_net,t	48	mm							
23		L_net,v	648	mm							
24		n	5			**Splitting || grain:**	Fv,ef,Rd:	172282,1	N		
25		n_ef	3,352			(all bolts)					
26		A_net,t	3360	mm^2			# bolts in one row:	5			
27		A_net,v (inner)	45360	mm^2							
28		A_net,v (outer)	34900,3	mm^2		**Block Shear:**	Fv,Rd:	173626,8	N		
29		A_net,v (tot)	115160,6	mm^2		(all bolts)					
30		# Shear planes	4				# bolts in one row:	5			
31		F_v,Ed	147550	N							
32		b_wood	120	mm							
33		h_wood	350	mm			bolt resistance, all:	560962,8	N		
34		b_alu	62,4	mm							
35		l_alu	145,6	mm		**Spacings:**	Wood part:	a1:	60	mm	
36								a2:	48	mm	
37		**Final aluminium plate dimension:**						a3,t:	84	mm	
38		b_min	200	mm				a4,c:	36	mm	
39		l_min	271,2	mm							
40		V bolts	39584,1	mm^3			Alu part:	e1:	15,6	mm	
41		V alu plates:	1084800,0	mm^3				e2:	15,6	mm	
42		V hexagonal:	2078461,0	mm^3				p1:	28,6	mm	
43		V total:	17570362,6	mm^3				p2:	31,2	mm	
44		**m total:**	**47,44**	**kg**							

Figure D.2: Aluminium nodes

Brun, Hansen, Zimmer

Development of a parametric workflow, form finding and structural analysis for timber gridshells

NTNU
Norwegian University of
Science and Technology